RESEARCH ARTICLE

Supporting Information

Ultrafast Charge Transfer of Stiboviologens for Electrochromism and Visible Light-Induced α-amino C(sp^3)−H Functionalization

Liang Xu,[a] Lei Zhang,[*b] Yi Qiao,[a] Haifeng Zheng,[a] Guoping Li,[a] Bin Rao,[c] Mingming Zhang,[e] Wenqiang Ma[*ad] and Gang He[*a]

[a.] Frontier Institute of Science and Technology, State Key Laboratory for Strength and Vibration of Mechanical Structures, Xi'an Key Laboratory of Electronic Devices and Material Chemistry, Engineering Research Center of Key Materials for Efficient Utilization of Clean Energy of Shaanxi Province, Future Industrial Innovation Institute of Emerging Information Storage and Smart Sensor, Xi'an Jiaotong University, Xi'an, Shaanxi Province, 710054, China. E-mail: ganghe@mail.xjtu.edu.cn, mawq2023@xjtu.edu.cn

[b.] School of Optoelectronic Engineering, Xidian University, Xi'an, Shaanxi Province, 710126, China. E-mail: leiz@xidian.edu.cn

[c.] School of Chemistry, Xi'an Jiaotong University, Xi'an, Shaanxi Province, 710054, China.

[d.] Department of Radiation Oncology, The First Affiliated Hospital of Xi'an Jiaotong University, Xi'an, Shaanxi Province, 710061, China.

[e.] School of Materials Science and Engineering Xi'an Jiaotong University Xi'an, Shaanxi Province, 710049, China.

Abstract: A series of antimony-bridged viologens derivatives, stiboviologens, were obtained by introducing an antimony atom into the viologens skeleton. By modifying them through *N*-alkylation and *N*-arylation, the optoelectronic properties of the stiboviologens were finely tuned. The stiboviologens displayed strong redox properties, high conjugation, and low energy gaps. Notably, the presence of the antimony atom significantly enhanced the ultrafast metal to ligand charge transfer (MLCT) process (approximately 1 ps), as determined by femtosecond transient absorption studies. Leveraging their excellent optoelectronic properties, the stiboviologens were successfully applied in electrochromism and utilized as both photosensitizers and electron transfer agents for catalyzing α-amino C(sp^3)-H functionalization reactions including oxidative cyclization reaction and cross dehydrogenative coupling reaction under visible light conditions. These findings highlight the potential of stiboviologens as promising materials in the field of optoelectronics and their versatile utilization in synthetic transformations

Table of Contents

Experimental Procedures

1. Materials and instrumentation

General. All reactions were performed using standard Schlenk and glovebox (Vigor) techniques under argon atmosphere. Et_2O, THF were distilled from sodium/benzophenone prior to use. Dry DMF, Anhydrous $Cu(OAc)_2$ (97%), Benzene (99%), Thiophene (99%), 3-Chloroperoxybenzoic acid (85%), I_2 (99.8%), Iodobenzene (98%) , *N,N*-Dimethylaniline were purchased from Energy Chemical Inc. p-Toluenesulfonic acid monohydrate (98%), *N*-Methylmaleimide, 1,2,3,4-Tetrahydroisoquinoline (96%) was purchased from Bide Pharmatech Ltd. Diphenyl iodonium triflate[1] and dithienyl iodonium triflate[2] were synthesized according to the references. $PhSbCl_2$ were synthesized according to the references.[3] *N*-phenyl-tetrahydroisoquinolines needed for CDC reactions were prepared by using the reported procedure.[4] If no other special indicated, other reagents and solvents were used as commercially available without further purification. Column chromatographic purification of products was accomplished using 200-300 mesh silica gel.

NMR spectra were measured on a Bruker Avance-400 spectrometer in the solvents indicated; chemical shifts are reported in units (ppm) by assigning TMS resonance in the ^1H spectrum as 0.00 ppm, DMSO-*d6* resonance in the ^{13}C spectrum as 39.50 ppm. Coupling constants are reported in Hz with multiplicities denoted as s (singlet), d (doublet), t (triplet), q (quartet) and m (multiplet). UV-vis measurements were performed using DH-2000-BAL Scan spectrophotometer. The cyclic voltammetry (CV) in solution were measured using CHI660E B157216, with a polished gold electrode as the working electrode, a Pt-net as counter electrode, and an Ag wire as reference electrode, using ferrocene/ferrocenium (Fc/Fc^+) as internal standard. EPR for **2**, **3**, **4** and **5** were measured using a Bruker EMX PLUS6/1 instrument at room temperature in dry degassed DMF. Scans were performed with magnetic field modulation amplitude of 0.1 G at room temperature in dry degassed DMF. Thermogravimetric analysis (TGA) measurements were carried out in the temperature range of 40-700 °C by using of a Mettler-Toledo TGA1 thermal analyzer in air, at a heating rate of 10 K•min^{-1}. High-resolution mass spectra (HRMS) were collected on a Bruker maxis UHR-TOF mass spectrometer in an ESI positive mode. photoluminescence spectra were measured using Horiba PL spectrometer (Fluorolog-3). The phosphorescence quantum efficiency, time-resolved phosphorescence spectra and lifetime were obtained using Edinburgh FLSP980 emission spectrophotometer equipped with a xenon lamp (Xe900), a picosecond pulsed laser (EPL-375), a microsecond flash-lamp (µF900) and an integrating sphere, respectively. Single crystal X-ray diffraction analysis was carried out on a Bruker Apex Duo instrument. Photographs were taken using a Nikon D5100 digital camera.

All the computational calculations reported in this work were performed using the Gaussian 09 code. To simulate the experimental UV-Vis in N,N-dimethylformamide (DMF), the Polarizable Continuum Model (PCM) as a self-consistent reaction field (SCRF) was used for the calculation of equilibrium geometries, vibrational frequencies and excited state calculations. The geometries for the ground state of these compounds in the DMF solution were optimized at the B3LYP level with the LANL08(d) basis set applied for the Sb atom and 6-31G(d) basis set for all other atoms. It should be pointed out that the structures of all stationary points in DMF solvent were fully optimized, and frequency calculations were performed at the same level. The frequency calculations confiifirmed the nature of all revealed equilibrium geometries: there were no imaginary frequencies.

The simulated UV–Vis spectra for optimized molecules were performed at the time dependent density functional theory (TD-DFT) at the ground-state equilibrium geometries in DMF solution, both low-lying singlet and triplet states were determined using the B3LYP, in association with the LANL08(d) basis set applied for the Sb atom and 6-311G(d,p) basis set for all other atoms.

In the solution-based ECD, Indium tin oxide (ITO)-coated glass (~ 15 Ω/sq) was utilized as the electrodes and **2,3,4** and **5** was used as active component. The two pieces of ITO glass were sealed together with a UV-cured gasket with 50 µm-thick intervals introduced by Baumgartner group.[5]

2. Synthetic procedures

Synthesis of stibodipydine 1.
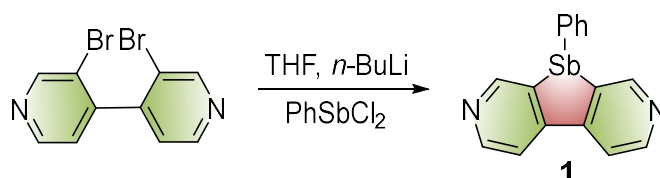
3,3'-dibromo-4,4'-bipyridine (628 mg, 2.0 mmol)[6] in dry THF (40 mL) was cooled to −85°C, and the solution of *n*-BuLi (2.5 M in hexanes, 1.7 mL, 4.2 mmol) was added dropwise. The mixture was stirred for 90 min at −85°C, followed by the addition of PhSbCl₂ (2.4 mmol in 10 mL of THF).[3] The mixture was allowed to warm to room temperature and stirred overnight. The volatiles were removed by vacuum distillation and the solid was dissolved in the mixture of water and ethyl acetate (40 mL × 3). The combined organic phase was dried over anhydrous sodium sulfate and concentrated, which was separated b y column chromatography (SiO$_2$, CH$_2$Cl$_2$: CH$_3$OH = 120:1 → 80:1) to give as a white solid. Yield: 250.2 mg (35.4 %).

^{1}H NMR (400 MHz, DMSO-*d6*) δ 9.13 (s, 2H), 8.70 (d, *J* = 5.2 Hz, 2H), 8.13 (d, *J* = 5.2 Hz, 2H), 7.35 (dd, *J* = 6.5, 3.0 Hz, 2H), 7.19-7.17 (m, 3H); ^{13}C NMR (101 MHz, DMSO-*d6*) δ 156.13, 155.60, 150.20, 142.66, 139.15, 135.28, 129.07, 128.72, 119.55; HRMS (ESI⁺) m/z: [M+H]⁺ calcd for C$_{16}$H$_{11}$SbN$_2$ 351.9960; found 351.9952; Mp (°C): 84.3°C -85.9°C.

Synthesis of methylstiboviologen 2.
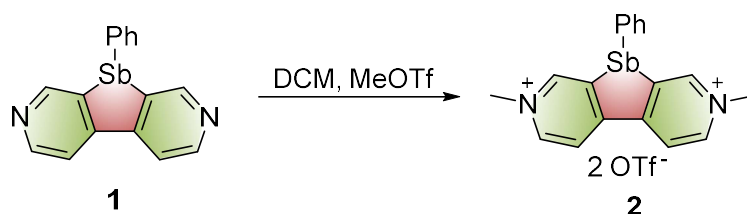
Stibodipyridine (70.6 mg, 0.2 mmol) was dissolved in dichloromethane (5 mL) and the solution was cooled to 0°C, followed by the addition of methyl triflate (113 μL, 1 mmol) dropwise. The reaction mixture was stirred at 0°C for 5 min, then it was allowed to warm to room temperature and stirred for 5 h. The yellow precipitate was collected via vacuum filtration, washed with dichloromethane and diethyl ether, and dried at 40°C under a vacuum: Yield: 118.7 mg (87.1%).

^{1}H NMR (400 MHz, DMSO-*d6*) δ 9.33 (s, 2H), 9.21 (d, *J* = 6.4 Hz, 2H), 9.02 (d, *J* = 6.4 Hz, 2H), 7.41 (d, *J* = 6.7 Hz, 2H), 7.25-7.21 (m, 3H), 4.42 (s, 6H); ^{13}C NMR (101 MHz, DMSO-*d6*) δ 158.59, 152.57, 150.87, 146.21, 139.61, 135.97, 129.29, 129.24, 124.38, 122.72, 119.51, 48.61; ^{19}F NMR (376 MHz, DMSO-*d6*) δ -73.02; HRMS (ESI⁺) m/z: [M-2OTf]⁺ calcd for C$_{18}$H$_{17}$SbN$_2$ 382.0430; found 382.0453; Mp (°C): 230.6°C -232.2°C.

Synthesis of benzylstiboviologen 3.

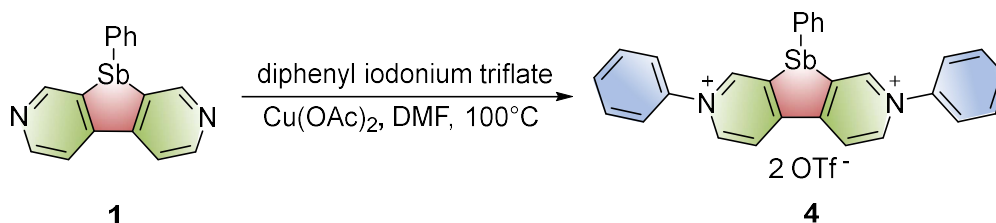Stibobipyridine (70.6 mg, 0.2 mmol) and benzyl bromide (2 mL, excess) were combined in a 10 mL of Schlenk. The reaction mixture was stirred at 60°C for 72 h, then it was allowed to warm to room temperature and the precipitate was collected via vacuum filtration, washed with dichloromethane. The precipitate was collected to obtain a dark red solid (120.0 mg, 86.3%).

The dark red solid (69.5 mg, 0.1 mmol) was dissolved in dichloromethane (3 mL) and the solution was cooled to 0°C, followed by the addition of methyl triflate (28 μL, 0.25 mmol) dropwise. The mixture was stirred at room temperature until the reaction underwent a significant color change. The yellow precipitate was collected via vacuum filtration, washed with dichloromethane and diethyl ether, and dried at 40°C under a vacuum: Yield: 63.2 mg (75.8%).

^{1}H NMR (400 MHz, DMSO-*d6*) δ 9.47 (d, *J* = 6.4 Hz, 4H), 9.07 (d, *J* = 6.4 Hz, 2H), 7.53 (d, *J* = 7.2 Hz, 4H), 7.47 (q, *J* = 7.2 Hz, 6H), 7.29 (d, *J* = 7.3 Hz, 2H), 7.21-7.16 (m, 3H), 5.98-5.90 (m, 4H); ^{13}C NMR (101 MHz, DMSO-*d6*) δ 159.25, 154.16, 149.73, 145.71, 140.04, 135.88, 134.82, 129.97, 129.82, 129.44, 129.18, 129.12, 125.09, 122.73, 119.53, 63.91; ^{19}F NMR (376 MHz, DMSO-*d6*) δ -77.76; HRMS (ESI[+]) m/z: [M-2OTf][+] calcd for $C_{30}H_{25}SbN_2$ 534.1056; found 534.1052; Mp (°C): 158.3°C -160.2°C.

Synthesis of phenylstiboviologen 4.

1 → **4**

Stibobipyridine (70.6 mg, 0.2 mmol), diphenyl iodonium triflate (258.1 mg, 0.6 mmol) and anhydrous Cu(OAc)₂ (1.8 mg, 0.01 mmol) was dissolved in degassed DMF (10 mL). The reaction mixture was stirred at 100°C for 8 h. The volatiles were removed under reduced pressure, the dark red oil was taken up in acetone/chloroform/diethyl ether (1:1:1), and filtered. The resulting residue was taken up in chloroform/acetone (5:1; 60 mL) and vigorously stirred for 30 min. The dark yellow precipitate was collected via vacuum filtration, washed with cold water and diethyl ether, and dried at 40°C under a vacuum: Yield: 76.5 mg (47.5%).

^{1}H NMR (400 MHz, DMSO-*d6*) δ 9.78 (d, *J* = 1.5 Hz, 2H), 9.68 (dd, *J* = 6.5, 1.5 Hz, 2H), 9.38 (d, *J* = 6.6 Hz, 2H), 7.99-7.94 (m, 4H), 7.83-7.81 (m, 6H), 7.54 (d,1.8 Hz, 2H), 7.26 (dd, *J* = 4.8, 1.8 Hz, 3H); ^{13}C NMR (101 MHz, DMSO-*d6*) δ 159.52, 153.00, 149.83, 145.80, 143.21, 139.48, 136.14, 132.02, 130.93, 129.43, 129.36, 125.16, 122.73, 119.52; ^{19}F NMR (376 MHz, DMSO-*d6*) δ -77.76; HRMS (ESI[+]) m/z: [M-2OTf][+] calcd for $C_{28}H_{21}SbN_2$ 506.0743; found 506.0745; Mp (°C): 246.8°C -248.3°C.

Synthesis of thienylstiboviologen 5.

1 → **5**
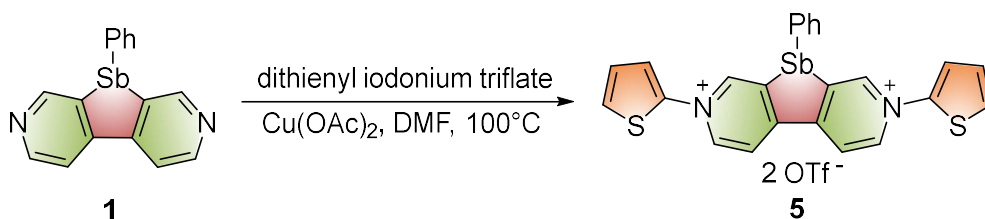
Stibobipyridine (35.3 mg, 0.1 mmol), dithienyl iodonium triflate (221.1 mg, 0.5 mmol) and anhydrous Cu(OAc)₂ (1 mg, 0.005 mmol) was dissolved in degassed DMF (5 mL). The reaction mixture was stirred at 40°C for 36 h. The volatiles were removed under reduced pressure, the dark red residue was taken up in THF (5 mL) and a mixture of dichloromethane /diethyl ether (1:1; 10 mL) was added. The dark brown precipitate was collected via vacuum filtration, dichloromethane and diethyl ether, and dried at 40°C under a vacuum: Yield: 70.4 mg (83.2 %).

^{1}H NMR (400 MHz, DMSO-*d6*) δ 9.79 (d, *J* = 1.7 Hz, 2H), 9.70 (dd, *J* = 6.7, 1.7 Hz, 2H), 9.29 (d, *J* = 6.7 Hz, 2H), 7.96 (s, 2H), 7.95 (s, 2H), 7.53-7.49 (m, 2H), 7.36 (t, *J* = 4.7 Hz, 2H), 7.29-7.24 (m, 3H); ^{13}C NMR (101 MHz, DMSO-*d6*) δ 159.15, 153.43, 148.98, 144.88, 143.61, 139.55, 136.19, 129.66, 129.42, 128.19, 125.72, 125.22; ^{19}F NMR (376 MHz, DMSO-*d6*) δ -77.76; HRMS (ESI[+]) m/z: [M-2OTf][+] calcd for $C_{18}H_{17}SbN_2S_2$ 517.9871; found 517.9860; Mp (°C): > 300°C.

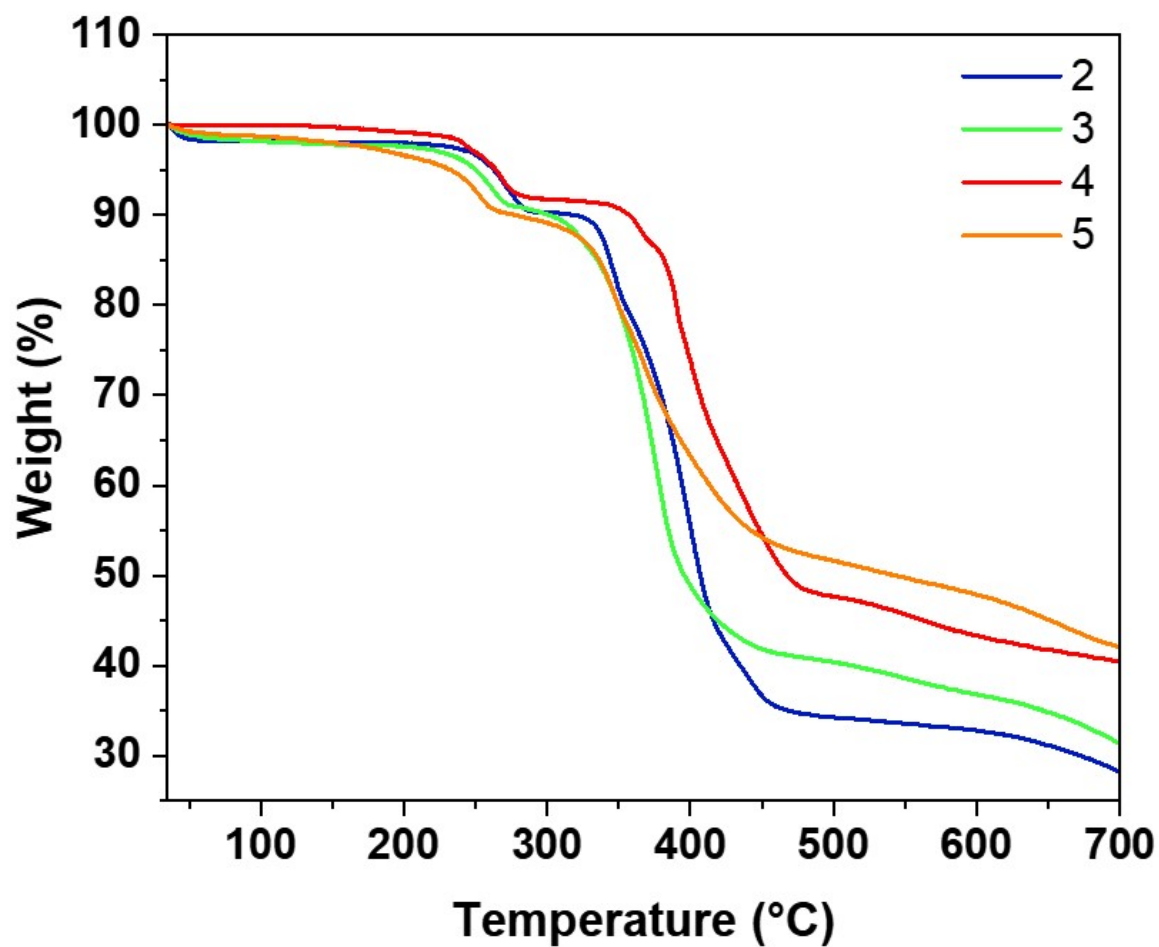### 3. TGA of antimony-bridged viologens

Figure S1. TGA of compound **2**, **3**, **4** and **5**.

4. Single-crystal X-ray structure determination

X-ray Crystallography: The X-ray-quality single crystals of **2−5**, suitable for single crystal X-ray diffraction experiments, were obtained by slowvapor diffusion of i-Pr$_2$O into a MeCN of **2−5** at room temperature. All data were collected using a Bruker APEX II CCD detector/D8 diffractometer using Mo/Cu Kα radiation. The data were corrected for absorption through Gaussian integration from indexing of the crystal faces. Structures were solved using the direct methods programs SHELXS-97, and refinements were completed using the program SHELXL-97.
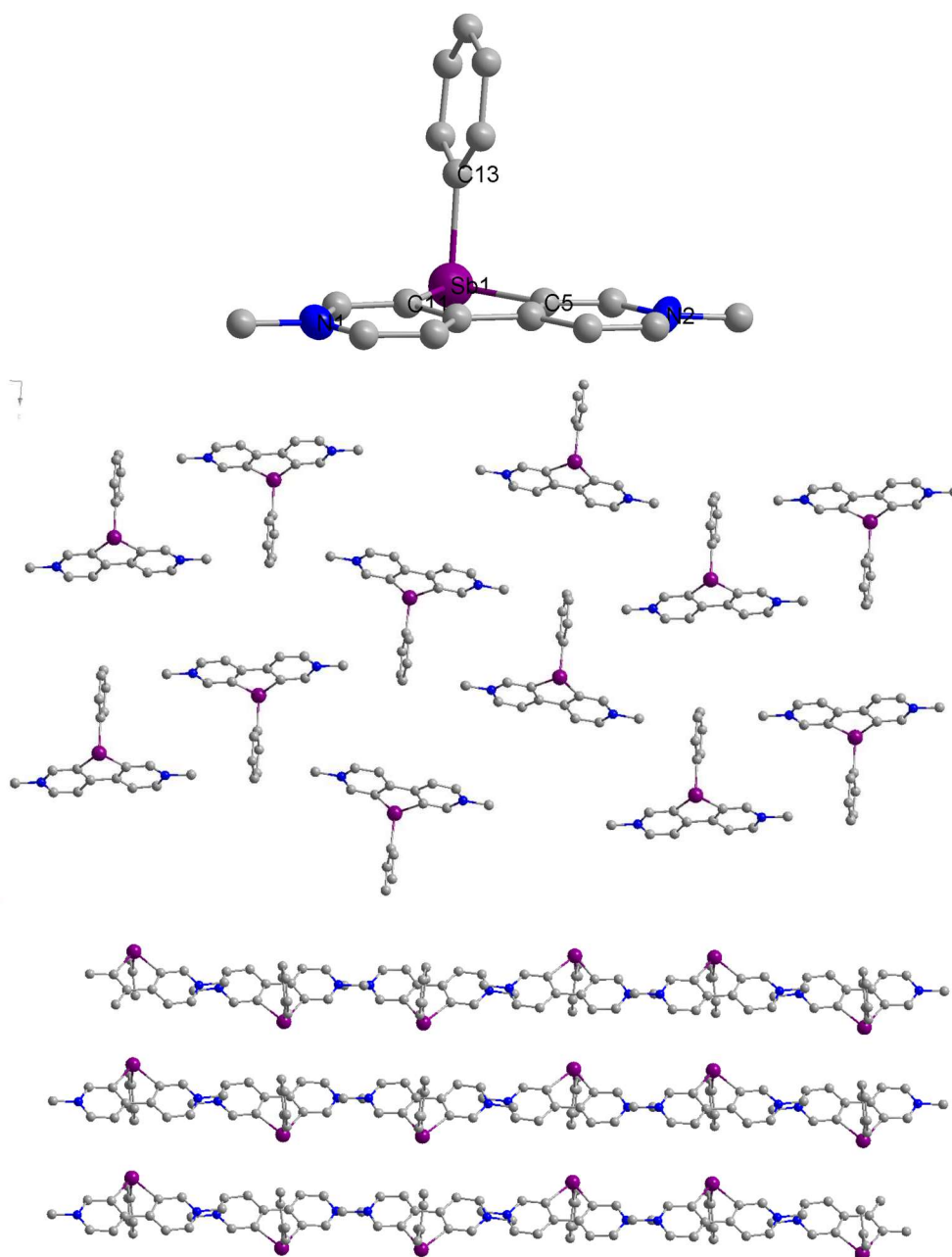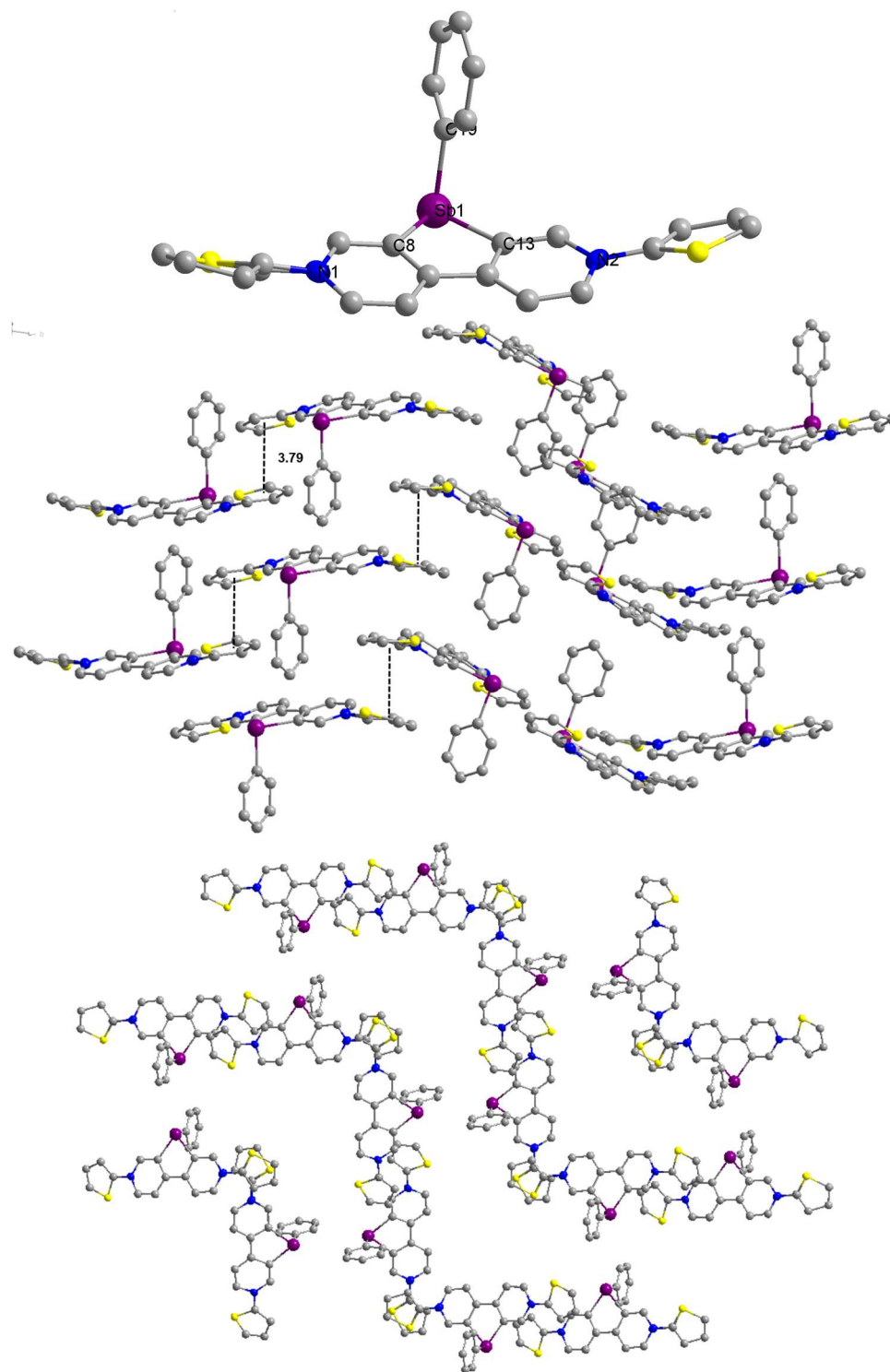

Figure S2. Molecular Structure of **2** with thermal ellipsoids presented at a 50% probability level. All hydrogen atoms have been omitted for clarity. Selected bond lengths (Å): Sb(1)-C(5), 2.17(5); Sb(1)-C(11), 2.17(5); Sb(1)-C(13), 2.13(6); Bond angles (deg): C(11)-Sb(1)-C(13), 78.0(19); C(13)-Sb(1)-C(5), 94.6(2); C(13)-Sb(1)-C(11), 98.3(2).

Table S1. Crystal data and structure refinement for **2**.

Empirical formula	$C_{20}H_{17}F_6N_2O_6S_2Sb$
Formula weight	681.31
Temperature	296.15 K
Wavelength	0.71073 Å
Crystal system，Space group	Monoclinic，P 1 21/c
Unit cell dimensions	a = 6.656(2) Å a= 90 deg
	b = 33.470(10) Å b= 101.728(4) deg
	c = 12.331(4) Å g = 90 deg
Volume	2689.8(14) Å ^3
Z，Density (calculated)	4，1.682 Mg/m^3
Absorption coefficient	1.260 mm^-1
F(000)	1344
Crystal size	0.24 x 0.22 x 0.2 mm^3
Theta range for data collection	2.080 to 27.680 deg
Index ranges	-8<=h<=8, -43<=k<=43, -16<=l<=16
Reflections collected / unique	30867/6245 [R(int) = 0.0358]
Completeness to theta = 25.242	99.7 %
Max. and min. transmission	0.7456 and 0.6286
Refinement method	Full-matrix least-squares on F^2
Data / restraints / parameters	6245 / 354 / 325
Goodness-of-fit on F^2	1.080
Final R indices [I>2sigma(I)]	R1 = 0.0574, wR2 = 0.1463
R indices (all data)	R1 = 0.0702, wR2 = 0.1525
Largest diff. peak and hole	0.672 and -1.025 e. Å ^3
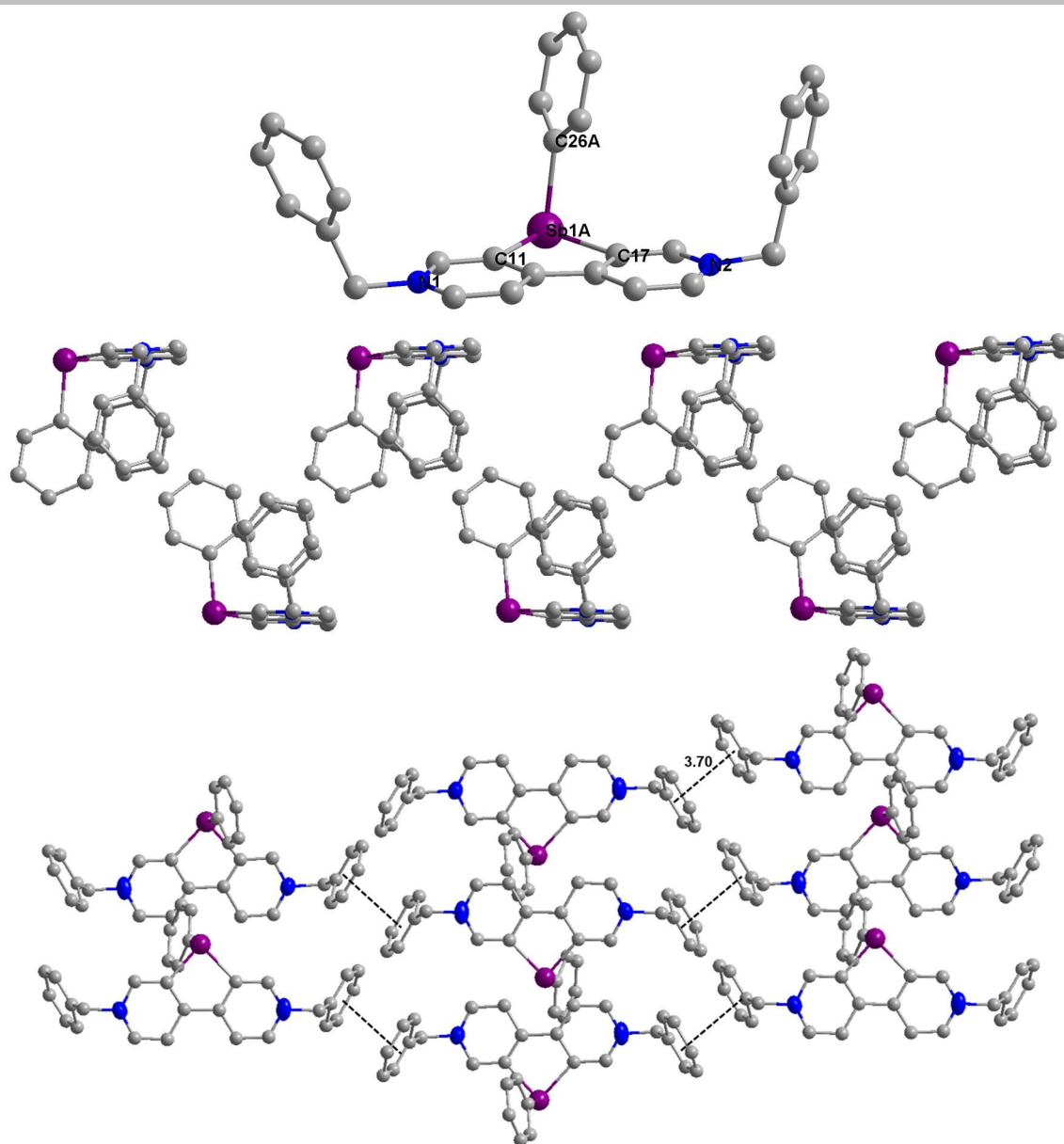
Figure S3. Molecular Structure of **3** with thermal ellipsoids presented at a 50% probability level. All hydrogen atoms have been omitted for clarity. Selected bond lengths (Å): Sb(1A)-C(17), 2.15(10); Sb(1A)-C(11), 2.16(10); Sb(1A)-C(26A), 2.15(14); Bond angles (deg): C(11)-Sb(1A)-C(17), 84.7(4); C(11)-Sb(1A)-C(26A), 93.3(7); C(11)-Sb(1A)-C(26A), 100.9(7).

Table S2. Crystal data and structure refinement for **3**.

Empirical formula	$C_{32}H_{25}F_6N_2O_6S_2Sb$
Formula weight	833.41
Temperature	193.00 K
Wavelength	0.71073 Å
Crystal system，Space group	orthorhombic, P $2_12_12_1$
Unit cell dimensions	a = 10.2451(5) Å a= 90 deg
	b = 12.6670(6) Å b= 90 deg
	c = 28.2436(12) Å g = 90 deg
Volume	3665.3(3) Å ^3
Z，Density (calculated)	4，1.510 Mg/m^3
Absorption coefficient	1.088 mm^-1
F(000)	1664.0
Crystal size	0.13 x 0.12 x 0.1 mm^3
Theta range for data collection	7.986 to 120.694 deg
Index ranges	-13<=h<=10, -16<=k<=16, -27<=l<=36
Reflections collected / unique	28920/8046 [R(int) = 0.0436]
Completeness to theta = 25.242	99.9 %
Max. and min. transmission	0.7455 and 0.6586
Refinement method	Full-matrix least-squares on F^2
Data / restraints / parameters	8046 / 171/ 483
Goodness-of-fit on F^2	1.268
Final R indices [I>2sigma(I)]	R1 = 0.0976, wR2 = 0.2863
R indices (all data)	R1 = 0.1099, wR2 = 0.3022
Largest diff. peak and hole	1.91and -0.90 e. Å ^3
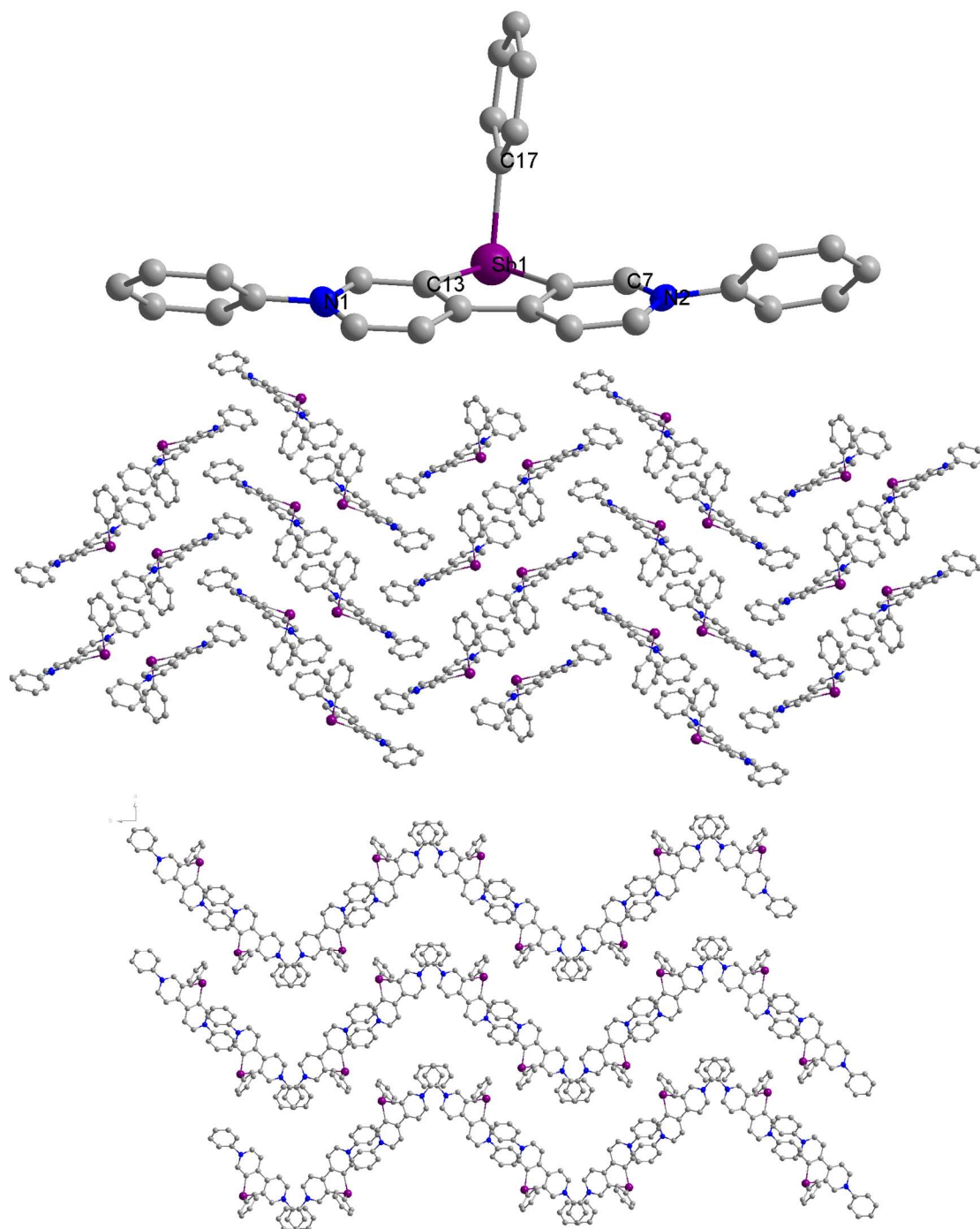
Figure S4. Molecular Structure of **4** with thermal ellipsoids presented at a 50% probability level. All hydrogen atoms have been omitted for clarity. Selected bond lengths (Å): Sb(1)-C(8), 2.17(4); Sb(1)-C(13), 2.18(3); Sb(1)-C(17), 2.14(4); Bond angles (deg): C(8)-Sb(1)-C(13), 77.6(13); C(17)-Sb(1)-C(8), 94.1(14); C(17)-Sb(1)-C(13), 98.4(13).

Table S3. Crystal data and structure refinement for **4**.

Empirical formula	$C_{30}H_{21}F_6N_2O_6S_2Sb$
Formula weight	805.36
Temperature	296.15 K
Wavelength	0.71073 Å
Crystal system，Space group	Monoclinic, P 1 21/c
Unit cell dimensions	a = 12.5955(17) Å a= 90 deg
	b = 29.107(4) Å b= 91.866(2) deg
	c = 8.6115(12) Å g = 90 deg
Volume	3155.5(7) Å ^3
Z，Density (calculated)	4，1.695 Mg/m^3
Absorption coefficient	1.088 mm^-1
F(000)	1600
Crystal size	0.25 x 0.22 x 0.21 mm^3
Theta range for data collection	1.399 to 27.274 deg
Index ranges	-16<=h<=16, -37<=k<=37, -11<=l<=11
Reflections collected / unique	30666/7057 [R(int) = 0.0344]
Completeness to theta = 25.242	99.9 %
Max. and min. transmission	0.7455 and 0.6586
Refinement method	Full-matrix least-squares on F^2
Data / restraints / parameters	7057 / 448 / 434
Goodness-of-fit on F^2	1.074
Final R indices [I>2sigma(I)]	R1 = 0.0418, wR2 = 0.1021
R indices (all data)	R1 = 0.0570, wR2 = 0.1102
Largest diff. peak and hole	1.407 and -0.736 e. Å ^3

Figure S5. Molecular Structure of **5** with thermal ellipsoids presented at a 50% probability level. All hydrogen atoms have been omitted for clarity. Selected bond lengths (Å): Sb(1)-C(8), 2.17(4); Sb(1)-C(13), 2.17(4); Sb(1)-C(19), 2.14(4); Bond angles (deg): C(8)-Sb(1)-C(13), 78.0(15); C(19)-Sb(1)-C(8), 97.3(14); C(17)-Sb(1)-C(13), 93.4(13).

Table S4. Crystal data and structure refinement for **5**.

Empirical formula	$C_{26}H_{17}F_6N_2O_6S_4Sb$
Formula weight	817.40
Temperature	193.00 K
Wavelength	0.71073 Å
Crystal system，Space group	Monoclinic, P 1 21/c
Unit cell dimensions	a = 12.4610(8) Å α= 90 deg
	b = 28.8323(18) Å β= 93.231(3) deg
	c = 8.3949(6) Å γ = 90 deg
Volume	3011.3(3) Å ^3
Z，Density (calculated)	4， 1.803 Mg/m^3
Absorption coefficient	1.088 mm^-1
F(000)	1616
Crystal size	0.13 x 0.12 x 0.1 mm^3
Theta range for data collection	6.18 to 120.542 deg
Index ranges	-15<=h<=12, -19<=k<=35, -10<=l<=10
Reflections collected / unique	22991/6514[R(int) = 0.0467]
Completeness to theta = 25.242	99.9 %
Max. and min. transmission	0.7455 and 0.6586
Refinement method	Full-matrix least-squares on F^2
Data / restraints / parameters	6514/543/561
Goodness-of-fit on F^2	1.042
Final R indices [I>2sigma(I)]	R1 = 0.0435, wR2 = 0.1138
R indices (all data)	R1 = 0.0505, wR2 = 0.1186
Largest diff. peak and hole	1.22 and -0.75

5. Emission spectra and lifetime
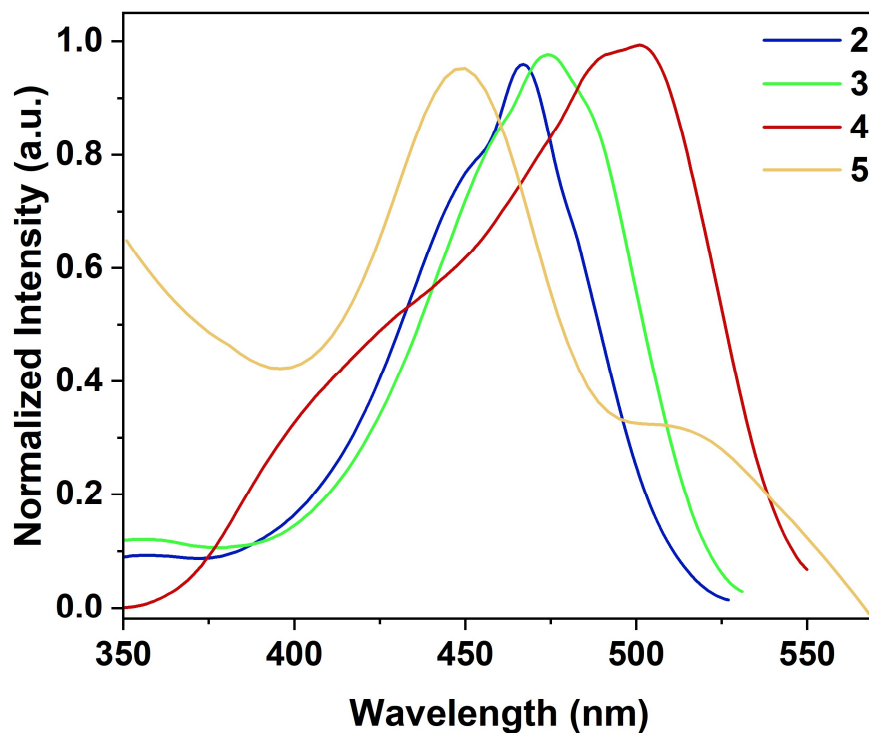
Figure S6. Excitation spectrum of **2**, **3**,4 and **5** in acetonitrile (c = 10^{-3} M) under ambient conditions.
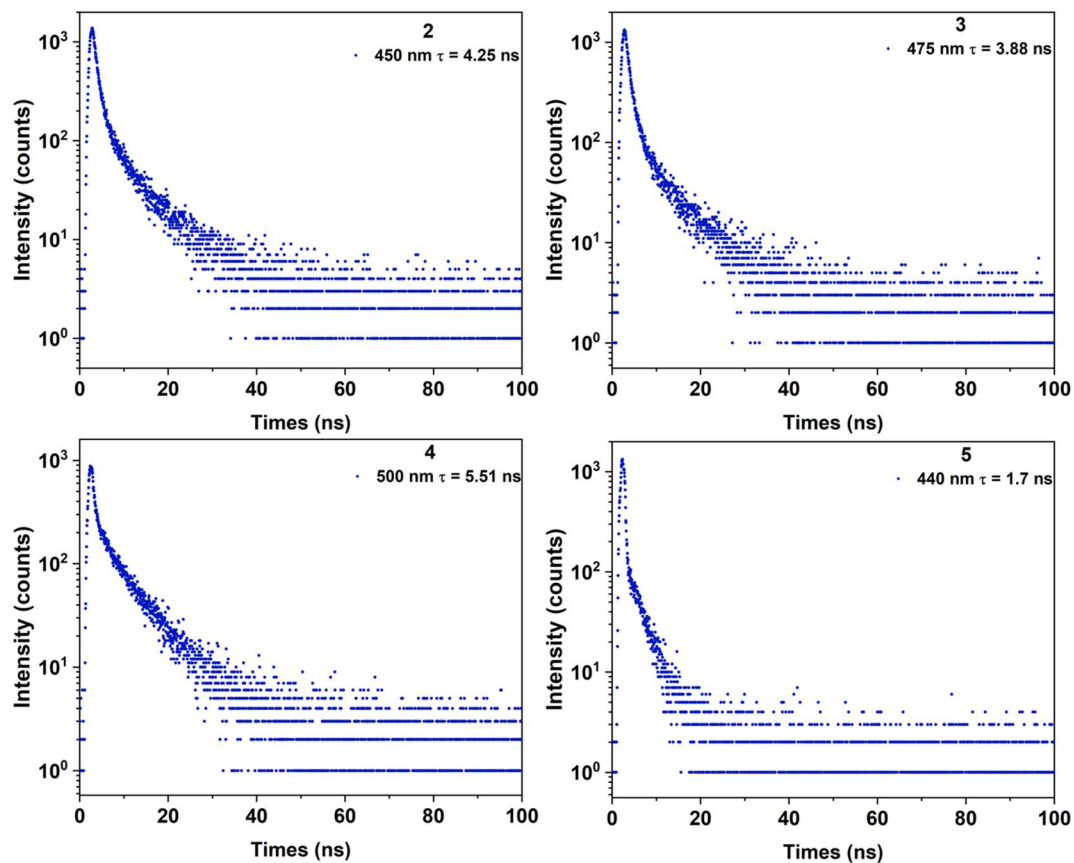
Figure S7. Lifetime decay profiles of emission bands of **2**, **3**,**4** and **5** in acetonitrile (c = 10^{-3} M) under ambient conditions.

S15

6. The cyclic voltammogram
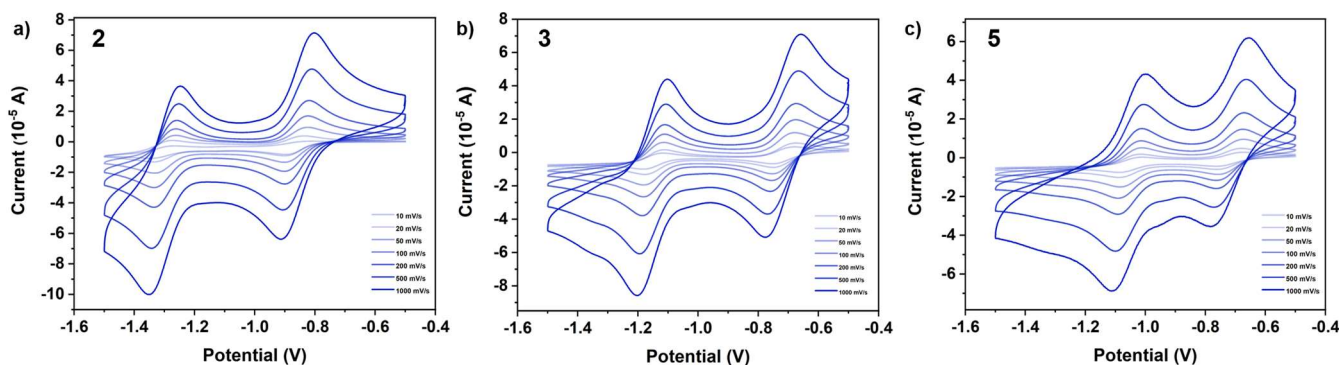
Figure S8. The cyclic voltammogram at different scan rates in DMF solution with tetrabutylammonium hexafluorophosphate (0.1 M) as supporting electrolyte, potential E referenced to Fc/Fc$^+$, c = 10^{-3} M.
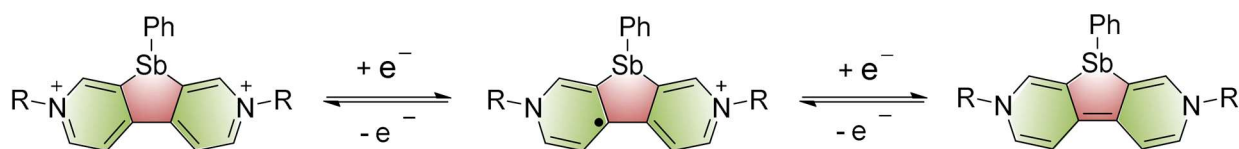
Scheme 1. Redox reaction of stibium-bridged viologens.

Compound	E_{red} [V]	E_g [eV][a]	(Calcd)[b]	E_{LUMO} [eV]	E_{HOMO} [eV]	E_{LUMO} [eV] calcd	E_{HOMO} [eV] calcd
2	-0.86, -1.28	3.84	3.45	-3.94	-7.78	-3.79	-7.24
3	-0.72, -1.15	3.71	3.45	-4.08	-7.79	-3.79	-7.24
4	-0.74, -1.10	3.12	3.33	-4.06	-7.18	-3.92	-7.25
5	-0.72, -1.05	2.62	3.06	-4.08	-6.70	-4.05	-7.11

Table S5. [a] Energy gap values were calculated from the absorption spectra in DMF.[7] [b] Theoretical calculations have been carried out by using the GAUSSIAN09 suite of programs.

7. Evaluation of electron-transfer constant k_{ET}

The electron-transfer constants k_{ET} were determinated using the Nicholson method according to our previous work.[8]

$$ip = 2.69 \times 10^5 AD_0^{1/2} v^{1/2} c^* = Rv^{1/2}$$

where electrode radius r = 0.15 cm, electrode area A = πr^2 = 0.07065 cm^2, concentration c* = 1 $\times 10^{-6}$ mol/cm^3.

When scan rate v = 0.1 V/s,

$$k_{ET} = \Psi(\pi D_0 Fv/RT)^{1/2} = 182\Psi R$$
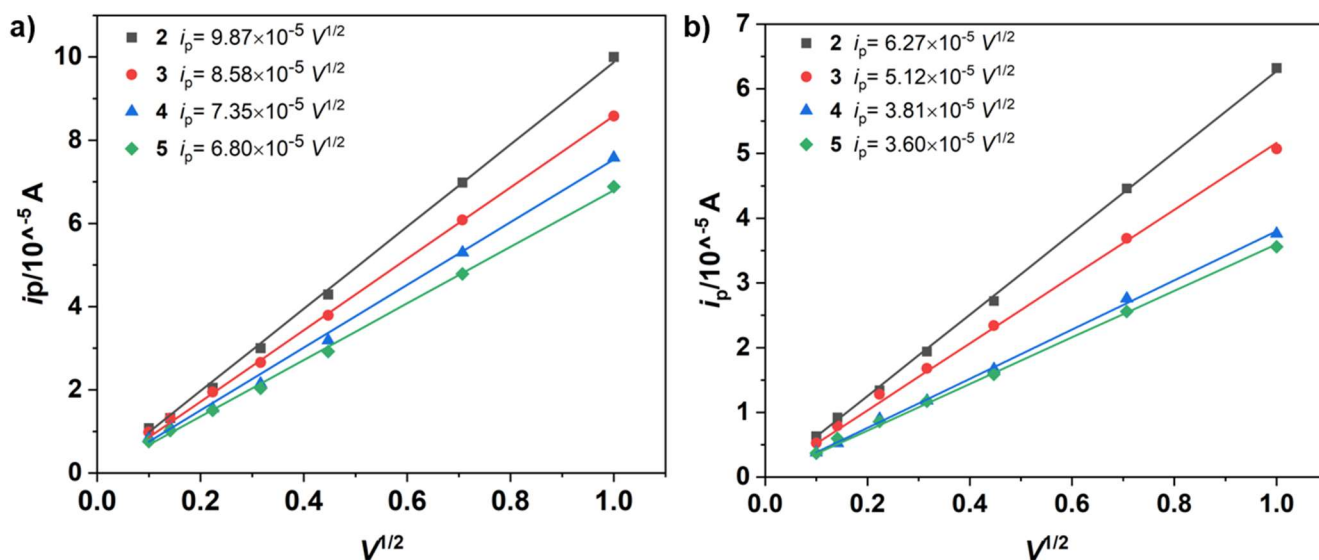
Figure S9. Peak current and scan rate diagrams of **2, 3, 4** and **5**: (a) first reduction and (b) second reduction.

Table S6. The electron-transfer constants kET of **2, 3, 4** and **5**.

Compound	R_1[a]	ΔE_{p1}[b]	Ψ_1[c]	R_1[a]	ΔE_{p2}[b]	Ψ_1[c]	k_{ET1}[d]	k_{ET2}[d]
2	6.27×10^{-5}	102	0.56	9.87×10^{-5}	100	0.60	6.4	10.77
3	5.12×10^{-5}	94	0.72	8.58×10^{-5}	95	0.69	6.8	10.87
4	3.81×10^{-5}	79	1.35	7.35×10^{-5}	81	1.22	9.7	16.31
5	3.60×10^{-5}	81	1.22	6.80×10^{-5}	82	1.16	8.1	14.35

[a] Slope of ip~v1/2 in Figure S8.

[b] ΔEp was calculated from CV.

[c] Ψ = (-0.6288+0.0021ΔEp)/(1-0.017ΔEp).

[d] Electron-transfer constant kET was evaluated according to Nicholson's formula.

8. Electrochromism of 2, 3, 4 and 5
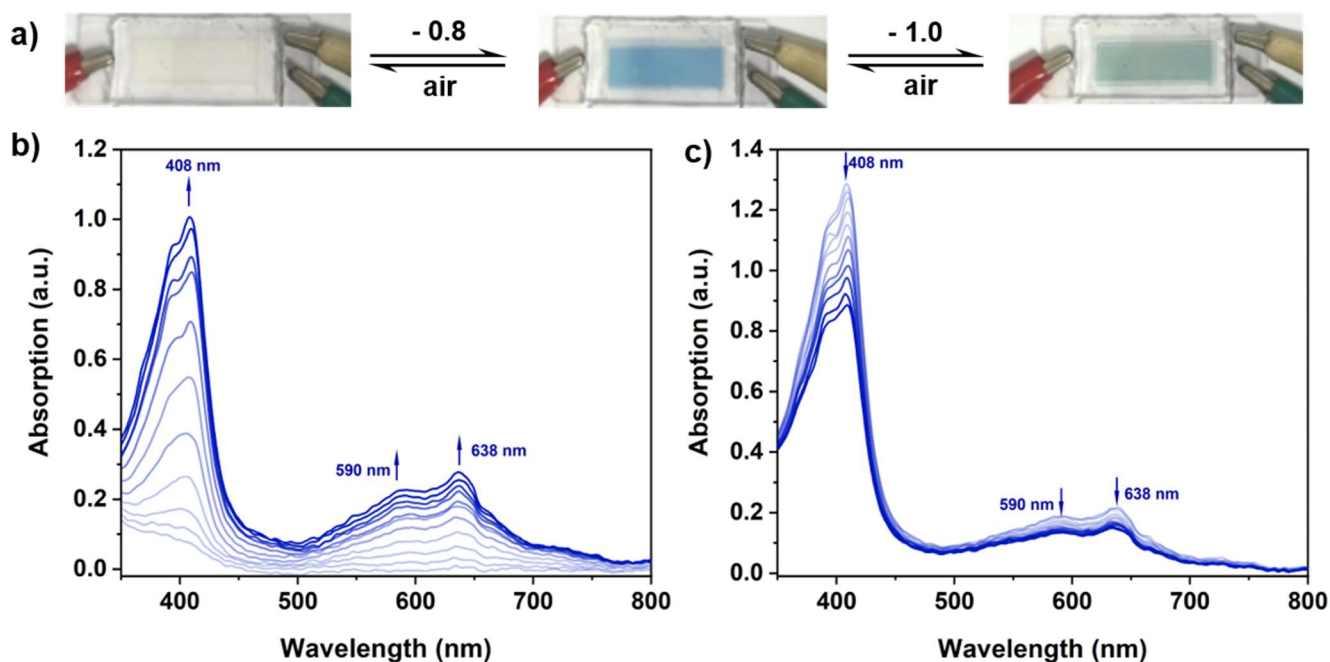
Figure S10. (a) Solution-based electrochromic device with **2** (no electrolyte). (b) Spectroelectrochemistry of **2** for first reduction. (c) Spectroelectrochemistry of for second reduction. *N,N*-Dimethylformamide (DMF) was used as the solvent.
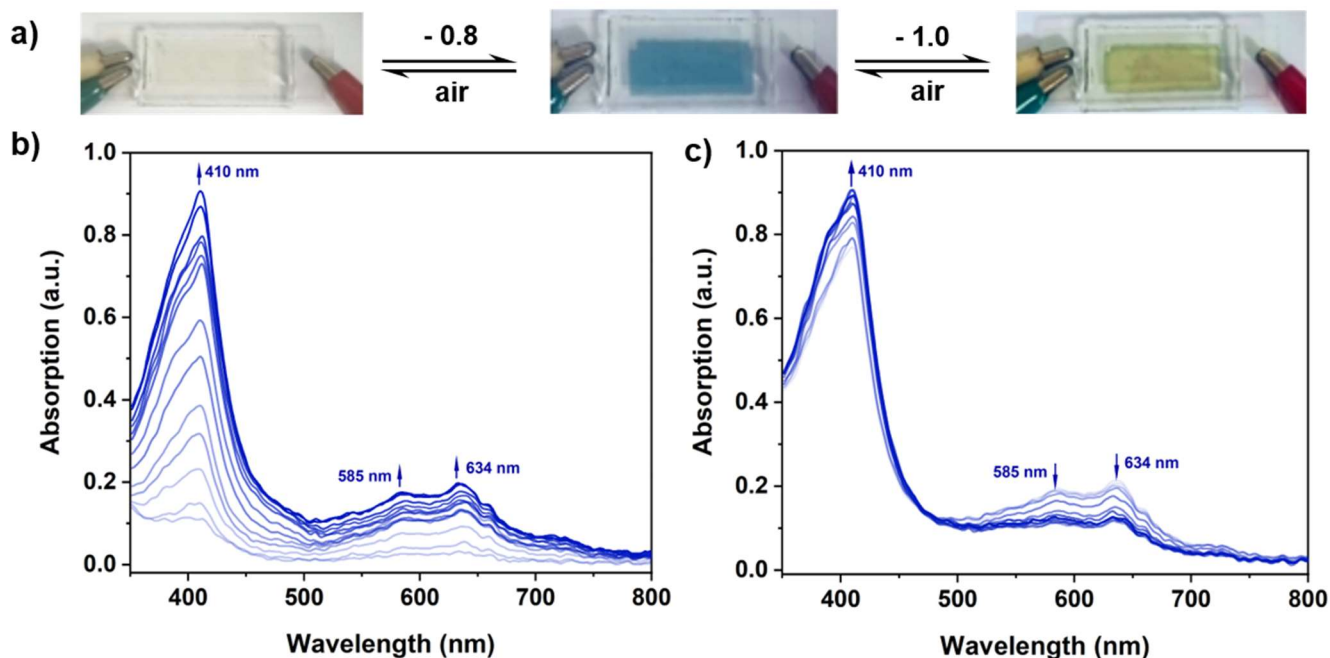
Figure S11. (a) Solution-based electrochromic device with **3** (no electrolyte). (b) Spectroelectrochemistry of **3** for first reduction. (c) Spectroelectrochemistry of for second reduction. *N,N*-Dimethylformamide (DMF) was used as the solvent.
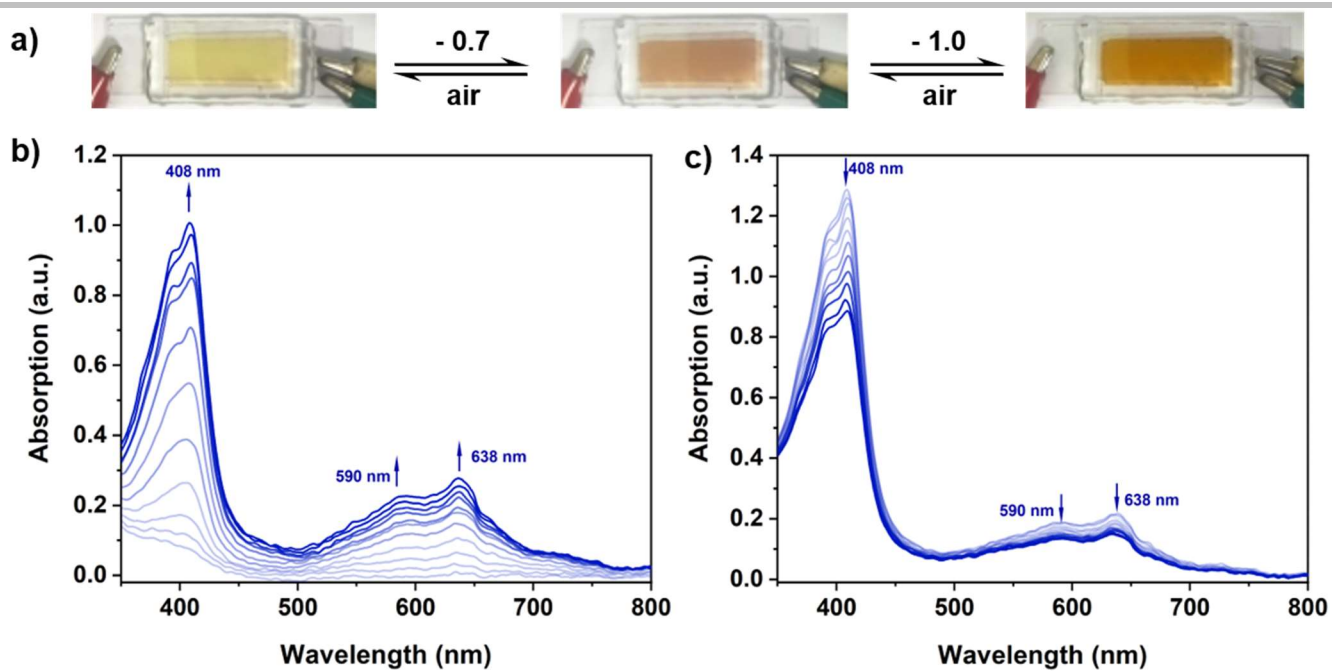
Figure S12. (a) Solution-based electrochromic device with **5** (no electrolyte). (b) Spectroelectrochemistry of **5** for first reduction. (c) Spectroelectrochemistry of for second reduction. *N,N*-Dimethylformamide (DMF) was used as the solvent.

9. Optical stability test for electrochromic switching of 4 and 4 + FeCp₂ complex

The optical stability for electrochromic switching of compound **4** and **4** + FeCp$_2$ were tested between 0 and -2.0 V. For compound **4**, the coloring time was set to 10 seconds, and the bleach time was 120 seconds. For compound **4** + FeCp$_2$, the coloring time was set to 5 seconds, and the bleach time was 80 seconds. The absorbance changes are all at 650 nm.
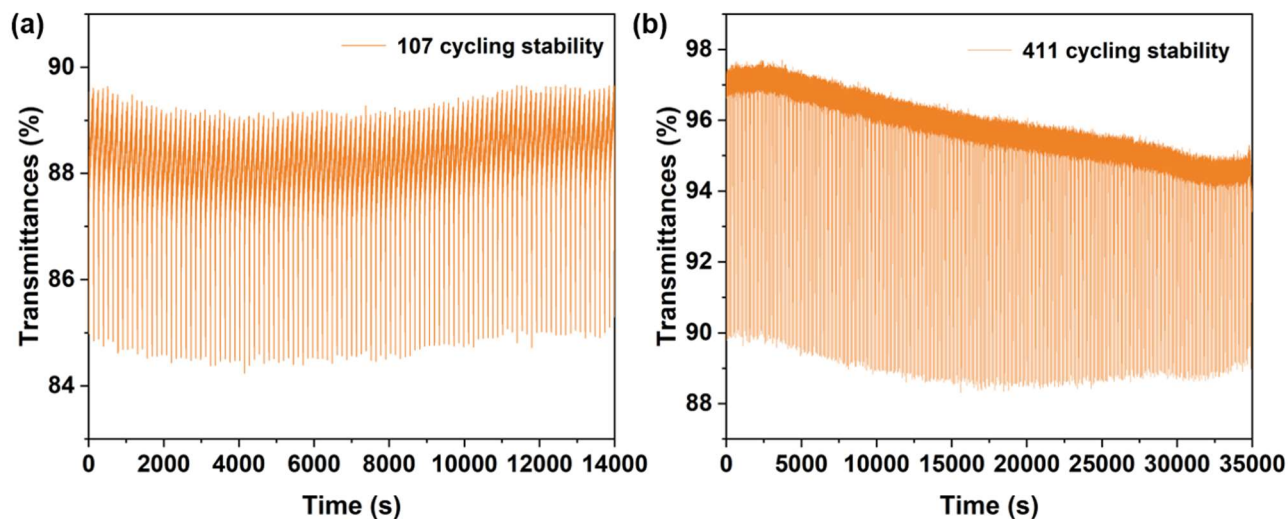
Figure S13. Optical stability test for ectrochromic switching of (a) **4**-based ECD and (b) **4** + FeCp$_2$-based ECD.

10. UV−Vis spectra of radical species and neutral species in DMF
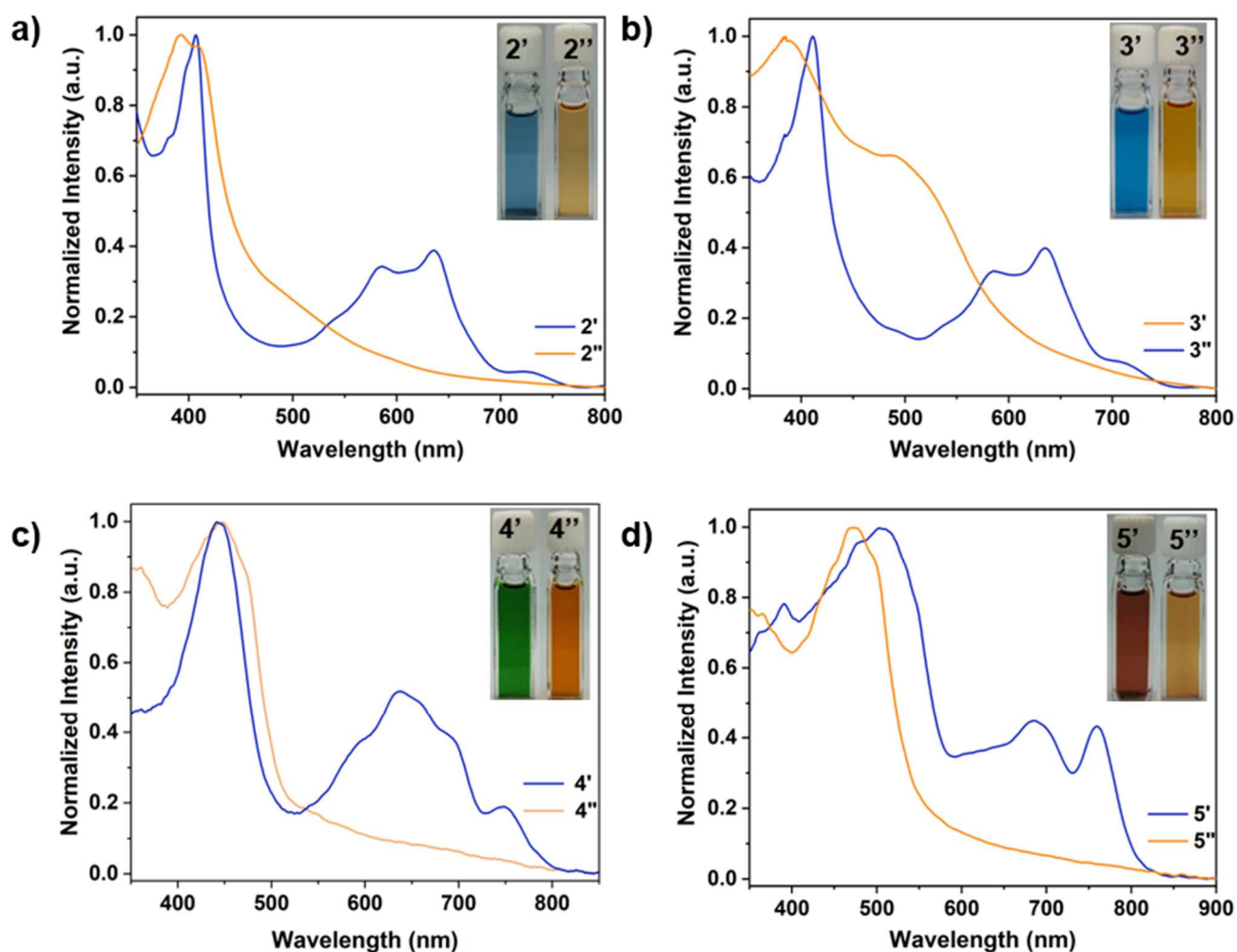
Figure S14. (a) UV−Vis spectra of **2** by chemical reduction with Zn (**2'**) and Na (**2"**), photographs are shown as the inset. (b) UV−Vis spectra of **3** by chemical reduction with Zn (**3'**) and Na (**3"**), photographs are shown as the inset. (c) UV−Vis spectra of **4** by chemical reduction with Zn (**4'**) and Na (**4"**), photographs are shown as the inset. (d) UV−Vis spectra of **5** by chemical reduction with Zn (**5'**) and Na (**5"**), photographs are shown as the inset.

11. EPR spectrum
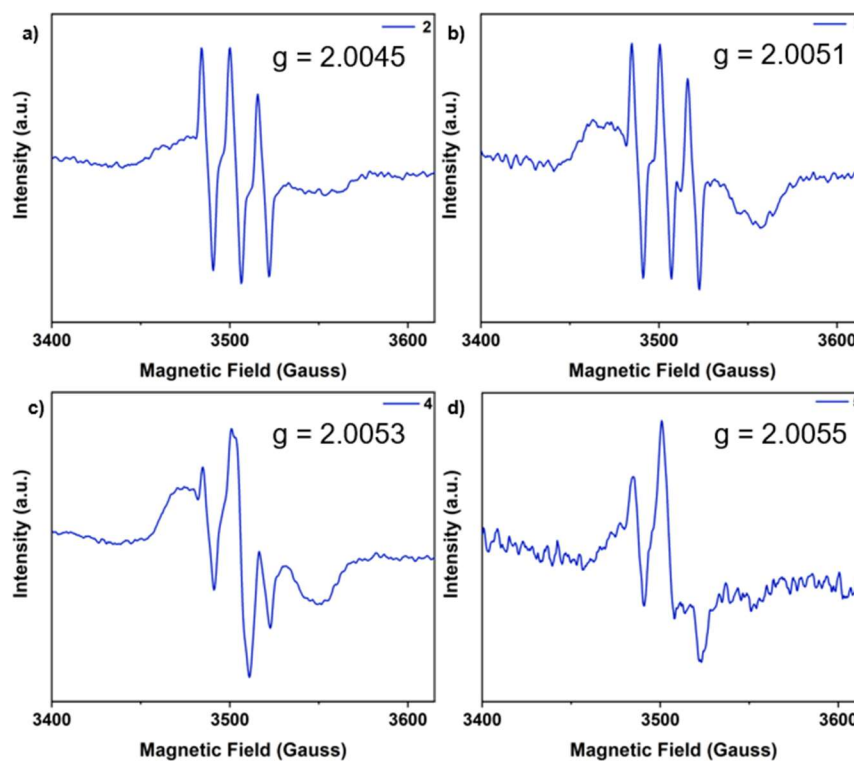
Figure S15. EPR spectrum of stiboviologens-based radicals by adding zinc powder at room temperature (c = 10^{-4} M) in *N,N*-dimethylformamide (DMF).
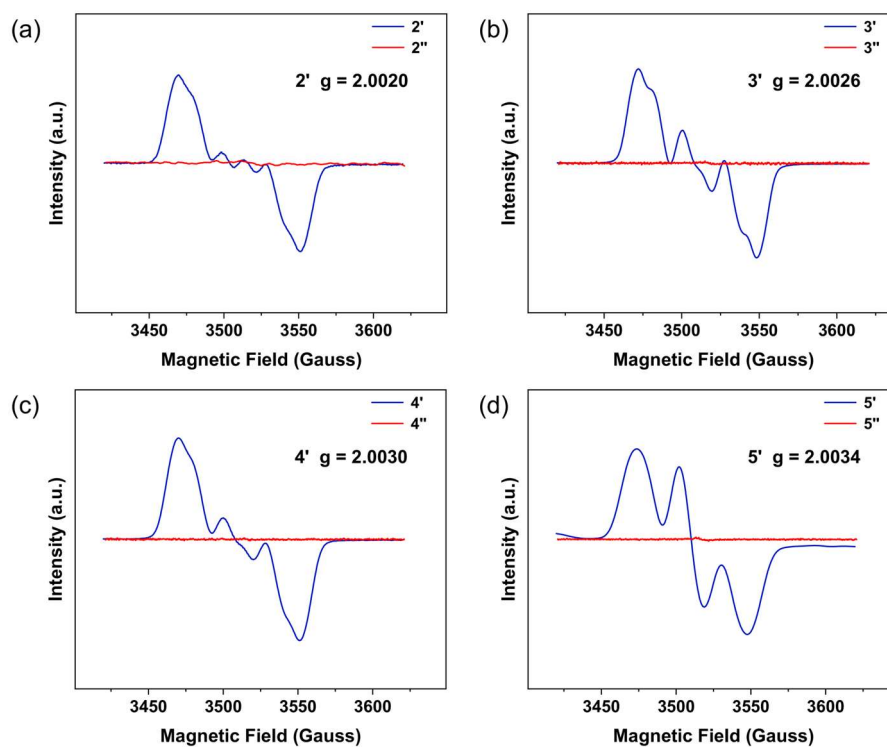
Figure S16. EPR spectrum of stiboviologens-based radicals by adding zinc powder and neutral species at room temperature by adding sodium (c = 10^{-3} M) in *N,N*-dimethylformamide (DMF).

12. Femtosecond transient absorption measurements

Femtosecond time-resolved measurements were done by means of transient absorption, and were performed using a commercial TA system (Time-Tech Spectra, LLC). Briefly, the output from a Light Conversion solid-state pump regeneration amplifier (100 kHz, λ = 1030 nm, fwhm 290 fs) was split into a pump and a probe part. Desired 370 nm and 410 nm pump wavelengths were obtained via a second harmonic generator (SHG) ORPHEUS-twins OPA (Light Conversion), and with neutral density filters the energy of each pulse was kept between ~500 nJ over ca. 3 mm2. The white light continuum probe was obtained by focusing part of the 1030 nm light on a sapphire plate. Polarization of the pump was set at magic angle, 54.7°, relative to the probe. Instrumental response time depends on pump and probe wavelengths, but is typically about 300 fs. All experiments were carried out at room temperature (i.e., T = 300 K).

Data analysis are done in TAS Analyzer (Time-Tech Spectra, Co., Ltd.), and graphed on Origin 2022, a robust trust-region reflective Newton nonlinear-least-squares method are used for the fits of time traces. Traces (ΔA vs. t) are fitted to two or three exponentials convolved with a Gaussian shaped response. Also included in the fits is an artifact signal that is due to cross phase modulation during pump and probe overlap. All spectra are corrected for chirp in the white light probe, time zero is set at maximum pump-probe temporal overlap.

Fit model: $y = C_0 + C_1 \cdot \exp(-x/t_1) + C_2 \cdot \exp(-x/t_2) + ... + C_n \cdot \exp(-x/t_n)$.
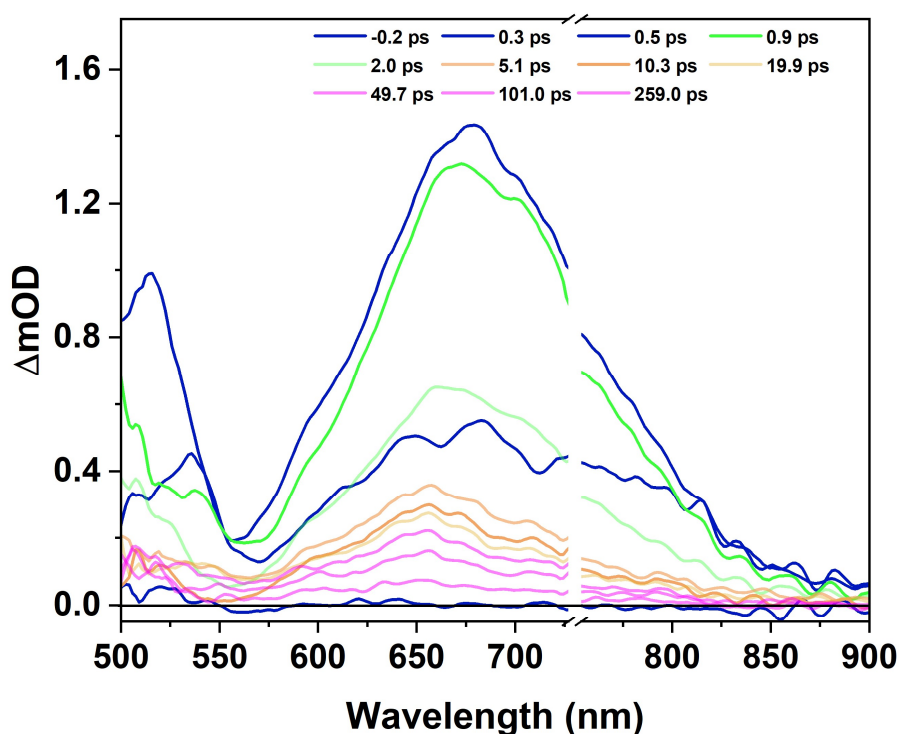
Figure S17. Transient absorption spectra **4** (0.5 M excited in 370 nm) in MeOH.
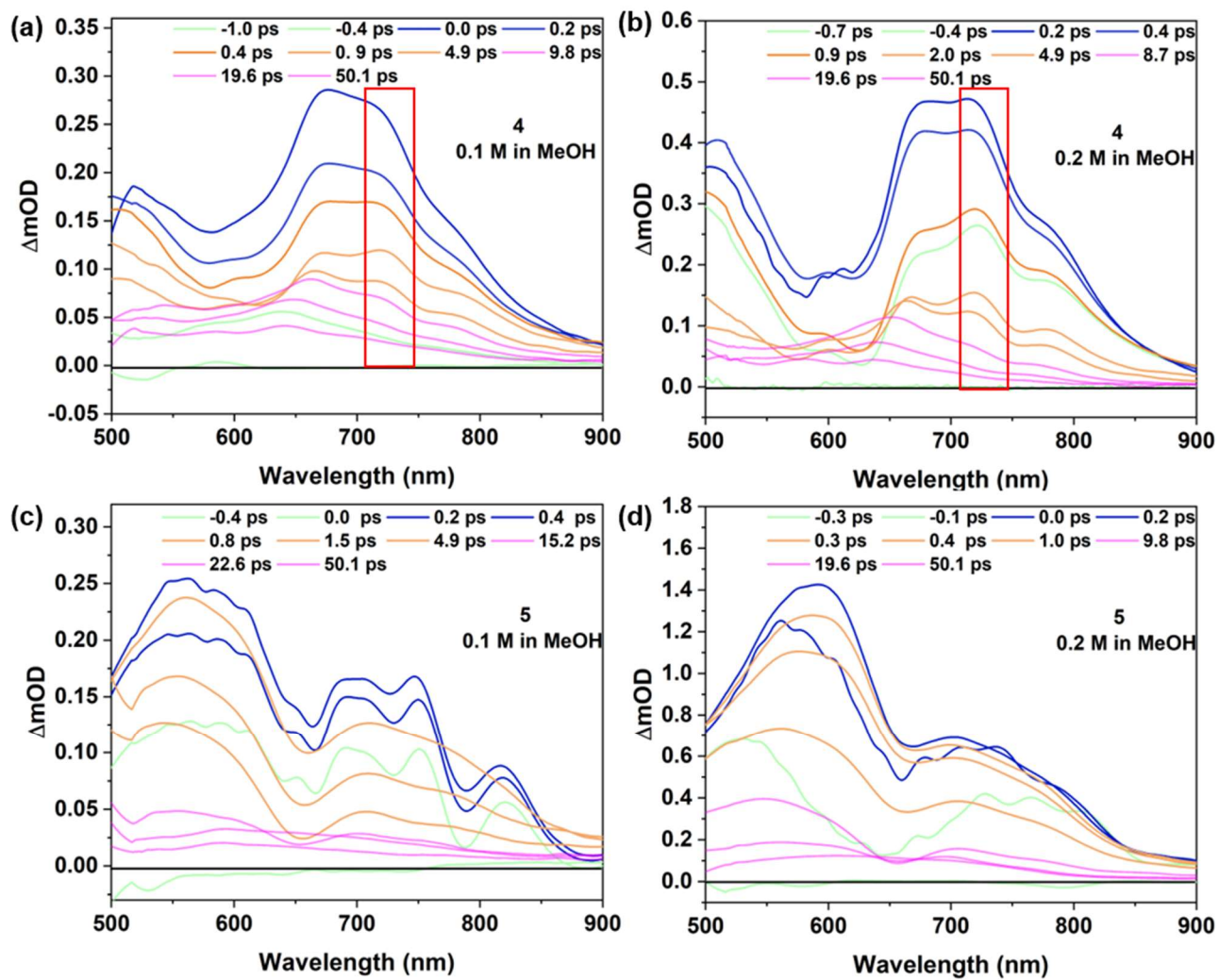
Figure S18. Transient absorption spectra **4** and **5** (0.1 M and 0.2 M excited in 410 nm) in MeOH.
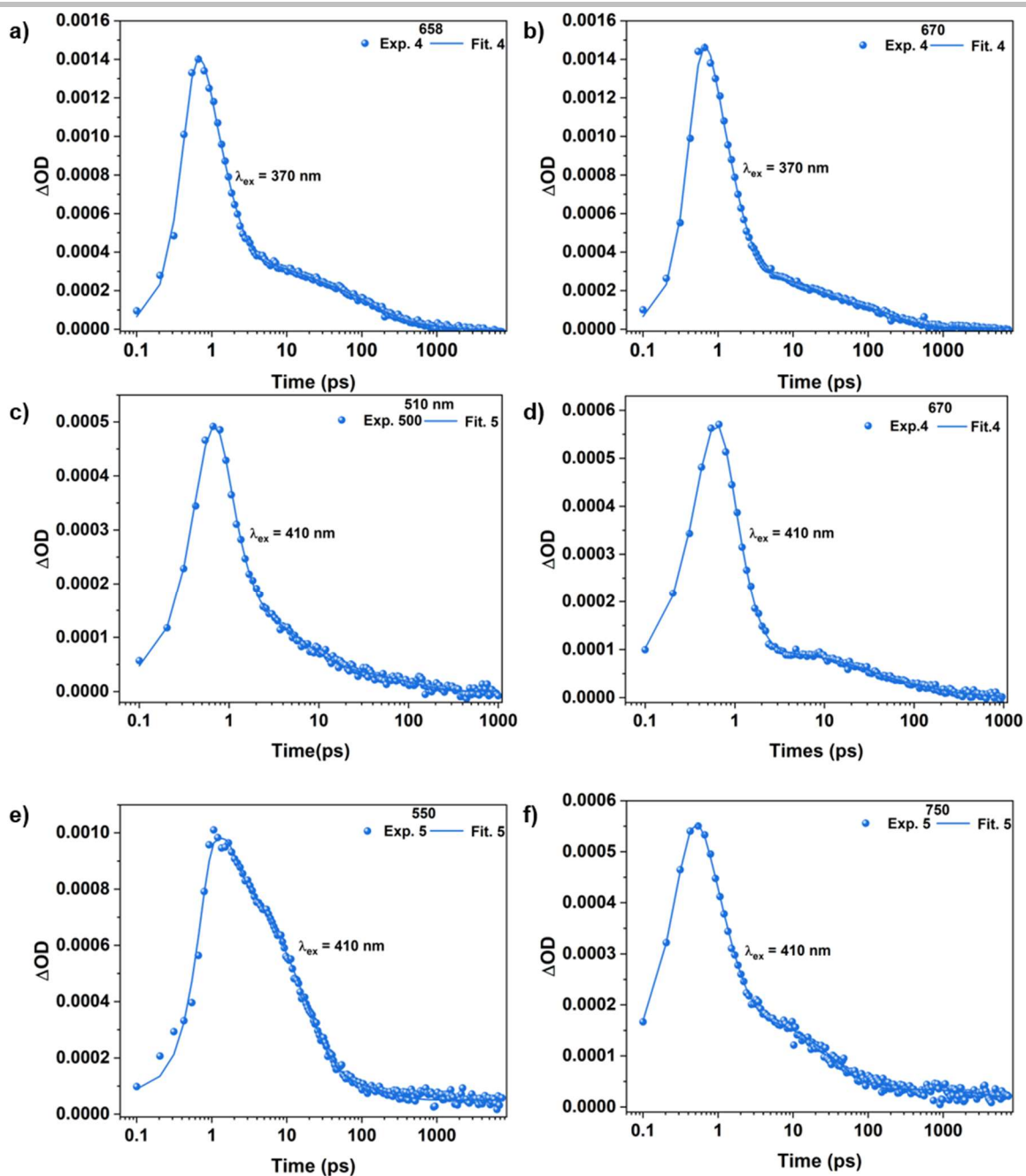
Figure S19. Decay curves in transient absorption of **4** at (a)-(b) 658 nm and 670 nm (λ_{ex} = 370 nm) , (c)-(d) 510 nm and 670 nm (λ_{ex} = 410 nm), and in transient absorption of **5** at (e)-(f) 550 nm and 750 nm (λ_{ex} = 410 nm).

Table S7. Time constants of multiple exponential fitting of femtosecond TA data of **4, 5** and **SeV^{2+}**,[9] with relative amplitudes given for a probe wavelength of 670 nm , 671 nm and 750 nm.

Compound	Wavelength	τ_1	A1	τ_2	A2	τ_3	A3
4 (370)	670	0.81	83%	16.2	7.5%	196	9.5%
4 (410)	670	0.83	92%	29.8	6%	156	2%
5 (410)	750	0.82	78%	33.5	21.5%	Inf	0.5%
SeV^{2+}	671	0.81	22%	233	74%	993	4%

13. Electrostatic potential surfaces of stiboviologens dications and radical species
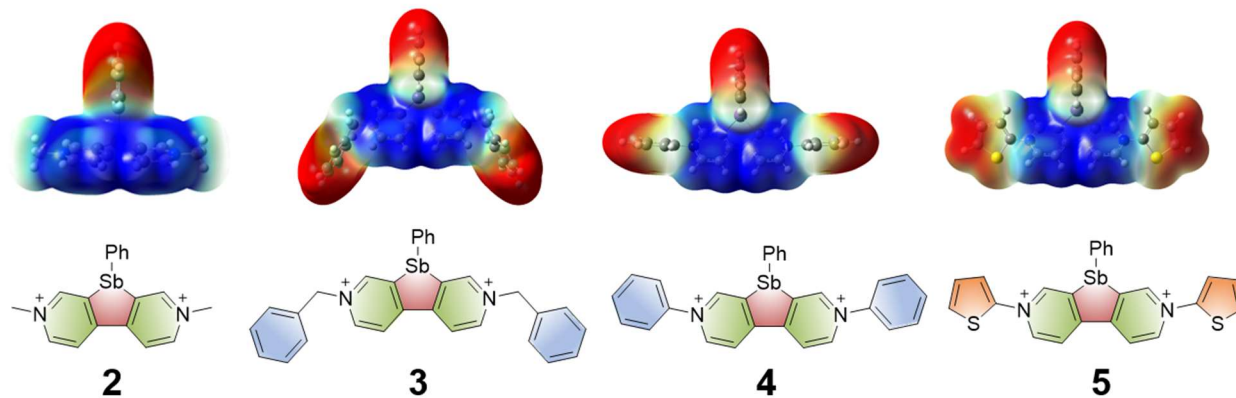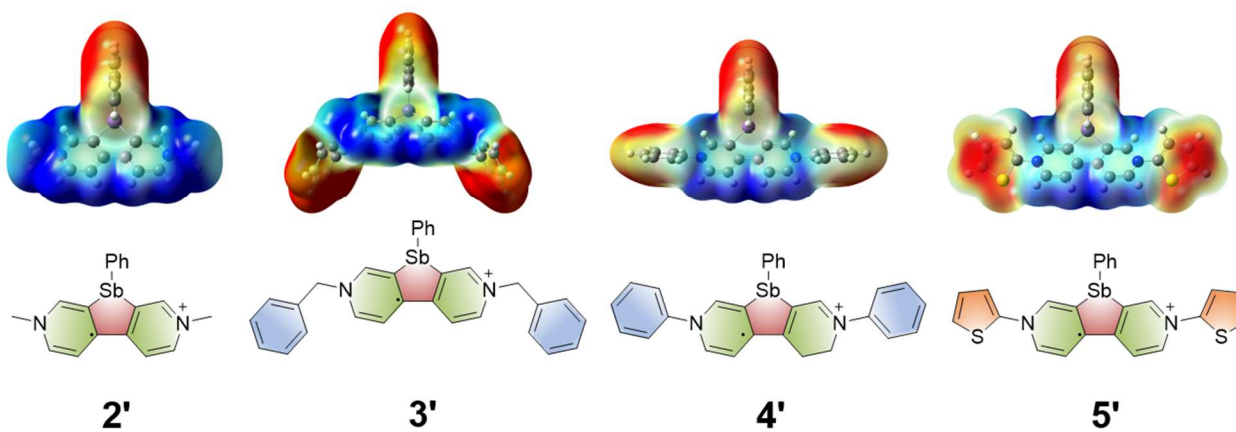
Figure S20. Electrostatic potential surfaces of stiboviologens dications and radical species.

14. DFT Calculations

2

LUMO + 1		- 2.36 eV
LUMO		- 3.79 eV
HOMO		- 7.24 eV
HOMO - 1		- 7.32 eV
HOMO - 2		- 7.53 eV
HOMO -3		- 8.67 eV

2'

LUMO + 1	
LUMO	
HOMO	
HOMO - 1	
α	β

2"

LUMO + 1		- 0.57 eV
LUMO		- 0.72 eV
HOMO		- 3.32 eV
HOMO - 1		- 6.29 eV

2

Ph
|
Sb

2 OTf⁻

2'

Ph
|
Sb

2 OTf⁻

2"

Ph
|
Sb

2 OTf⁻
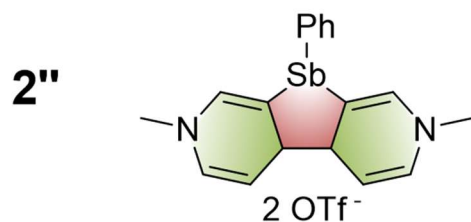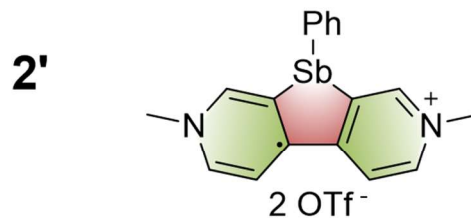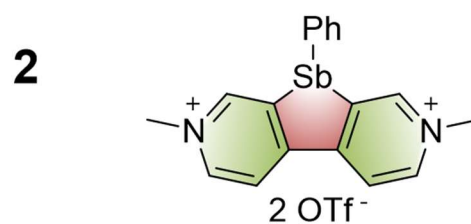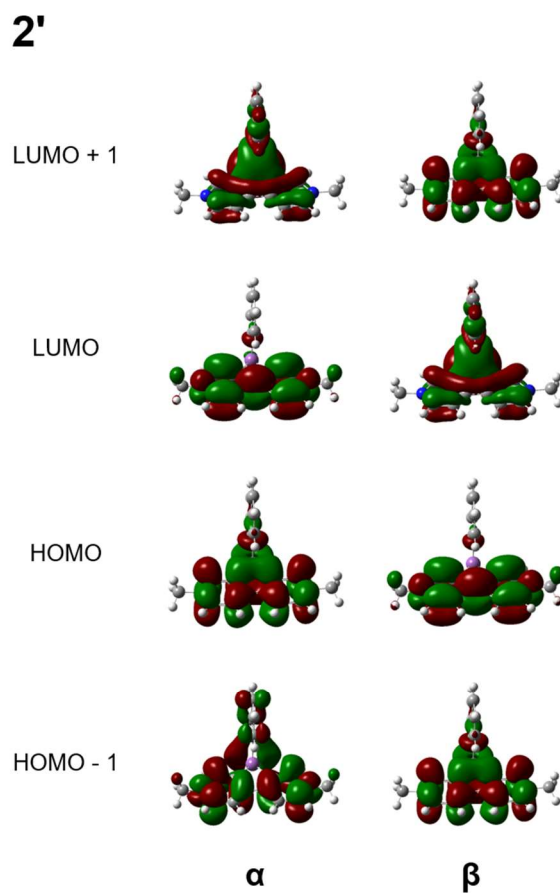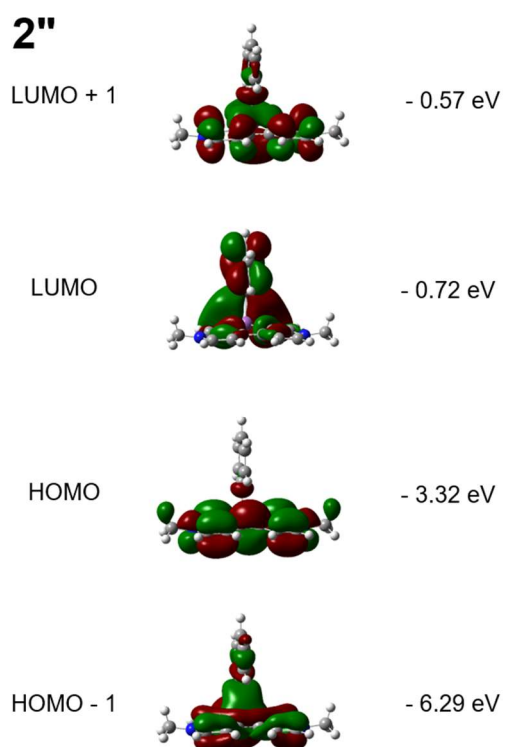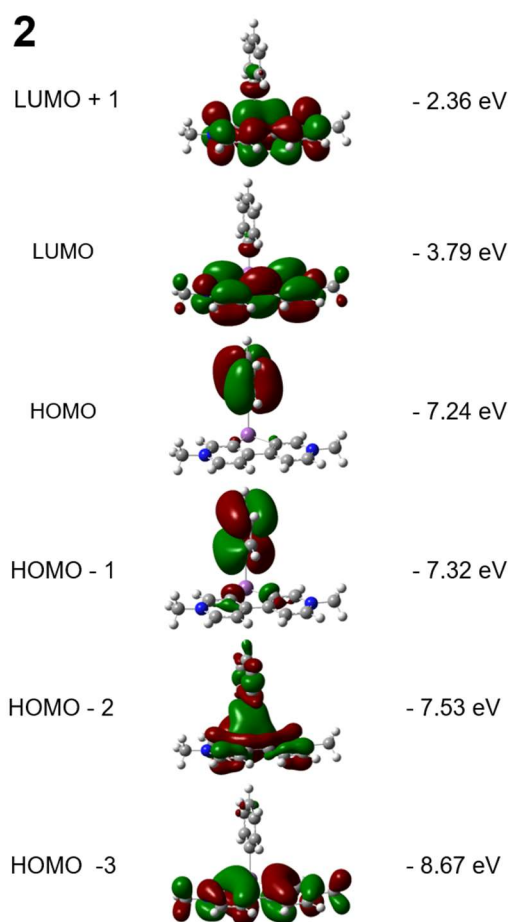
3
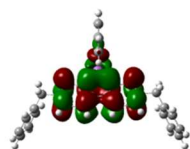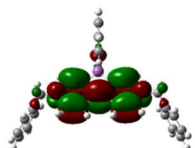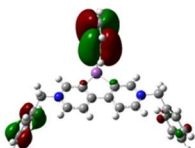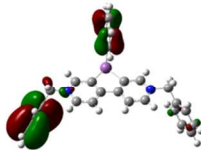
LUMO + 1		- 2.36 eV
LUMO		- 3.79 eV
HOMO		- 7.24 eV
HOMO - 1		- 7.25 eV
HOMO - 2		- 7.27 eV
HOMO - 3		- 7.30 eV

3'

	α	β
LUMO + 1		
LUMO		
HOMO		
HOMO - 1		
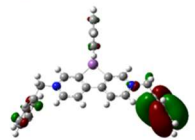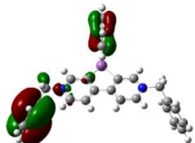
3"
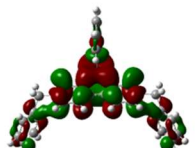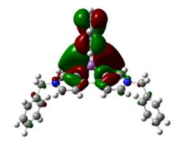
LUMO + 1		- 0.63 eV
LUMO		- 0.75 eV
HOMO		- 3.34 eV
HOMO - 1		- 6.27 eV

3

3'

3"
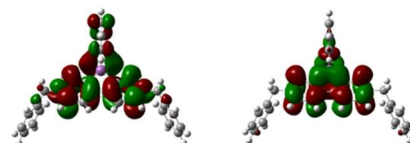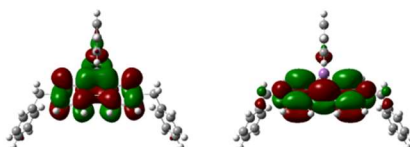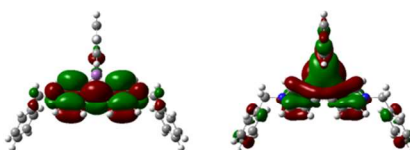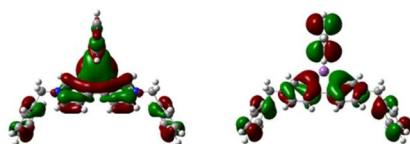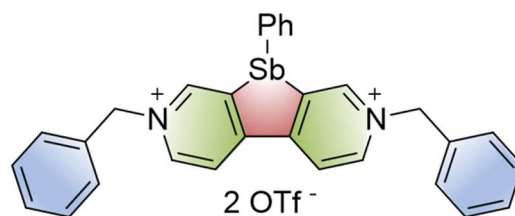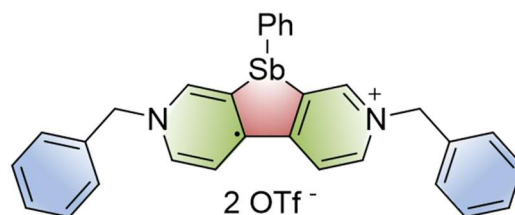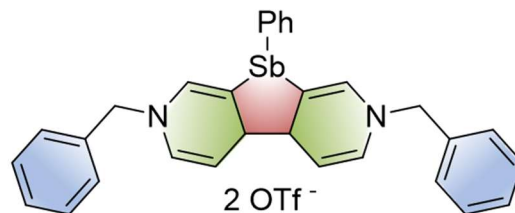
4

LUMO + 1		- 2.40 eV
LUMO		- 3.92 eV
HOMO		- 7.25 eV
HOMO - 1		- 7.32 eV
HOMO - 2		- 7.54 eV
HOMO -3		- 7.57 eV

4'

	α	β
LUMO + 1		
LUMO		
HOMO		
HOMO - 1		

4"

LUMO + 1		- 0.75 eV
LUMO		- 0.88 eV
HOMO		- 3.61 eV
HOMO - 1		- 6.10 eV

4

4'

4"
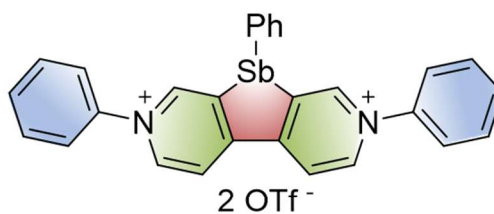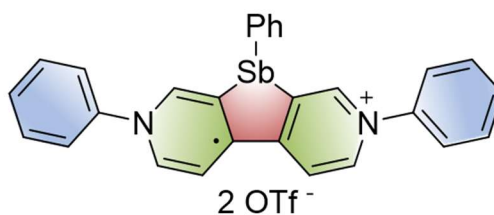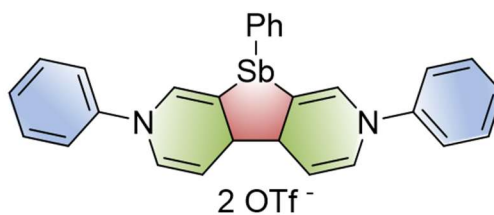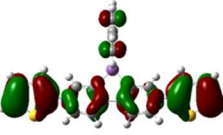
5

LUMO + 1   - 2.44 eV

LUMO   - 4.05 eV

HOMO   - 7.11 eV
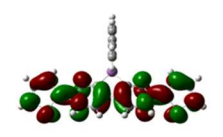
HOMO - 1   - 7.27 eV

HOMO - 2   - 7.32 eV

HOMO -3   - 7.35 eV

5'

LUMO + 1

LUMO

HOMO

HOMO - 1

α   β

5"

LUMO + 1   - 0.88 eV

LUMO   - 1.07 eV

HOMO   - 3.73 eV

HOMO - 1   - 5.85 eV

5
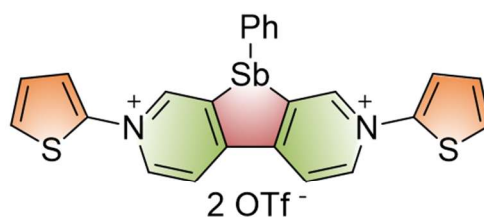
5'
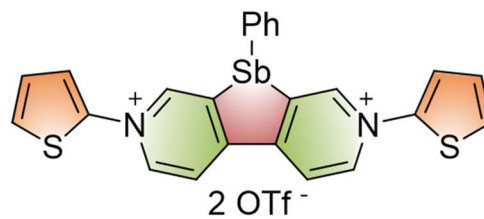
5"
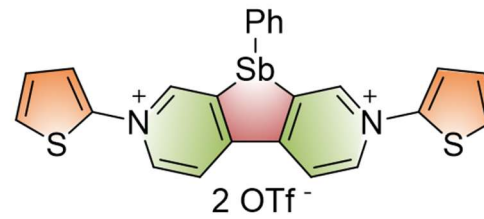
Figure S21. The calculated orbitals of **2, 2', 2", 3, 3', 3", 4, 4', 4", 5, 5', 5".**

15. Computed UV-vis spectra

The simulated UV–Vis spectra for optimized molecules were performed at the time dependent density functional theory (TD-DFT) at the ground-state equilibrium geometries in DMF solution, both low-lying singlet and triplet states were determined using the B3LYP, in association with the LANL08(d) basis set applied for the Sbe atom and 6-311G(d,p) basis set for all other atoms.

Table S8. Calculated (λ_{TD-DFT}) wavelengths (nm) of **2**. Molecular orbitals (MOs) involved in the main electronic transition, f corresponds to the oscillator strength.

λ_{TD-DFT}	MOs	Oscillator, Strength, f	
413.08	HOMO-2 -> LUMO	0.0861	77.6 %
	HOMO-1 -> LUMO		15.0 %
	HOMO -> LUMO		6.5 %
291.78	HOMO-3 -> LUMO	0.4317	90.8 %
	HOMO -> LUMO+1		2.8 %
282.42	HOMO-6 -> LUMO	0.2093	2.0 %
	HOMO-5 -> LUMO		86.9 %
	HOMO-2 -> LUMO+1		7.5 %
258.59	HOMO-7 -> LUMO	0.1385	36.2 %
	HOMO-2 -> LUMO+2		28.4 %
	HOMO-2 -> LUMO+3		26.0 %
	HOMO-2 -> LUMO+4		3.0 %

Table S9. Calculated (λ_{TD-DFT}) wavelengths (nm) of **3**. Molecular orbitals (MOs) involved in the main electronic transition, f corresponds to the oscillator strength.

λ_{TD-DFT}	Mos	Oscillator Strength, f	
417.14	HOMO-6 -> LUMO	0.0649	33.8 %
	HOMO-5 -> LUMO		3.8 %
	HOMO-4 -> LUMO		7.8 %
	HOMO-3 -> LUMO		11.2 %
	HOMO-2 -> LUMO		19.8 %
	HOMO-1 -> LUMO		22.3 %
291.47	HOMO-7 -> LUMO	0.5037	89.5 %
	HOMO-1 -> LUMO+1		2.9 %
283.02	HOMO-10 -> LUMO	0.1797	58.5 %
	HOMO-9 -> LUMO		12.4 %
	HOMO-7 -> LUMO+1		2.7 %
	HOMO-4 -> LUMO+1		2.5 %
	HOMO-2 -> LUMO+1		6.6 %
257.93	HOMO-12 -> LUMO	0.1075	25.1 %
	HOMO-7 -> LUMO+3		46.3 %
	HOMO-5 -> LUMO+3		48.6 %
	HOMO-4 -> LUMO+3		3.5 %
	HOMO-3 -> LUMO+3		6.0 %
	HOMO-2 -> LUMO+3		3.4 %

Table S10. Calculated (λ_{TD-DFT}) wavelengths (nm) of **4**. Molecular orbitals (MOs) involved in the main electronic transition, f corresponds to the oscillator strength.

λ_{TD-DFT}	Mos	Oscillator Strength, f	
428.23	HOMO-2-> LUMO	0.0589	70.5 %
	HOMO-1-> LUMO		26.0 %
	HOMO-> LUMO		2.4 %
297.61	HOMO-3-> LUMO	0.7168	98.9 %
285.91	HOMO-8-> LUMO	0.2284	5.0 %
	HOMO-2-> LUMO+1		90.2 %
	HOMO-1> LUMO+1		2.2 %
278.77	HOMO-9-> LUMO	0.2789	80.6 %
	HOMO-3-> LUMO+1		9.5 %
	HOMO-2-> LUMO+3		4.5 %

Table S11. Calculated (λ_{TD-DFT}) wavelengths (nm) of **5**. Molecular orbitals (MOs) involved in the main electronic transition, f corresponds to the oscillator strength.

λ_{TD-DFT}	Mos	Oscillator Strength, f	
489.26	HOMO-> LUMO	0.8050	98.7 %
454.36	HOMO-4-> LUMO	0.0511	23.9 %
	HOMO-2-> LUMO		75.0 %
285.23	HOMO-10-> LUMO	0.1999	4.1 %
	HOMO-8-> LUMO		8.0 %
	HOMO-4-> LUMO+1		77.8 %
	HOMO-2-> LUMO+1		5.5 %
277.92	HOMO-6-> LUMO	0.4826	35.6 %
	HOMO-4-> LUMO		2.2 %
	HOMO-2-> LUMO+2		56.1 %
	HOMO-> LUMO+1		2.2 %
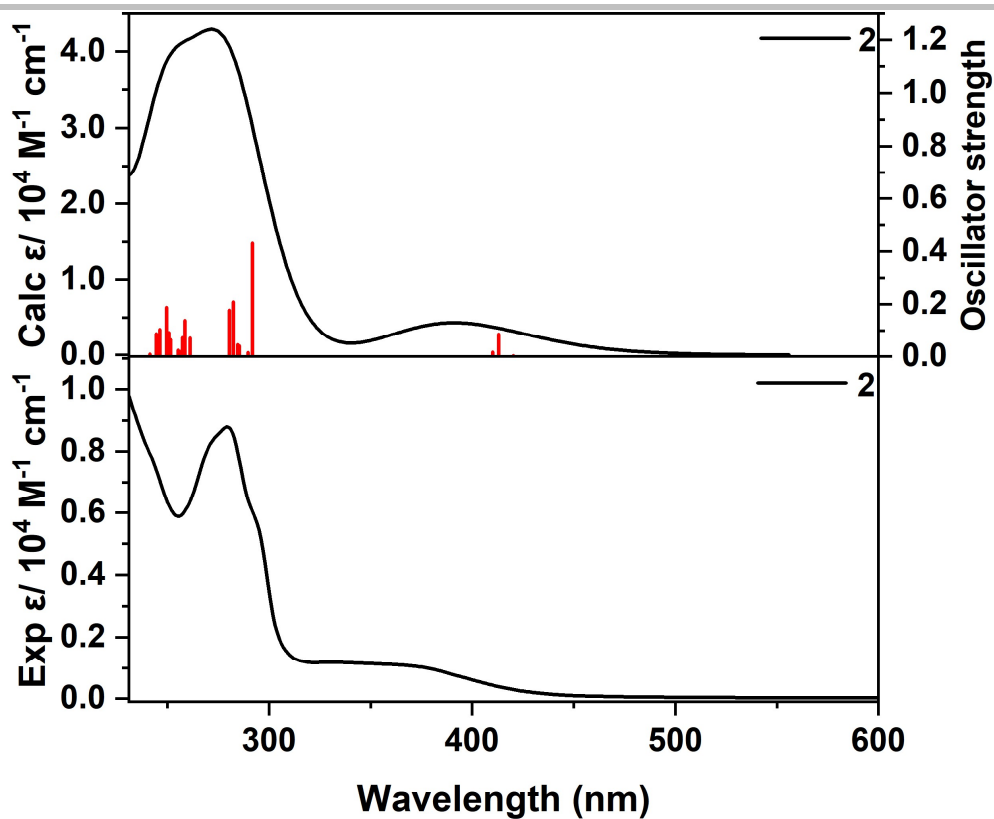
Figure S22. Computed UV/Vis absorbance spectrum at the TD-B3LYP/6-311G(d,p) [LANL08(d) for Sb] level of theory in DMF, and experimental UV-vis spectra in DMF of **2**.
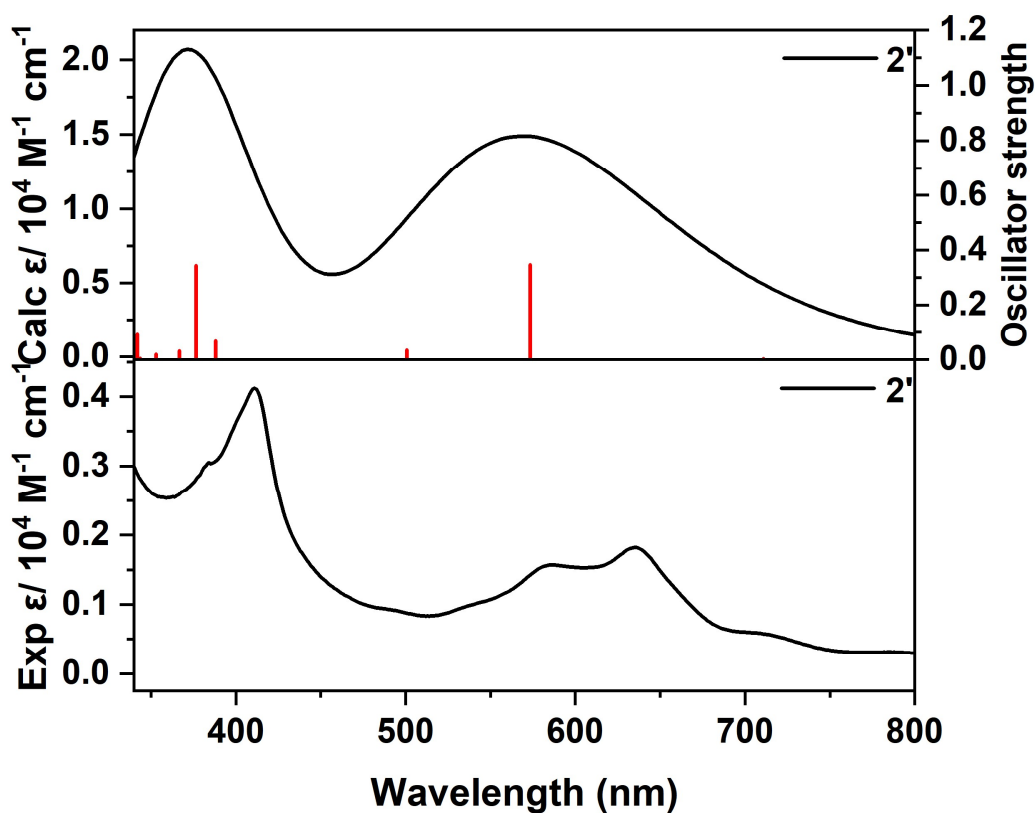
Figure S23. Computed UV/Vis absorbance spectrum at the TD-B3LYP/6-311G(d,p) [LANL08(d) for Sb] level of theory in DMF, and experimental UV-vis spectra in DMF of **2'**.
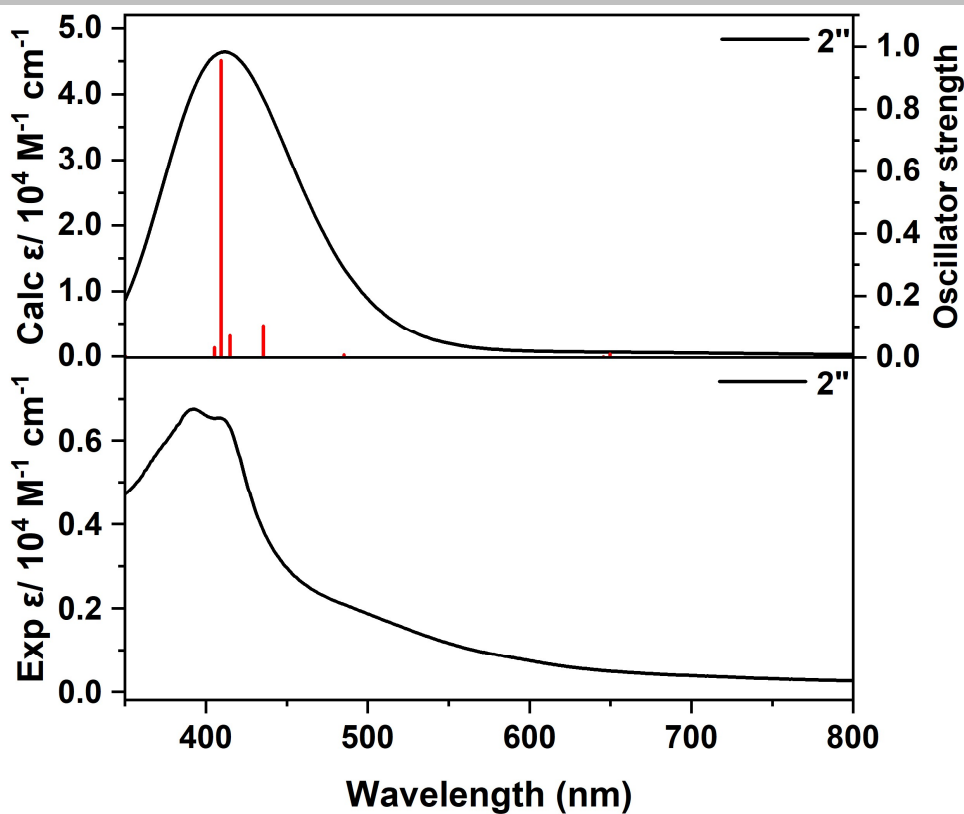
Figure S24. Computed UV/Vis absorbance spectrum at the TD-B3LYP/6-311G(d,p) [LANL08(d) for Sb] level of theory in DMF, and experimental UV-vis spectra in DMF of **2"**.
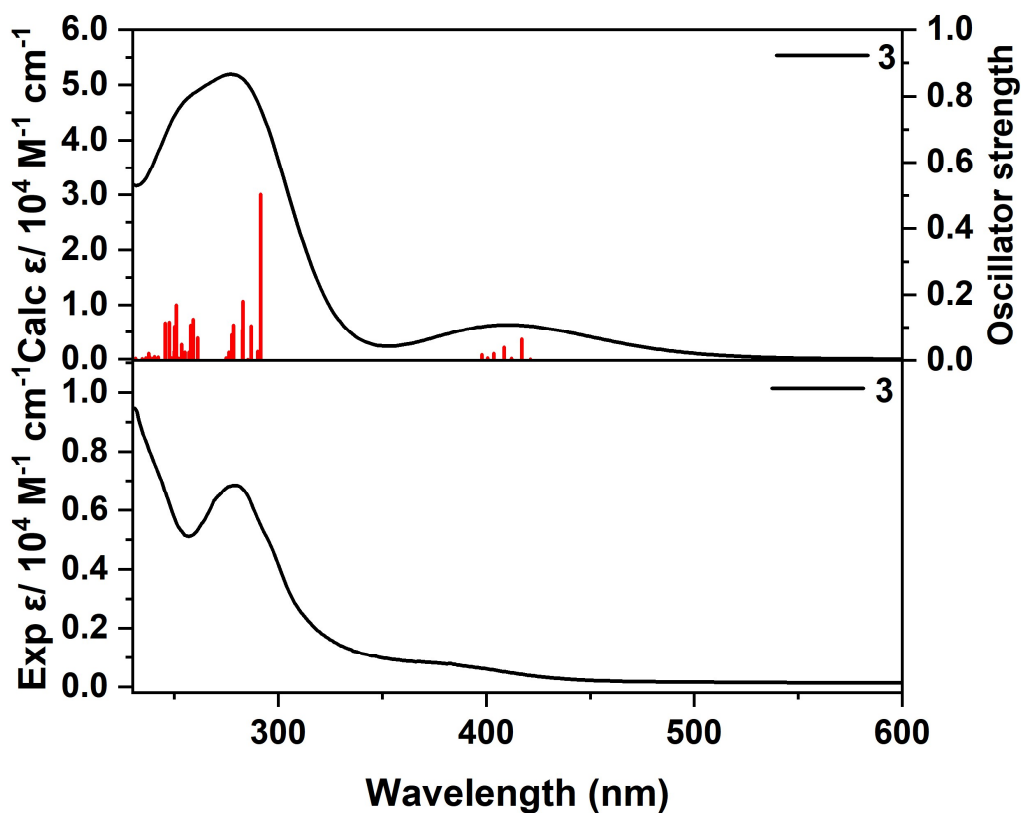
Figure S25. Computed UV/Vis absorbance spectrum at the TD-B3LYP/6-311G(d,p) [LANL08(d) for Sb] level of theory in DMF, and experimental UV-vis spectra in DMF of **3**.
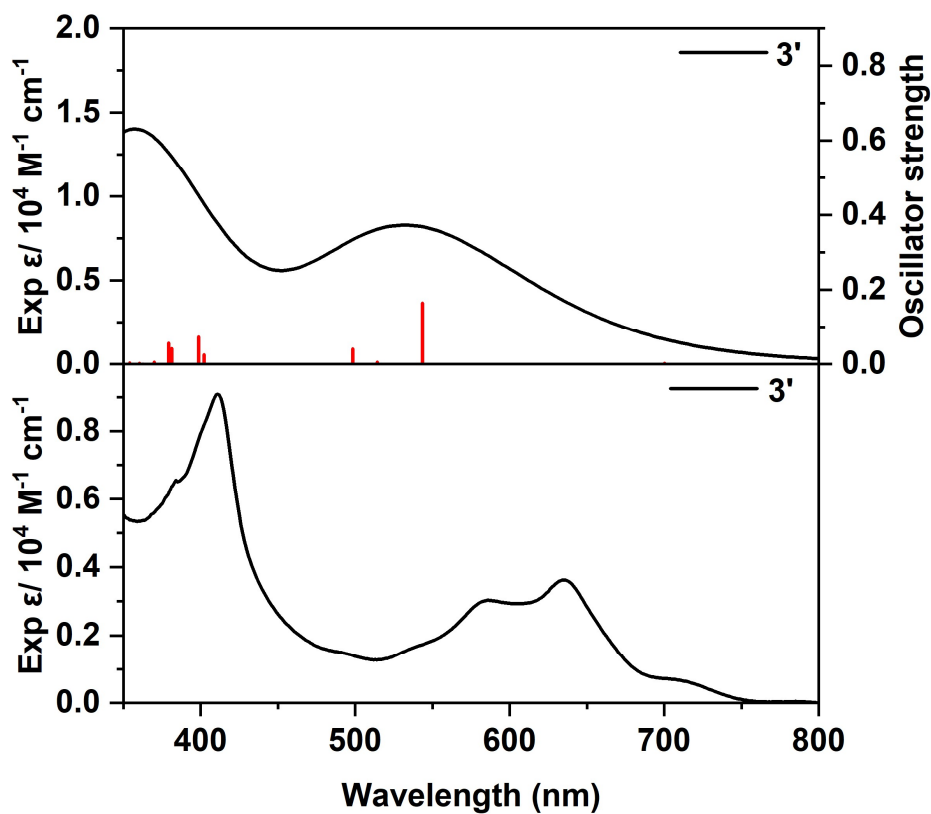
Figure S26. Computed UV/Vis absorbance spectrum at the TD-B3LYP/6-311G(d,p) [LANL08(d) for Sb] level of theory in DMF, and experimental UV-vis spectra in DMF of **3'**.
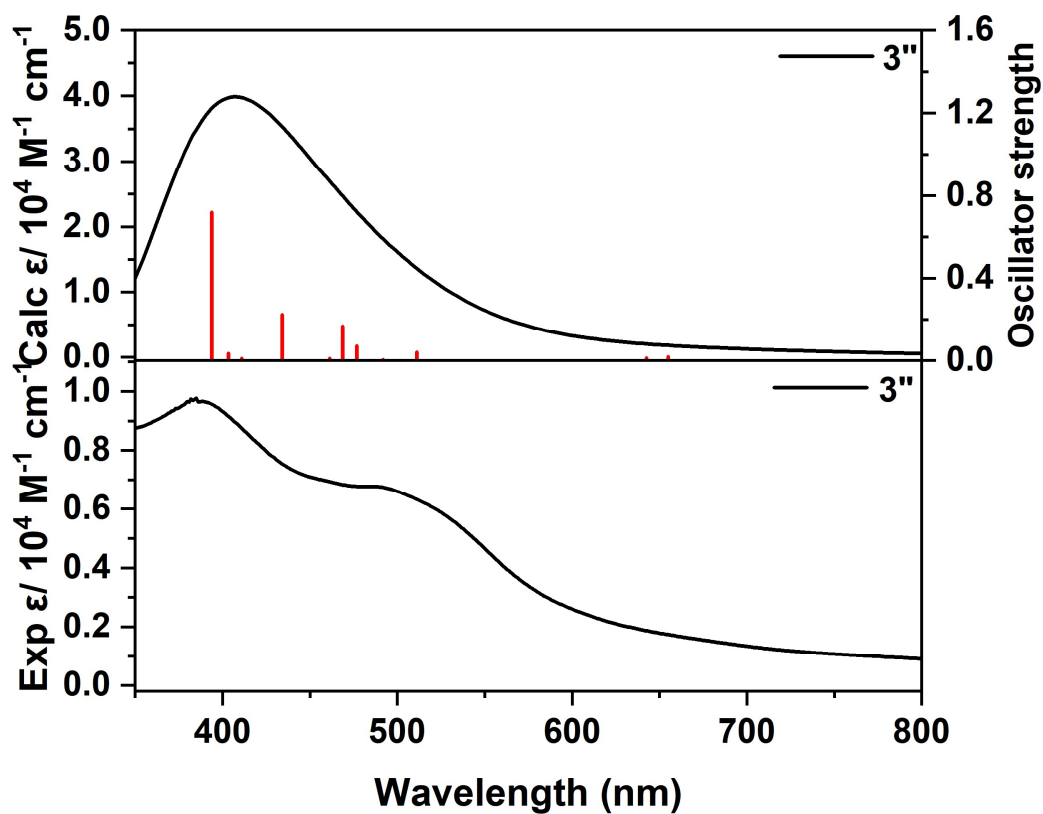
Figure S27. Computed UV/Vis absorbance spectrum at the TD-B3LYP/6-311G(d,p) [LANL08(d) for Sb] level of theory in DMF, and experimental UV-vis spectra in DMF of **3"**.
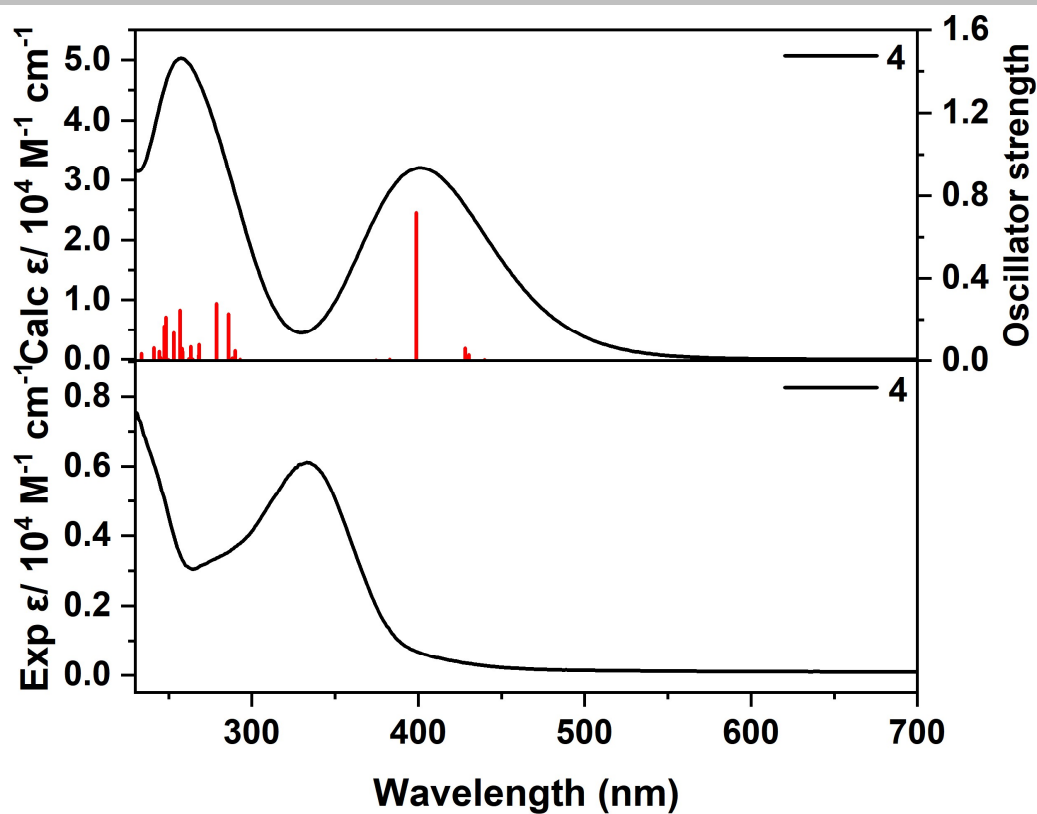
Figure S28. Computed UV/Vis absorbance spectrum at the TD-B3LYP/6-311G(d,p) [LANL08(d) for Sb] level of theory in DMF, and experimental UV-vis spectra in DMF of **4**.
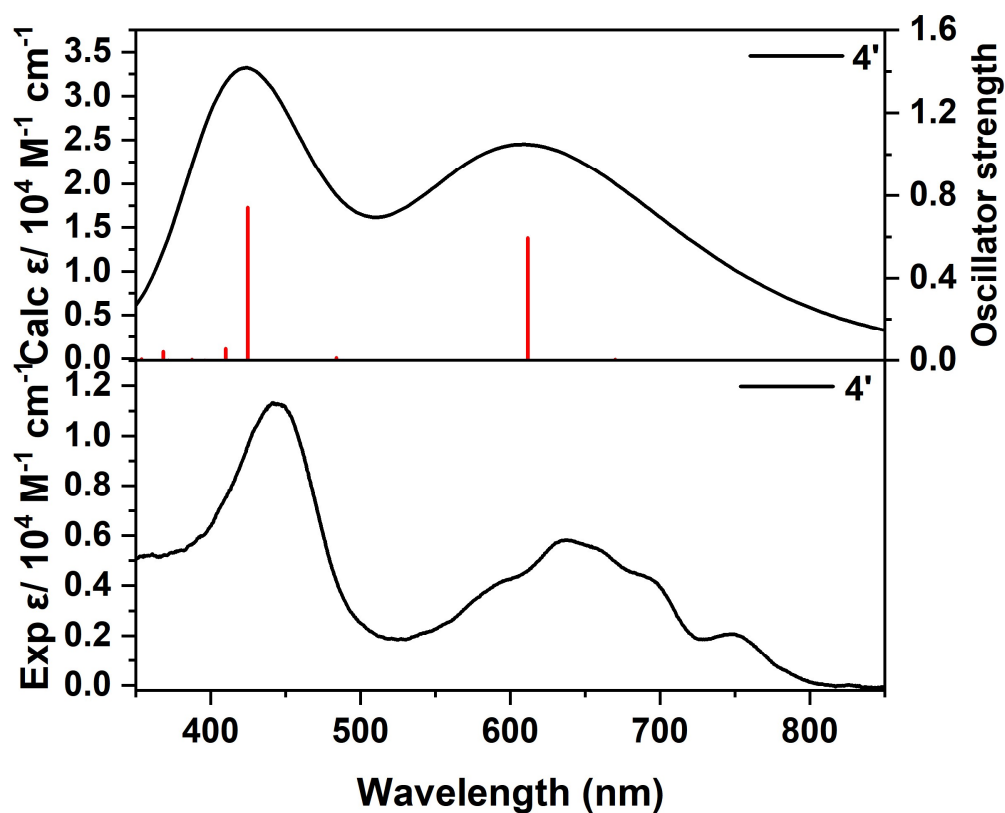
Figure S29. Computed UV/Vis absorbance spectrum at the TD-B3LYP/6-311G(d,p) [LANL08(d) for Sb] level of theory in DMF, and experimental UV-vis spectra in DMF of **4'**.
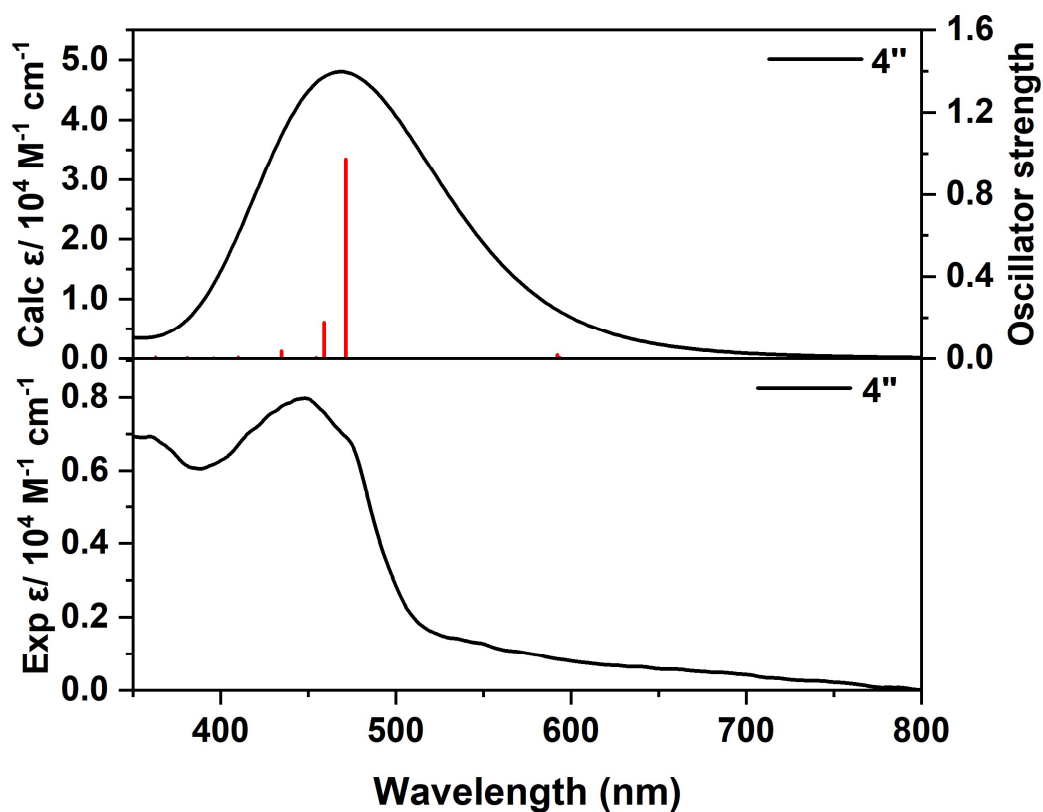
Figure S30. Computed UV/Vis absorbance spectrum at the TD-B3LYP/6-311G(d,p) [LANL08(d) for Sb] level of theory in DMF, and experimental UV-vis spectra in DMF of **4"**.
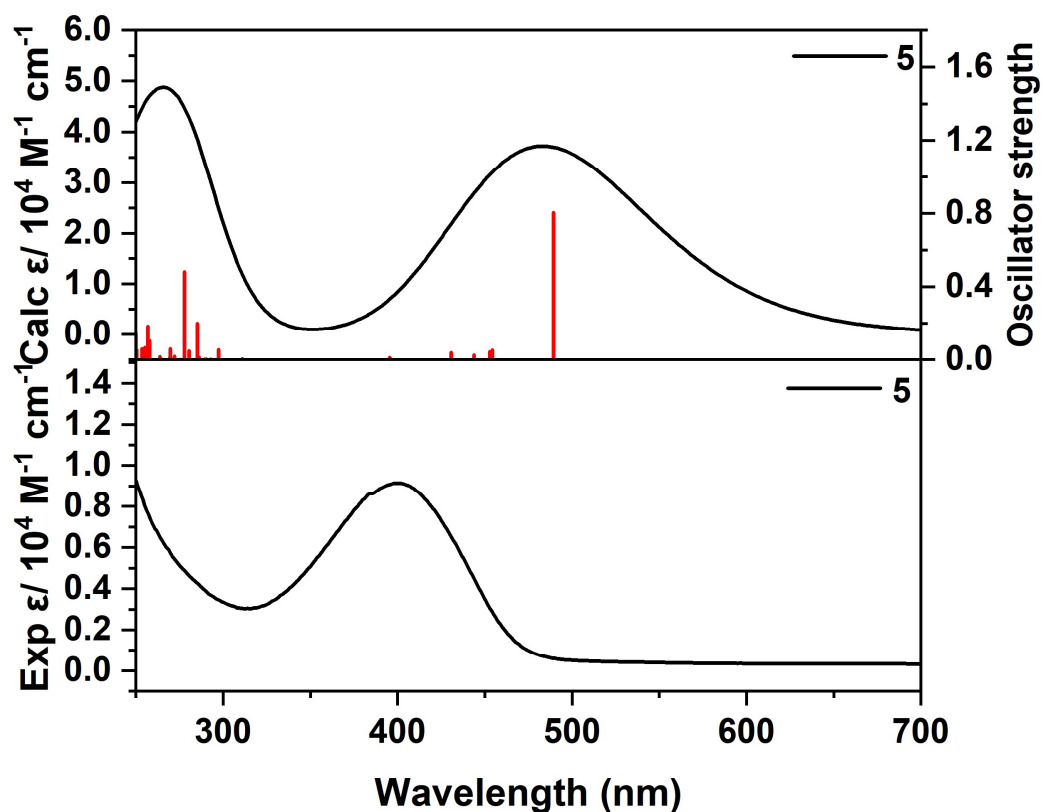
Figure S31. Computed UV/Vis absorbance spectrum at the TD-B3LYP/6-311G(d,p) [LANL08(d) for Sb] level of theory in DMF, and experimental UV-vis spectra in DMF of **5**.
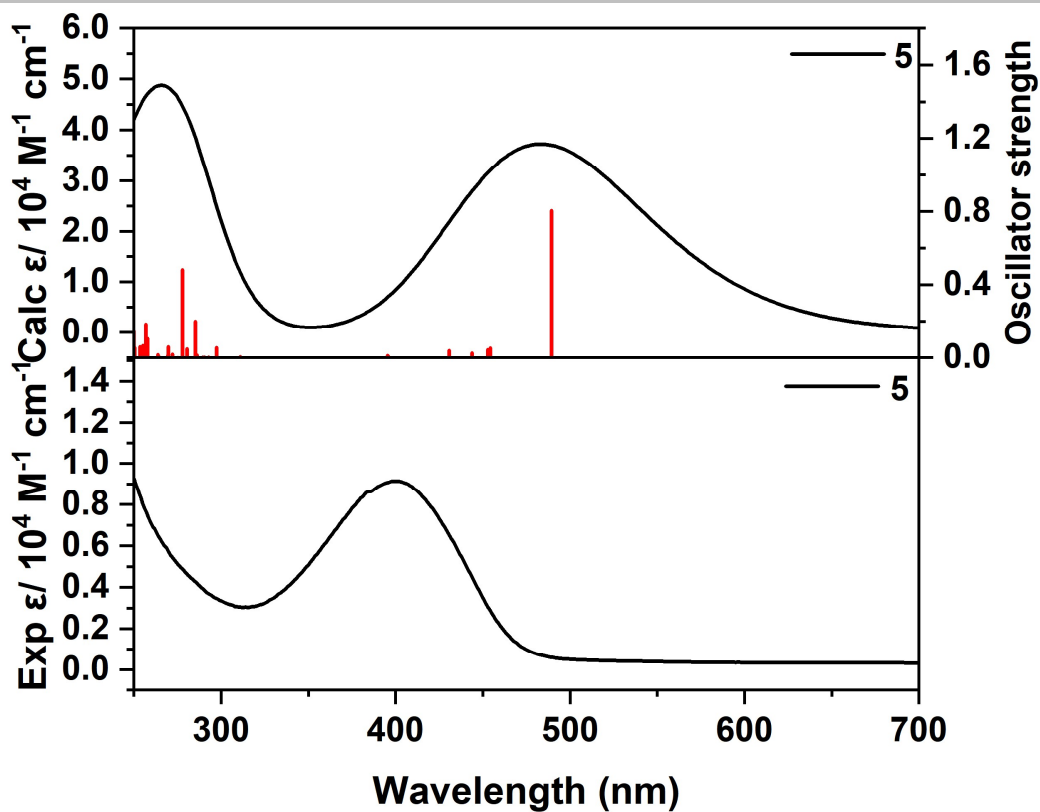
Figure S32. Computed UV/Vis absorbance spectrum at the TD-B3LYP/6-311G(d,p) [LANL08(d) for Sb] level of theory in DMF, and experimental UV-vis spectra in DMF of **5'**.
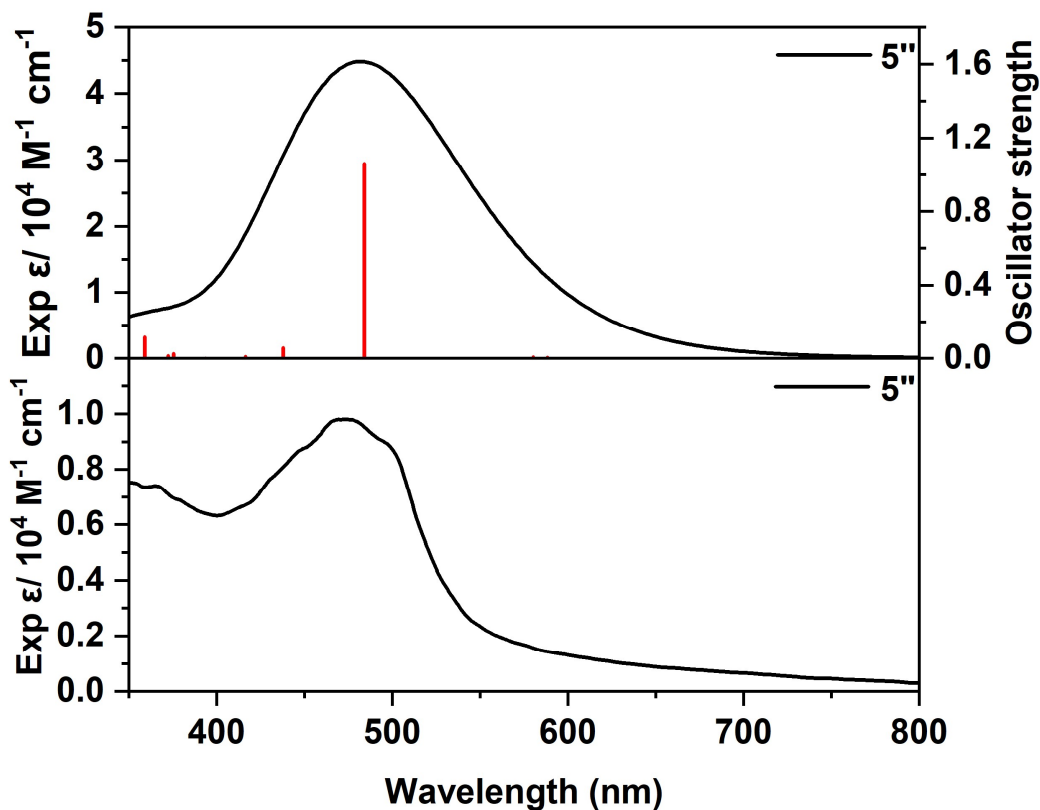
Figure S33. Computed UV/Vis absorbance spectrum at the TD-B3LYP/6-311G(d,p) [LANL08(d) for Sb] level of theory in DMF, and experimental UV-vis spectra in DMF of **5''**.

16. Calculated spin density plots for the radical species
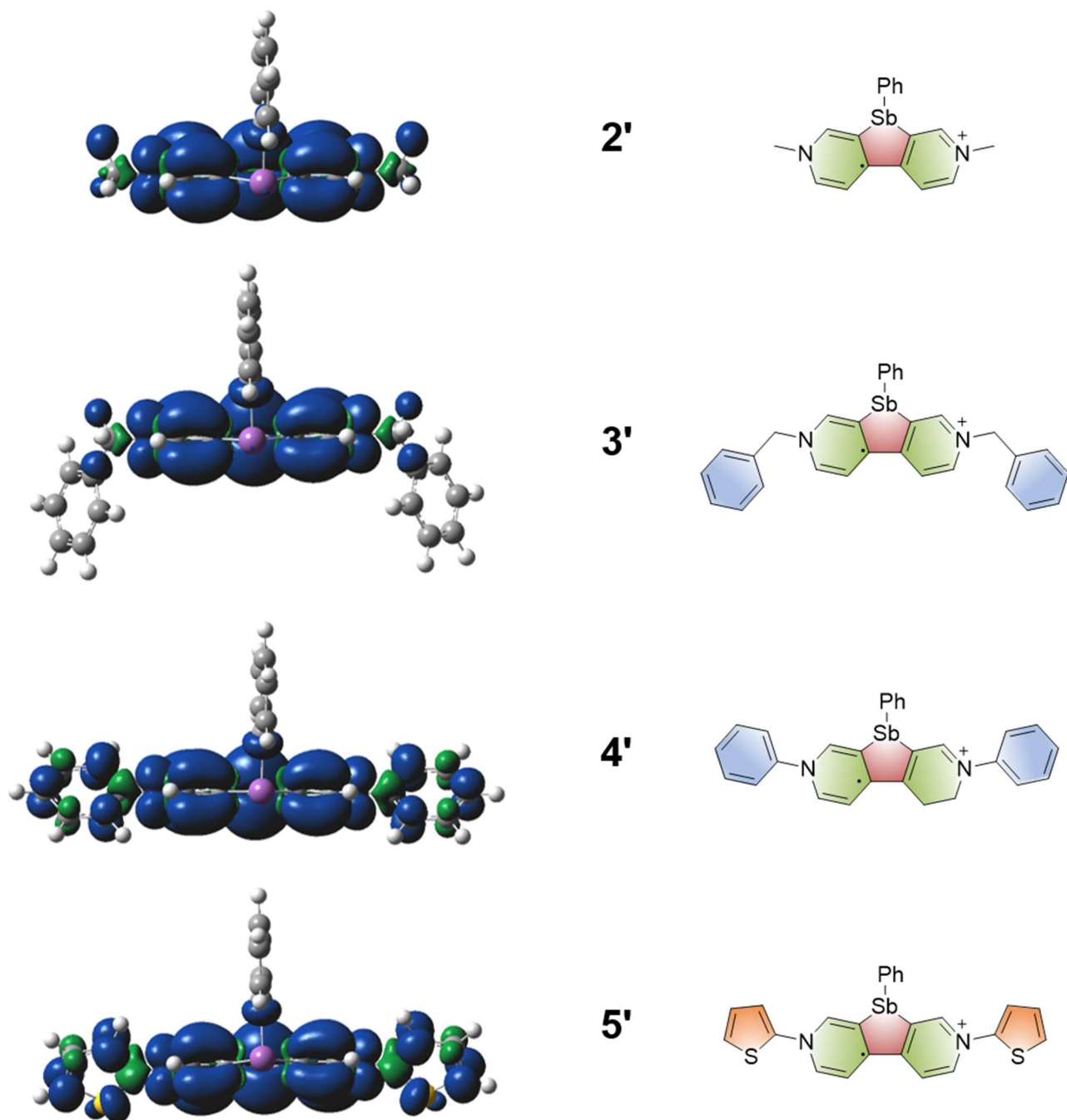
Figure S34. The calculated spin density plots for the radical species.

17. Mulliken charge distribution

Color Range: -0.735 to 0.735

Color Range: -0.603 to 0.603

Color Range: -0.455 to 0.455

2 (Sb: 0.735, N: -0.319)

2 (Sb: 0.603, N: -0.347)

2 (Sb: 0.455, N: -0.379)

Color Range: -0.731 to 0.731

Color Range: -0.603 to 0.603

Color Range: -0.457 to 0.457

3 (Sb: 0.731, N: -0.316)

3 (Sb: 0.603, N: -0.344)

3 (Sb: 0.457, N: -0.373)

Color Range: -0.737 to 0.737

Color Range: -0.618 to 0.618

Color Range: -0.497 to 0.497

4 (Sb: 0.737, N: -0.390)

4 (Sb: 0.618, N: -0.419)

4 (Sb: 0.497, N: -0.472)

Color Range: -0.734 to 0.734

Color Range: -0.629 to 0.629

Color Range: -0.514 to 0.514

5 (Sb: 0.734, N: -0.356)

5 (Sb: 0.629, N: -0.396)

5 (Sb: 0.514, N: - 0.416)

Figure S35. The calculated Mulliken charge distribution for the stiboviologen and their radicals.

18. Natural bond orbital (NBO) charge distribution

Color Range: -1.416 to 1.416

2 (Sb: 1.416, N: -0.285)

Color Range: -1.320 to 1.320

2 (Sb: 1.320, N: -0.344)

Color Range: -1.218 to 1.218

2 (Sb: 1.218, N: -0.422)

Color Range: -1.415 to 1.415

3 (Sb: 1.415, N: -0.286)

Color Range: -1.322 to 1.322

3 (Sb: 1.322, N: -0.346)

Color Range: -1.223 to 1.223

3 (Sb: 1.223, N: -0.416)

Color Range: -1.417 to 1.417

4 (Sb: 1.417, N: -0.287)

Color Range: -1.331 to 1.331

4 (Sb: 1.331, N: -0.344)

Color Range: -1.235 to 1.235

4 (Sb: 1.235, N: -0.401)

Color Range: -1.423 to 1.423

5 (Sb: 1.423, N: -0.298)

Color Range: -1.340 to 1.340

5 (Sb: 1.340, N: -0.355)

Color Range: -1.244 to 1.244

5 (Sb: 1.244, N: -0.410)

Figure S36. The natural bond orbital (NBO) charge distribution of stiboviologen and their radicals.

19. Visible light-induced oxidative cyclization reaction - reaction 1

General porocedure oxidative cyclization reaction.

N,N-dimethylaniline (62.5 μL, 0.5 mmol), N-methylmaleimide (11.1 mg, 0.1mmol) and 3 (2 mmol %) were mixed in the 2 mL DMSO with magnetic stirring bar. The tube was irradiated by blue LEDs for 24 h. After cooling to ambient temperature, the aqueous layer was extracted in the mixture of water and ethyl acetate (8 mL × 3), and the combined organic layer was dried by MgSO$_4$. The solvent was removed by rotary evaporation and purified by column chromatography on silica gel using petroleum ether/ethyl acetate (15:1 → 8:1) as eluent.

Table S12. Oxidative cyclization reaction by visible light photocatalysis.
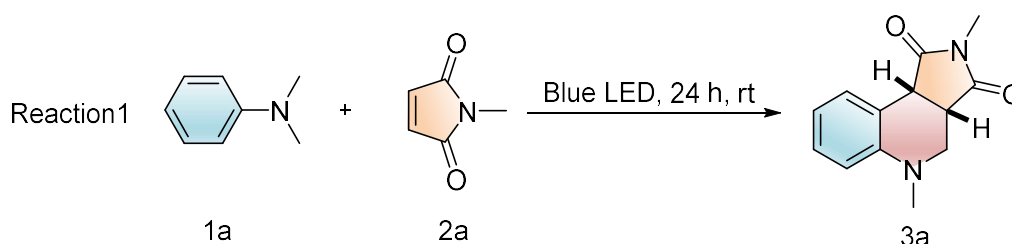
entry[a]	Catalyst	Solvent	Yield(%)[b]
1	4 (1 mol%)	MeOH	37
2	4 (1 mol%)	CH$_3$CN	47
3	4 (1 mol%)	DMF	70
4	4 (1 mol%)	DMSO	85
5	4 (2 mol%)	DMSO	87
5	2 (2 mol%)	DMSO	81
6	3 (2 mol%)	DMSO	83
7	5 (2 mol%)	DMSO	77
8	-	DMSO	n.r.
9	4 (2 mol%)	DMSO	76
10[c]	4 (2 mol%)	DMSO	n.r.
11[d]	4 (2 mol%)	DMSO	n.r.
12	MV^{2+} (2 mol%)	DMSO	48
13	PhV^{2+} (2 mol%)	DMSO	50
14	Se-PhV^{2+} (2 mol%)	DMSO	57
15	Te-PhV^{2+} (2 mol%)	DMSO	71
16	Bi-PhV^{2+} (2 mol%)	DMSO	77

[a]. Reaction conditions: 1a (0.5 mmol), 2a (0.1 mmol), blue light irradiationb [b] Isolated yield. The yields detected by ^{1}H NMR spectroscopy using mesitylene as an internal standard. [c]No air, under Ar [d] No light.

Substrate scope of General Procedure Oxidative Cyclization.

Dimethylaniline and maleimide Imide with different substituents were purchased from Energy Chemical Inc. The data of all the various substrates and corresponding products were all consistent with the previous report.[10]

2,5-Dimethyl-3a,4,5,9b-tetrahydro-1H-pyrrolo[3,4-c]quinoline-1,3(2H)-dione(3aa).
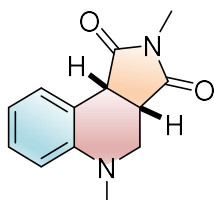
^{1}H NMR (400 MHz, CDCl$_3$) δ 7.48 (dt, J = 7.4, 1.1 Hz, 1H), 7.21 – 7.19 (m, 1H), 6.89 (td, J = 7.4, 1.1 Hz, 1H), 6.70 (dd, J = 8.2, 1.1 Hz, 1H), 4.01 (d, J = 9.4 Hz, 1H), 3.55-3.52 (m, 1H), 3.38-3.35 (m, 1H), 3.04 (dd, J = 11.5, 4.4 Hz, 1H), 2.99 (s, 3H), 2.79 (s, 3H); ^{13}C NMR (101 MHz, CDCl$_3$) δ 178.76 , 176.81 , 148.33 , 130.20 , 128.60 , 119.70 , 118.72 , 112.55 , 50.47 , 43.57 , 42.02 , 39.45 , 25.39.

5-Methyl-2-phenyl-3a,4,5,9b-tetrahydro-1H-pyrrolo[3,4-c]quinoline-1,3(2H)-dione(3ab).
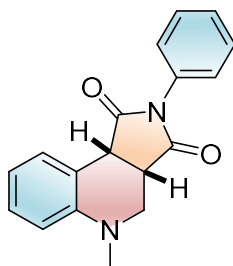
^{1}H NMR (400 MHz, CDCl$_3$) δ 7.54 (d, J = 7.5 Hz, 1H), 7.43 (t, J = 7.5 Hz, 2H), 7.36 (t, J = 7.5 Hz, 1H), 7.29-7.22 (m, 3H), 6.92 (t, J = 7.4 Hz, 1H), 6.76 (d, J = 8.2 Hz, 1H), 4.17 (d, J = 9.6 Hz, 1H), 3.62 (dd, J = 11.5, 2.8 Hz, 1H), 3.56 (s, 1H), 3.14 (dd, J = 11.5, 4.4 Hz, 1H), 2.85 (s, 3H); ^{13}C NMR (101 MHz, CDCl$_3$) δ 175.79 , 148.51 , 130.34 , 129.02 , 128.71 , 128.54 , 126.37 , 119.70 , 118.55 , 112.56 , 50.67 , 43.59 , 42.15 , 39.47.

2-(4-Methoxyphenyl)-5-methyl-3a,4,5,9b-tetrahydro-1*H*-pyrrolo- [3,4-*c*]quinoline-1,3(2*H*)-dione(3ac).
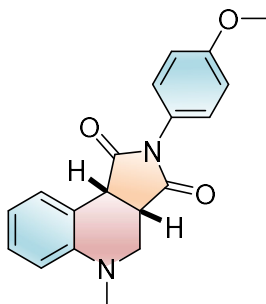
^{1}H NMR (400 MHz, CDCl$_3$) δ 7.53 (d, J = 7.6 Hz, 1H), 7.20 (dd, J = 20.5, 7.6 Hz, 3H), 6.94-6.89 (m, 3H), 6.75 (d, J = 8.2 Hz, 1H), 4.15 (d, J = 9.6 Hz, 1H), 3.80 (s, 3H), 3.61 (dd, J = 11.6, 2.5 Hz, 1H), 3.53 (dd, J = 9.6, 4.0 Hz, 1H), 3.12 (dd, J = 11.5, 4.4 Hz, 1H), 2.84 (s, 3H); ^{13}C NMR (101 MHz, CDCl$_3$) δ 177.94 , 176.00 , 159.40 , 148.47 , 130.35 , 128.66 , 127.59 , 124.63 , 119.69 , 114.31 , 112.55 , 55.49 , 50.69 , 43.50 , 42.07 , 39.48.

8-Bromo-2,5-dimethyl-3a,4,5,9b-tetrahydro-1H-pyrrolo[3,4-c]quinoline-1,3(2H)-dione(3ad).
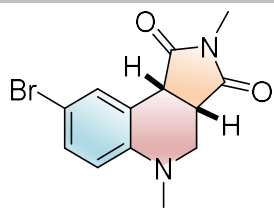
¹H NMR (400 MHz, CDCl₃) δ 7.59 (d, *J* = 2.4 Hz, 1H), 7.29 (d, *J* =8.7 Hz, 1H), 6.56 (d, *J* = 8.7 Hz, 1H), 3.95 (d, *J* = 9.4 Hz, 1H), 3.53 (dt, *J* = 11.7, 1.7 Hz, 1H), 3.38 – 3.35 (m, 1H), 3.04 – 3.00 (m, 4H), 2.78 (s, 3H); ¹³C NMR (101 MHz, CDCl₃) δ 178.30 , 176.13 , 147.41 , 132.59 , 131.34 , 120.55 , 114.17 , 111.68 , 50.24 , 43.34 , 41.69 , 39.44 , 25.48.

8-Bromo-5-methyl-2-phenyl-3a,4,5,9b-tetrahydro-1H-pyrrolo-[3,4-c]quinoline-1,3(2H)-dione(3ae).
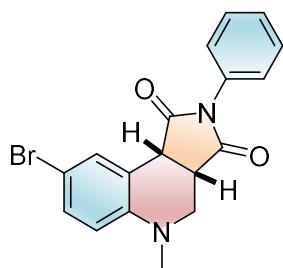
¹H NMR (400 MHz, CDCl₃) δ 7.65 (dd, *J* = 2.4, 0.8 Hz, 1H), 7.46-7.42 (m, 2H), 7.39-7.37 (m, 1H), 7.32 (dd, *J* = 8.7, 2.4 Hz, 1H), 7.28-7.25 (m, 2H), 6.61 (d, *J* = 8.7 Hz, 1H), 4.11 (d, *J* = 9.6 Hz, 1H), 3.61 (dd, *J* = 11.5, 2.8 Hz, 1H), 3.55-3.53 (m, 1H), 3.11 (dd, *J* = 11.5, 4.4 Hz, 1H), 2.82 (s, 3H); ¹³C NMR (101 MHz, CDCl₃) δ 177.24 , 175.12 , 147.49 , 132.73 , 131.47 , 129.07 , 128.66 , 126.30 , 120.35 , 114.23 , 111.71 , 77.23 , 50.38 , 43.30 , 417.

8-Bromo-2-(4-methoxyphenyl)-5-methyl-3a,4,5,9b-tetrahydro-1*H*-pyrrolo[3,4-c]quinoline-1,3(2*H*)-dione(3af).
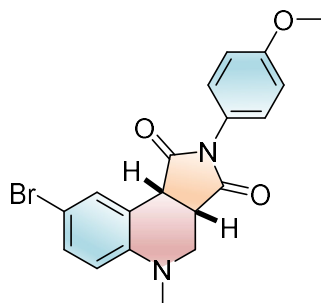
¹H NMR (400 MHz, CDCl₃) δ 7.64 (s, 1H), 7.31 (d, *J* = 8.9 Hz, 1H), 7.23-7.16 (m, 2H), 6.95-6.93 (m, 2H), 6.61 (d, *J* = 8.9 Hz, 1H), 4.09 (d, *J* = 9.5 Hz, 1H), 3.81 (d, *J* = 2.0 Hz, 3H), 3.60 (d, *J* = 11.6 Hz, 1H), 3.52 (d, *J* = 8.0 Hz , 1H), 3.13-3.09 (m, 1H), 2.82 (d, *J* = 1.9 Hz, 3H); ¹³C NMR (101 MHz, CDCl₃) δ 159.48 , 147.48 , 132.73 , 131.43 , 127.53 , 124.45 , 120.44 , 114.35 , 114.21 , 111.70 , 77.23 , 76.79 , 55.50 , 50.40 , 43.23 , 41.73 , 39.48.

2,5,8-Trimethyl-3a,4,5,9b-tetrahydro-1*H*-pyrrolo[3,4-*c*]quinoline-1,3(2*H*)-dione(3ag).
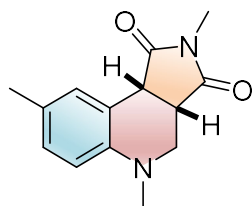
¹H NMR (400 MHz, CDCl₃) δ 7.29 (d, *J* = 2.1 Hz, 1H), 7.01 (dd, *J* = 8.4, 2.1 Hz, 1H), 6.61 (d, *J* = 8.2 Hz, 1H), 3.96 (d, *J* = 9.4 Hz, 1H), 3.51 (dd, *J* = 11.5, 2.3 Hz, 1H), 3.35 (dq, *J* = 7.2, 2.2 Hz, 1H), 2.99-2.95 (m, 4H), 2.76 (s, 3H), 2.30 (s, 3H);¹³C NMR (101 MHz, CDCl₃) δ 177.82 , 146.36 , 130.82 , 129.25 , 129.02 , 128.99 , 128.50 , 126.38 , 118.49 , 112.55 , 50.96 , 43.60 , 42.19 , 39.59 , 20.46.

5,8-Dimethyl-2-phenyl-3a,4,5,9b-tetrahydro-1*H*-pyrrolo[3,4-c]quinoline-1,3(2*H*)-dione(3ah).
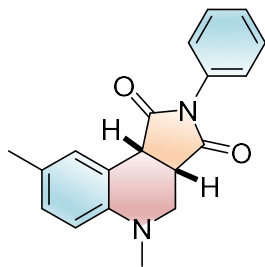
^{1}H NMR (400 MHz, CDCl$_3$) δ 7.45-7.41 (m, 2H), 7.38-7.35 (m, 2H), 7.28 (d, *J* = 1.6 Hz, 1H), 7.04 (dd, *J* = 8.3, 2.0 Hz, 1H), 6.65 (d, *J* = 8.3 Hz, 1H), 4.12 (d, *J* = 9.5 Hz, 1H), 3.57 (s, 1H), 3.54-3.51 (m, 1H), 3.06 (dd, *J* = 11.4, 4.3 Hz, 1H), 2.81 (s, 3H), 2.30 (s, 3H); ^{3}C NMR (101 MHz, CDCl$_3$) δ 177.82 , 146.36 , 130.82 , 129.25 , 129.02 , 128.99 , 128.50 , 126.38 , 118.49 , 112.55 , 50.96 , 43.60 , 42.19 , 39.59 , 20.46.

2-(4-Methoxyphenyl)-5,8-dimethyl-3a,4,5,9b-tetrahydro-1*H*-pyrrolo[3,4-c]quinoline-1,3(2*H*)-dione(3ai).
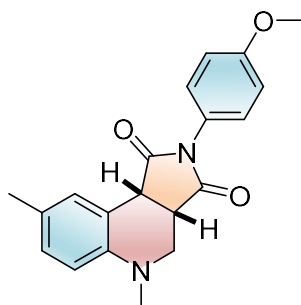
^{1}H NMR (400 MHz, CDCl$_3$) δ 7.34 (s, 1H), 7.19-7.16 (m, 2H), 7.04 (d, *J* = 8.3 Hz, 1H), 6.94-6.92 (m, 2H), 6.65 (d, *J* = 8.3 Hz, 1H), 4.10 (d, *J* = 9.6 Hz, 1H), 3.80 (d, *J* = 1.6 Hz, 3H), 3.57 (d, *J* = 6.7 Hz , 1H), 3.52-3.46 (m, 1H), 3.05 (dd, *J* = 11.5, 4.3 Hz, 1H), 2.80 (s, 3H), 2.30 (s, 3H). ^{13}C NMR (101 MHz, CDCl$_3$) δ 178.07 , 176.11 , 159.38 , 146.37 , 130.82 , 129.20 , 128.98 , 127.61 , 124.67 , 118.59 , 114.29 , 112.52 , 55.48 , 50.98 , 43.52 , 42.13 , 39.59 , 20.46.

20. Visible light-induced cross-dehydrogenative coupling - reaction 2

General Procedure Cross-Dehydrogenative Coupling Reaction.

N-phenyl-tetrahydroisoquinoline (**12**) (20.9 mg, 0.1 mmol),[11] nucleophile (1 mmol, 10 eq) and catalyst (the molar amount of the SbV^{2+} moiety is 2 mmol %) were mixed in the 2 mL solvent with magnetic stirring bar. The tube was irradiated by blue LED for about 24 h. After the solvent was removed by rotary evaporation and the crude products were purified by column chromatography on silica gel using petroleum ether/ethyl acetate (10:1) as eluent, the target products were obtained.

Table S13.Cross-coupling reaction by visible light photocatalysis.
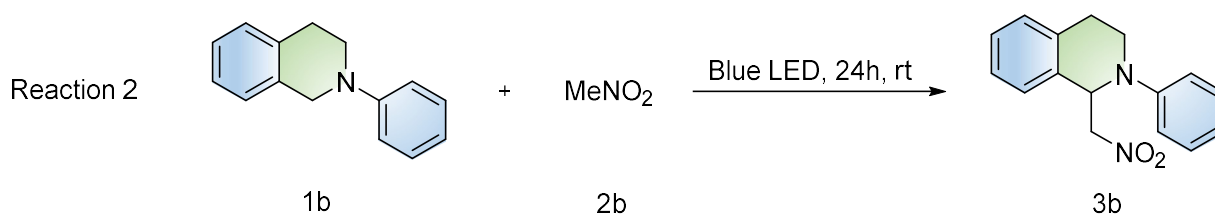
entry[a]	Catalyst	Solvent	Yield(%)[b]
1	4 (1 mol%)	EtOH	53
2	4 (1 mol%)	CH$_3$CN	48
3	4 (1 mol%)	DMSO	37
4	4 (1 mol%)	MeOH	81
5	4 (2 mol%)	MeOH	85
6	2 (2 mol%)	MeOH	74
7	3 (2 mol%)	MeOH	80
8	5 (2 mol%)	MeOH	61
9	-	MeOH	19
10[c]	4 (2 mol%)	MeOH	n.r.
11[d]	4 (1 mol%)	MeOH	n.r.
12	MV^{2+} (1 mol%)	MeOH	15
13	PhV^{2+} (1 mol%)	MeOH	19
14	Se-PhV^{2+} (1 mol%)	MeOH	45
15	Te-PhV^{2+} (1 mol%)	MeOH	73
16	Bi-PhV^{2+} (1 mol%)	MeOH	81

[a]. Reaction **1** conditions: 1b (0.1 mmol), 2b (1 mmol) , under air at 298 K with blue LED irradiation for 24 h. [b] The yields detected by ^{1}H NMR spectroscopy using mesitylene as an internal standard. [c] No air, under Ar [d] No light.

Substrate scope of General Procedure Cross-Dehydrogenative Coupling Reaction.

In addition to nitromethane, nimethyl malonate and niethyl malonate were also selected as nucleophilic reagents. *N*-phenyl Tetrahydroisoquinoline with different substituents was synthesized through literature reports. The data of all thevarious substrates and corresponding products were all consistent with the previous report.[12]

1-Nitromethyl-2-phenyl-1,2,3,4-tetrahydroisoquinoline (3ba).
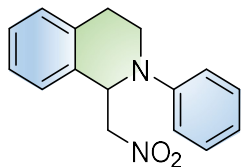
^{1}H NMR (400 MHz, CDCl$_3$) δ 7.30 (dq, *J* = 24.0, 7.7 Hz, 5H), 7.19 (d, *J* = 7.7 Hz, 1H), 7.05 (d, *J* = 8.1 Hz, 2H), 6.91 (t, *J* = 7.7 Hz, 1H), 5.61 (t, *J* = 8.1 Hz 1H), 4.93 (dd, *J* = 11.9, 8.1 Hz, 1H), 4.62 (dd, *J* = 11.9, 8.1 Hz, 1H), 3.71 (s, 2H), 3.15 (dt, *J* = 15.3, 7.1 Hz, 1H), 2.85 (d, *J* = 16.6 Hz, 1H); ^{13}C NMR (101 MHz, CDCl$_3$) δ 148.43, 135.31, 132.93, 129.55, 129.23, 128.16, 127.03, 126.73, 119.46, 115.13, 78.80, 58.24, 42.10, 26.47.

Dimethy 2-(2-phenyl-1,2,3,4-tetrahydroisoquinolin-1-yl)malonate (3bb)
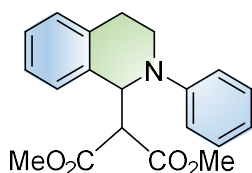
^{1}H NMR (400 MHz, CDCl$_3$) δ 7.28 (td, *J* = 13.7, 11.3, 6.1 Hz, 4H), 7.20 (d, *J* = 8.3 Hz, 2H), 7.07 (d, *J* = 8.3 Hz, 2H), 6.84 (t, *J* = 7.5 Hz, 1H), 5.78 (d, *J* = 9.5 Hz, 1H), 4.04 (dd, *J* = 9.5, 2.7 Hz, 1H), 3.74 (d, *J* = 2.7 Hz, 5H), 3.63 (d, *J* = 2.7 Hz, 3H), 3.14 (d, *J* = 8.2 Hz, 1H), 2.98-2.93 (m, 1H); ^{13}C NMR (101 MHz, CDCl$_3$) δ 168.30, 167.41, 148.78, 135.67, 134.79, 129.12, 129.00, 127.65, 127.06, 126.06, 118.63, 115.20, 59.13, 58.20, 52.58, 42.19, 26.06.

Diethyl 2-(2-phenyl-1,2,3,4-tetrahydroisoquinolin-1-yl)malonate (3bc).
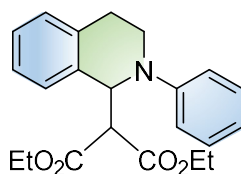
^{1}H NMR (400 MHz, CDCl$_3$) δ 7.26 (ddd, *J* = 20.7, 14.2, 7.3 Hz, 4H), 7.17 (d, *J* = 8.3 Hz, 2H), 7.03 (d, *J* = 8.3 Hz, 2H), 6.80 (t, *J* = 7.3 Hz, 1H), 5.78 (d, *J* = 9.2 Hz, 1H), 4.18-4.03 (m, 4H), 3.97-3.94 (m, 1H), 3.78-3.66 (m, 2H), 3.11 (q, *J* = 8.2 Hz, 1H), 2.96-2.91 (m, 1H), 1.22 (t, *J* = 7.3 Hz, 3H), 1.14 (t, *J* = 6.9 Hz, 3H). ^{13}C NMR (101 MHz, CDCl$_3$) δ 167.98, 167.14, 148.86, 135.97, 134.83, 129.08, 128.91, 127.53, 127.19, 126.02, 118.45, 115.08, 61.53, 59.57, 57.90, 42.29, 26.14, 13.97, 13.91.

2-(4-Fluorophenyl)-1-nitromethyl-1,2,3,4-tetrahydroisoquinoline (3bd).
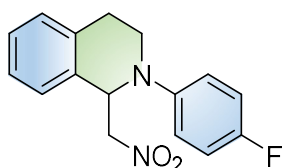
^{1}H NMR (400 MHz, CDCl$_3$) δ 7.25 (ddd, J = 34.7, 13.7, 8.1 Hz, 4H), 7.00-6.96 (m, 4H), 5.48 (t, J = 7.4 Hz, 1H), 4.89 (dd, J = 12.0, 9.0 Hz, 1H), 4.62 (dd, J = 12.6, 5.7 Hz, 1H), 3.65 (dd, J = 7.5, 4.1 Hz, 2H), 3.08 (dt, J = 16.3, 7.9 Hz, 1H), 2.78 (d, J = 16.6 Hz, 1H); ^{13}C NMR (101 MHz, CDCl$_3$) δ 158.36, 155.98, 145.31, 145.28, 135.26, 132.53, 129.47, 128.12, 126.96, 126.78, 117.98, 117.90, 115.99, 115.77, 78.85, 58.75, 42.85, 25.77; ^{19}F NMR (376 MHz, CDCl$_3$) δ -124.25.

Dimethy-2-(2-(4-fluorophenyl)-1,2,3,4-tetrahydroisoquinolin-1-yl)malonate (3be).
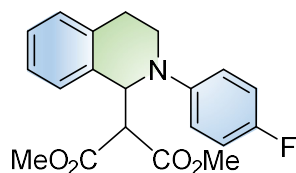
^{1}H NMR (400 MHz, CDCl$_3$) δ 7.28-7.19 (m, 4H), 6.97 (dd, J = 6.6, 2.2 Hz, 4H), 5.62 (d, J = 9.5 Hz, 1H), 4.01 (dd, J = 9.5, 2.4 Hz, 1H), 3.78-3.72 (m, 4H), 3.65 (d, J = 2.3 Hz, 4H), 3.08 (d, J = 8.3 Hz, 1H), 2.89 (d, J = 16.0 Hz, 1H); ^{13}C NMR (101 MHz, CDCl$_3$) δ 168.21, 167.41, 157.76, 155.39, 145.54, 129.12, 127.70, 127.04, 126.13, 117.32, 117.24, 115.60, 115.38, 77.37, 77.05, 76.73, 59.16, 58.85, 52.60, 42.92, 25.68; ^{19}F NMR (376 MHz, CDCl$_3$) δ -125.78.

Diethyl-2-(2-(4-fluorophenyl)-1,2,3,4-tetrahydroisoquinolin-1-yl)malonate (3bf).
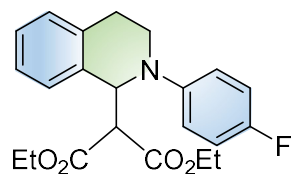
^{1}H NMR (400 MHz, CDCl$_3$) δ 7.33-7.19 (m, 4H), 7.02-6.90 (m, 4H), 5.64 (d, J = 9.3 Hz, 1H), 4.19 (dd, J = 13.6, 8.7 Hz, 4H), 3.95 (s, 1H), 3.80-3.72 (m, 1H), 3.62 (dd, J = 13.3, 5.8 Hz, 1H), 3.14-3.06 (m, 1H), 2.90 (dd, J = 16.6, 4.8 Hz, 1H), 1.24 (td, J = 7.2, 2.3 Hz, 3H), 1.21 – 1.14 (m, 3H); ^{13}C NMR (101 MHz, CDCl$_3$) δ 167.89, 167.11, 157.65, 155.28, 145.61, 145.59, 135.58, 134.65, 129.02, 127.58, 127.18, 126.09, 117.10, 117.03, 115.54, 115.32, 61.63, 61.58, 61.53, 59.55, 58.57, 42.99, 25.76, 14.08, 13.96, 13.94; ^{19}F NMR (376 MHz, CDCl$_3$) δ -126.11.

1-Nitromethyl-2-p-tolyl-1,2,3,4-tetrahydroisoquinoline (3bg).
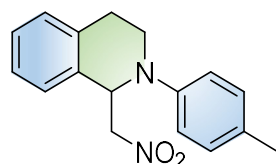
^{1}H NMR (400 MHz, CDCl$_3$) δ 7.20 (dddd, J = 25.7, 16.6, 7.1, 1.6 Hz, 4H), 7.09 (d, J = 7.1 Hz, 2H), 6.91-6.89 (m, 2H), 5.51 (dd, J = 8.0, 6.4 Hz, 1H), 4.89-4.84 (m, 1H), 4.58 (d, J = 6.3 Hz, 1H), 3.71-3.54 (m, 2H), 3.07 (ddd, J = 15.5, 9.3, 5.8 Hz, 1H), 2.76 (dt, J = 16.4, 4.6 Hz, 1H), 2.28 (s, 3H); ^{13}C NMR (101 MHz, CDCl$_3$) δ 146.39, 135.38, 132.95, 130.00, 129.31, 129.12, 128.03, 127.00, 126.65, 115.91, 78.85, 58.42, 42.32, 26.24, 20.40.

Dimethy -2-(2-(p-tolyl)-1,2,3,4-tetrahydroisoquinolin-1-yl)malonate (3bh).
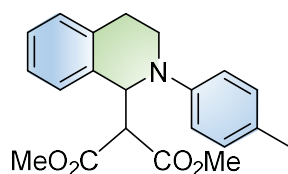
^{1}H NMR (400 MHz, CDCl$_3$) δ 7.21-7.15 (m, 2H), 7.11-7.09 (m, 2H), 7.01 (d, J = 8.3 Hz, 2H), 6.90-6.88 (m, 2H), 5.61 (d, J = 9.4 Hz, 1H), 3.96 (d, J = 9.4 Hz, 1H), 3.61 (d, J = 26.3 Hz, 8H), 3.05 (ddd, J = 16.2, 9.6, 6.4 Hz, 1H), 2.80 (d, J = 16.6 Hz, 1H), 2.22 (s, 3H); ^{13}C NMR (101 MHz, CDCl$_3$) δ 168.34, 167.48, 146.76, 135.53, 134.80, 129.63, 129.10, 127.54, 127.10, 125.96, 115.87, 59.18, 58.58, 52.59, 52.54, 42.29, 25.74, 20.35.

Diethyl-2-(2-(p-tolyl)-1,2,3,4-tetrahydroisoquinolin-1-yl)malonate (3ai).
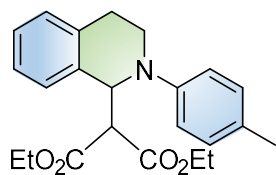
^{1}H NMR (400 MHz, CDCl$_3$) δ 7.26-7.24 (m, 1H), 7.17-7.15 (m, 3H), 7.11-7.09 (m, 2H), 6.90-6.88 (m, 2H), 5.64 (d, J = 9.2 Hz, 1H), 4.14-4.02 (m, 4H), 3.91 (d, J = 9.2 Hz, 1H), 3.69-3.63 (m, 2H), 3.08-3.02 (m, 1H), 2.81 (dt, J = 16.5, 4.7 Hz, 1H), 2.23 (s, 3H), 1.14 (dt, J = 18.5, 7.1 Hz, 6H); ^{13}C NMR (101 MHz, CDCl$_3$) δ 168.02, 167.20, 146.82, 135.81, 134.82, 129.58, 129.00, 127.98, 127.41, 127.24, 125.91, 115.74, 61.55, 59.55, 58.32, 42.34, 25.82, 20.33, 14.09, 13.97, 13.95.

21. Quantum yield measurements

According to the procedure of Yoon, the photon flux of the spectrophotometer was determined by standard ferrioxalate actinometry. Firstly, prepare solutions **A** and **B**. The preparation of **A** was as follows: Potassium ferrate (1.47 g) was dissolved in 20 ml sulfuric acid solution (0.05 M) to obtain a 0.15 M potassium ferrate solution, which was then stored in the dark for future use. The preparation of **B** was as follows : 1,10-phenanthroline (25 mg) and acetate was dissolved in 25 ml sulfuric acid solution (0.5 M) to obtain a buffer solution of 1,10-phenanthroline, which was then stored in the dark for future use.

Next, measure the absorption strengths A1 and A2. Under dark conditions, 2ml of solution **A** was added to a quartz colorimetric dish and irradiated at 433nm for 90 seconds. Then 0.35ml of solution **B** was added and placed in darkness for one hour to ensure complete complexation of ferrous ions with 1,10-phenanthroline. The absorption intensity of the mixed solution at 510 nm was recorded as A1 = 2.143. Repeating the above operation under no light conditions, and the absorption intensity of the mixed solution at 510nm was recorded as A2 = 0.045 .

According to formula (1), calculate the Mol Fe^{2+}

$$\text{Mol Fe}^{2+} = \frac{V \cdot \Delta A}{l \cdot \varepsilon} = \frac{0.00235 \text{ L} \times 2.098}{1.000 \text{ cm} \times 11100 \text{ L} \cdot \text{mol}^{-1} \cdot \text{cm}^{-1}} = 4.44 \times 10^{-7} \text{ mol} \qquad (1)$$

The total volume V= 0.00235 L，difference in absorbance intensity: ΔA = A1 - A2 = 2.098, the optical path length: l = 1.000 cm and the absorption coefficient at 510 nm: ε = 11100 L·mol^{-1}·cm^{-1}.

According to formula (2)，calculate the the photon flux.

$$\text{Photon flux} = \frac{\text{mol Fe}^{2+}}{\phi \cdot t \cdot f} = \frac{4.44 \times 10^{-7} \text{ mol}}{1.03 \times 90 \text{ s} \times 0.99145} = 4.73 \times 10^{-9} \text{ einstein s}^{-1} \qquad (2)$$

$$f = 1 - 10^{-A} = 1 - 10^{-2.068} = 0.99145 \qquad (3)$$

The quantum yield of solution **A** at 433 nm: ϕ = 1.03, the excitation time: t = 90 s, according to formula (3)，calculate the f, the absorption intensity of solution **A** at 433 nm: A = 2.068.

For reaction **1**, the determination of quantum yield value of photocatalyst **4**: 0.1mmol *N,N*-dimethylaniline, 0.1 mmol *N*-Methylmaleimide, 0.002 mmol catalyst **4** and DMSO (2mL) were added to a quartz cuvette with a lid. Excitation was performed at 433 nm for 18000 s. After excitation, the reaction yield was determined to be γ**1 =** 45% by ^{1}H NMR spectroscopy using 1,3,5-trimethoxybenzene as the internal standard.

According to formula (4), calculate the the photon flux ϕ_{4-1}

$$\phi_{4-1} = \frac{\text{mol}(prod)}{\text{flux} \cdot t \cdot f} = \frac{0.45 \times 0.1 \times 10^{-3}}{4.73 \times 10^{-9} \times 18000 \times 0.99145} = 0.53 \qquad (4)$$

For reaction **2,** the determination of quantum yield value of photocatalyst **4**: 0.1 mmol 2-phenyl-1,2,3,4-tetrahydroisoquinoline, 1 mmol nitromethane, 0.002 mmol catalyst **4** and MeOH (2 mL) were added to a quartz cuvette with a lid. Excitation was performed at 433 nm for 18000 s. After excitation, the reaction yield was determined to be γ**2 =** 38 % by ^{1}H NMR spectroscopy using 1,3,5-trimethoxybenzene as the internal standard.

According to formula (4), calculate the the photon flux ϕ_{4-2}

$$\phi_{4-2} = \frac{\text{mol (prod)}}{\text{flux} \cdot t \cdot f} = \frac{0.38 \times 0.1 \times 10^{-3}}{4.73 \times 10^{-9} \times 18000 \times 0.99145} = 0.45 \qquad (4)$$

22. Estimation of excited state redox potential

According to the Rehm-Weller equation

$$E^*(X^*/X^-) = E(X/X^-) + E_{00}(X^*/X)$$

The E (X/X$^-$) can be estimated by CV.The excited-state energy $E_{0,0}$ of **2, 3, 4 and 5** was read from the cross-point of the UV-vis absorption and luminescence spectra at 452 nm, 447 nm, 443 nm and 478 nm. From Table S5, E (**2/2'**) = -0.82 V vs. Fc, E (**3/3'**) = -0.72 V vs. Fc, E (**4/4'**) = -0.74 V vs. Fc and E (**5/5'**) = -0.72 V vs. Fc.

$$E(\mathbf{2^*/2'}) = E(\mathbf{2/2'}) + E_{0,0} + 0.4\ V = -0.86\ V + 1240/452\ V + 0.4\ V = +2.28\ V\ vs.\ SCE$$

$$E(\mathbf{3^*/3'}) = E(\mathbf{3/3'}) + E_{0,0} + 0.4\ V = -0.72\ V + 1240/447\ V + 0.4\ V = +2.45\ V\ vs.\ SCE$$

$$E(\mathbf{4^*/4'}) = E(\mathbf{4/4'}) + E_{0,0} + 0.4\ V = -0.74\ V + 1240/443\ V + 0.4\ V = +2.46\ V\ vs.\ SCE$$

$$E(\mathbf{5^*/5'}) = E(\mathbf{5/5'}) + E_{0,0} + 0.4\ V = -0.72\ V + 1240/478\ V + 0.4\ V = +2.27\ V\ vs.\ SCE$$

23. ^{1}H, ^{13}C, ^{19}F, NMR spectra

^{1}H NMR (400 MHz, DMSO-*d6*) spectrum of **1.**
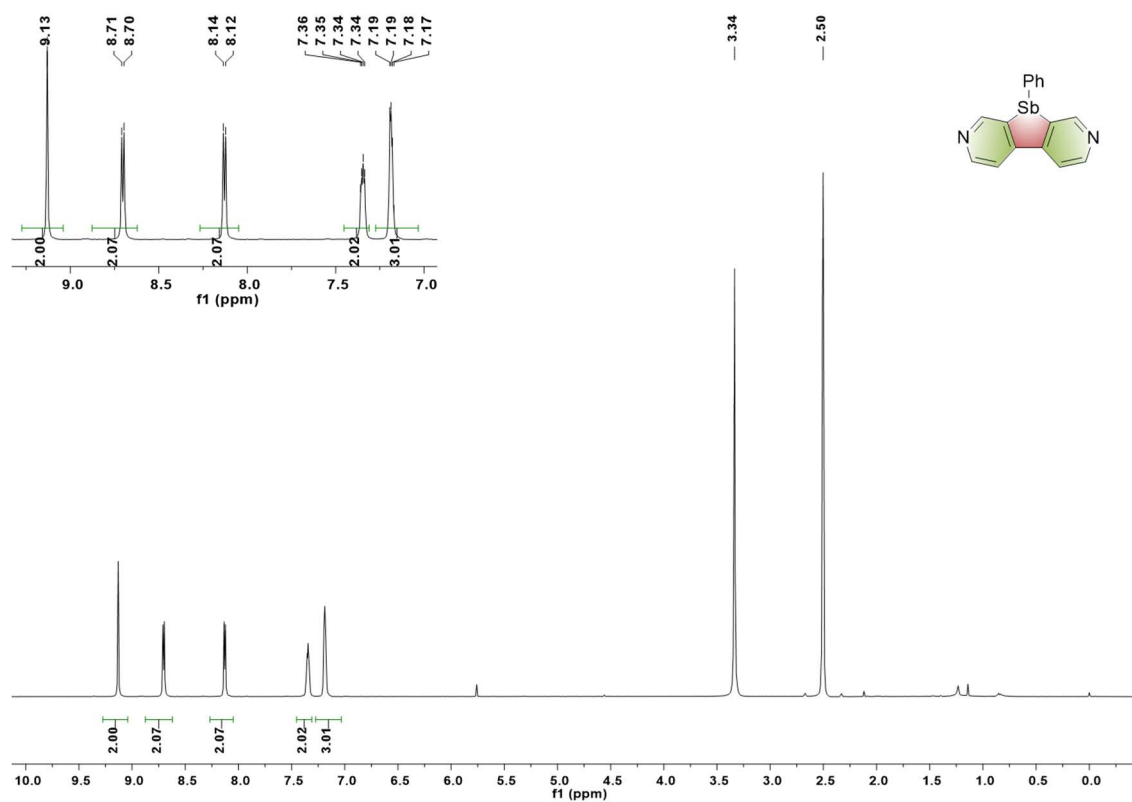
^{13}C NMR (101 MHz, DMSO-*d6*) spectrum of **1.**
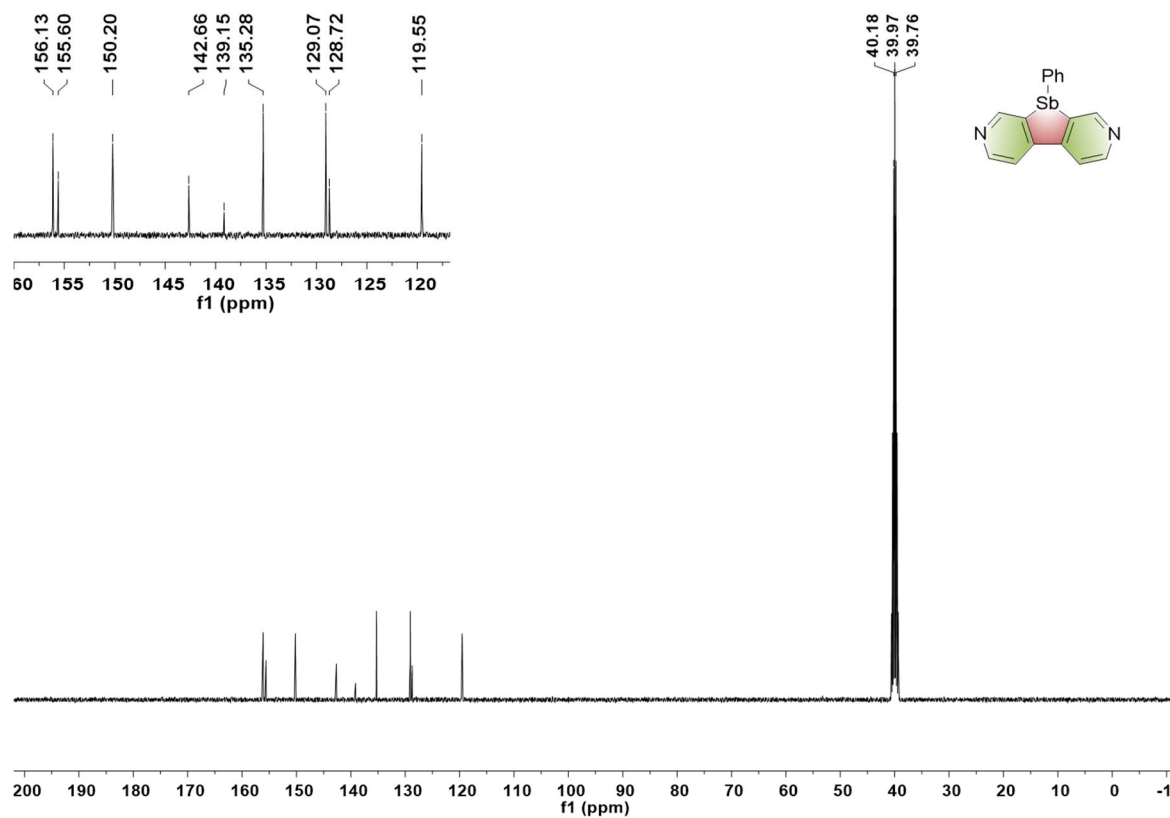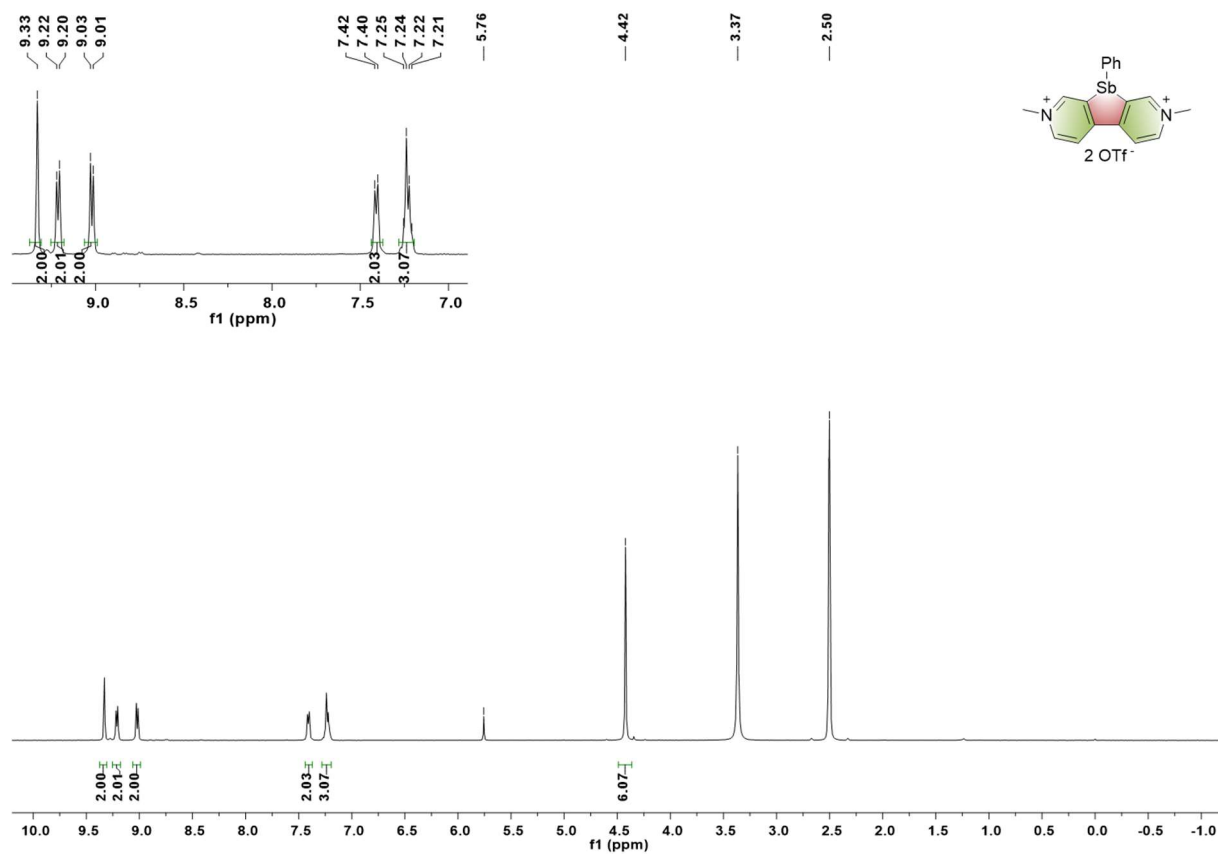
^{1}H NMR (400 MHz, DMSO-*d6*) spectrum of **2**.

^{13}C NMR (101 MHz, DMSO-*d6*) spectrum of **2**.
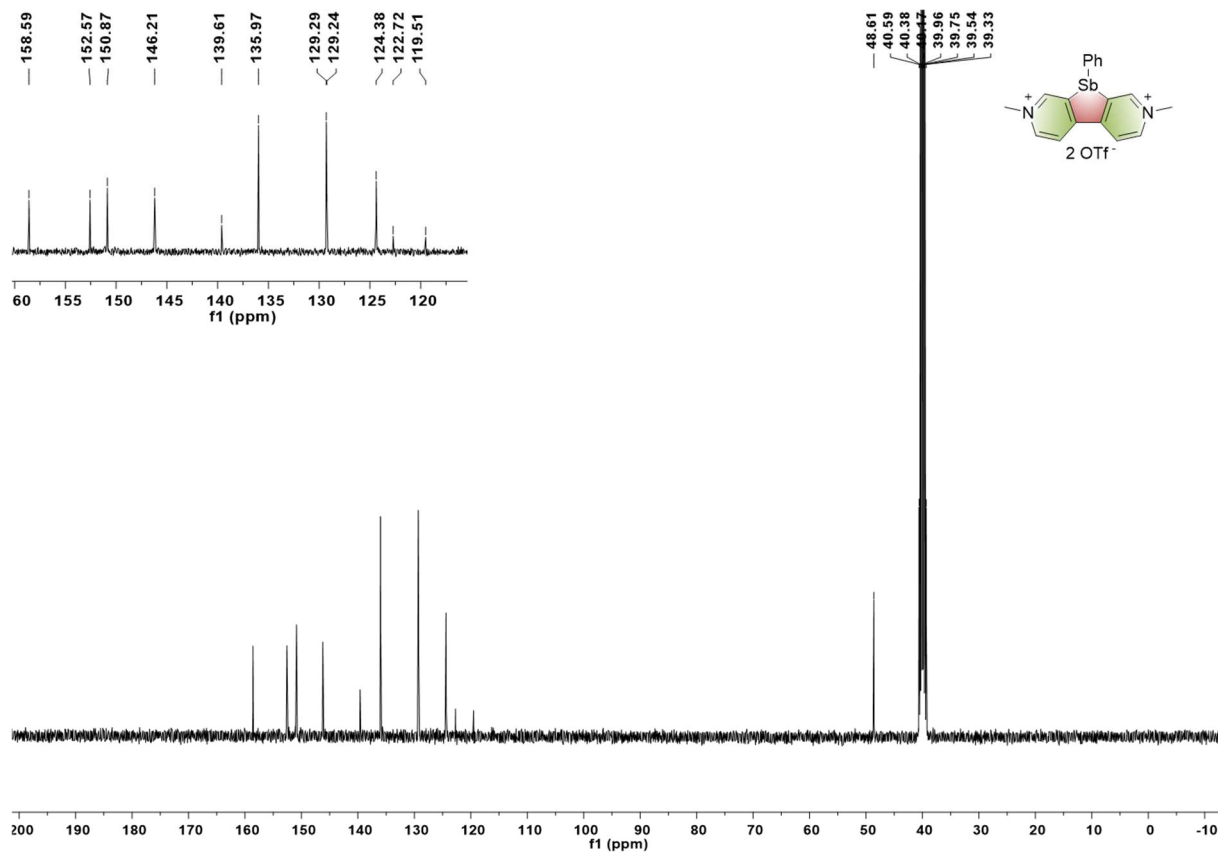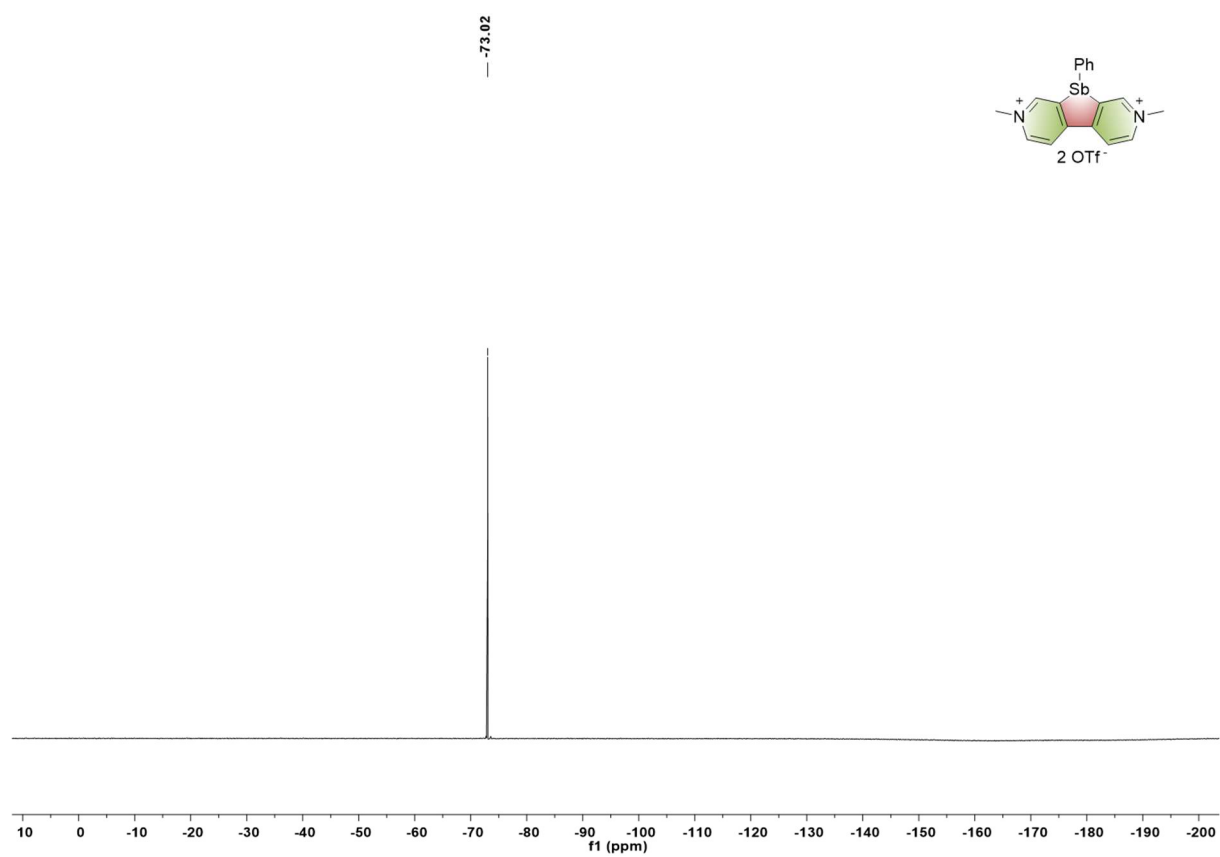
^{19}F NMR (376 MHz, DMSO-*d6*) spectrum of **2**.

¹H NMR (400 MHz, DMSO-*d6*) spectrum of **3.**

¹³C NMR (101 MHz, DMSO-*d6*) spectrum of **3.**
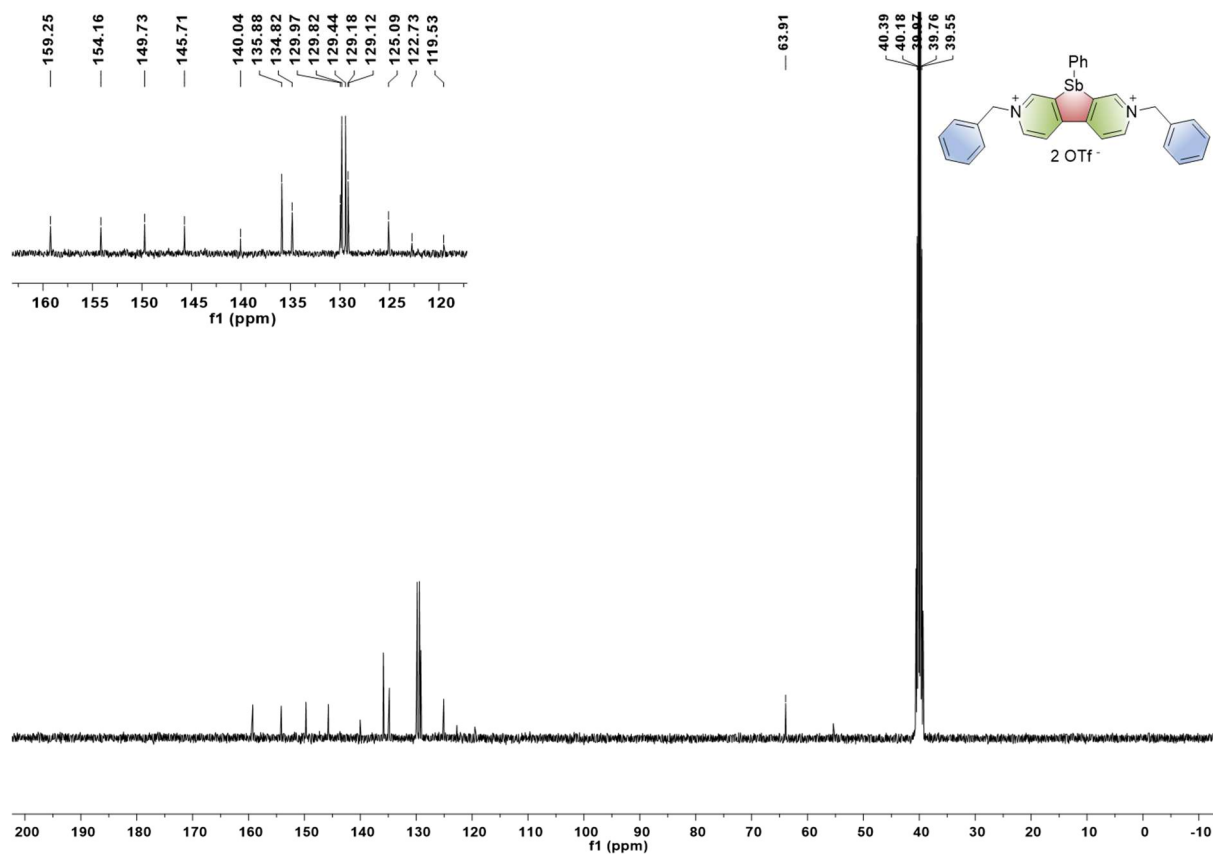
^{19}F NMR (376 MHz, DMSO-*d6*) spectrum of **3**.

—−77.76

f1 (ppm)
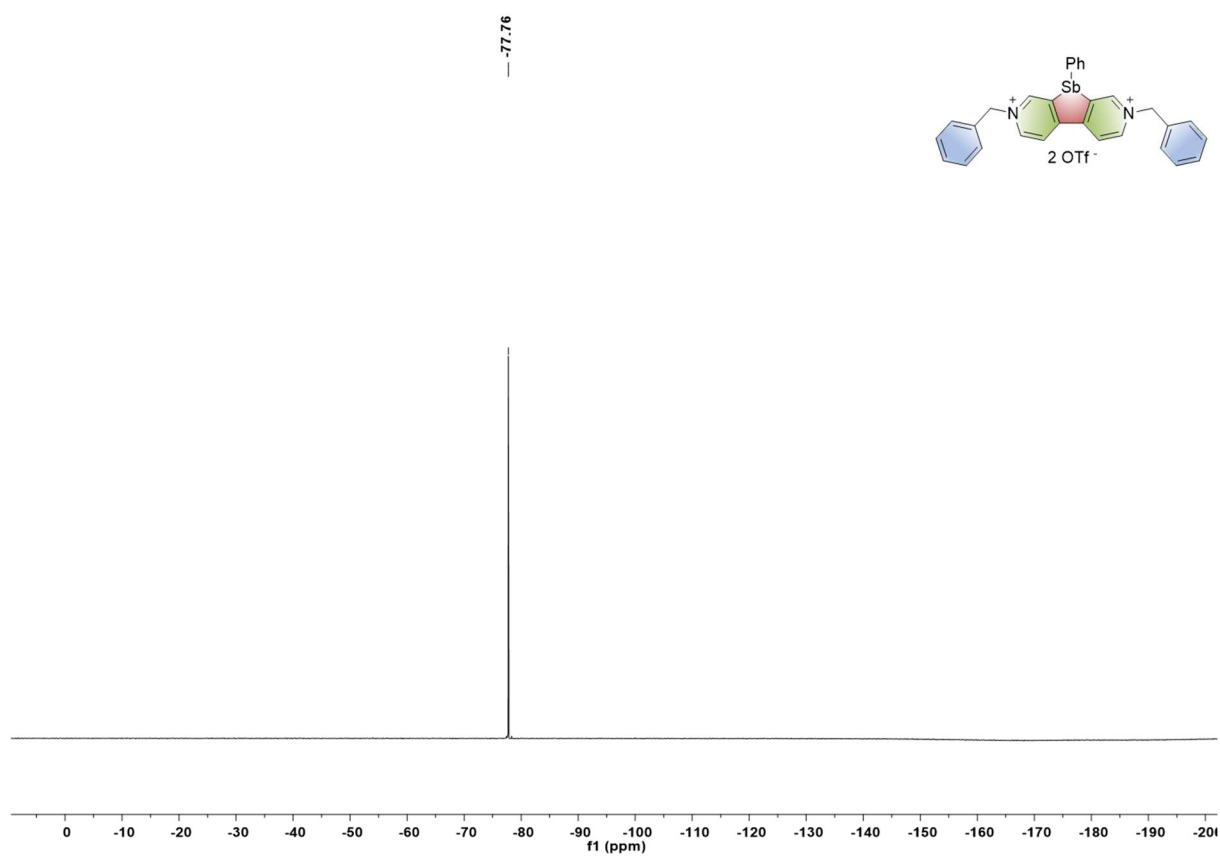
^{1}H NMR (400 MHz, DMSO-*d6*) spectrum of **4.**

^{13}C NMR (101 MHz, DMSO-*d6*) spectrum of **4.**
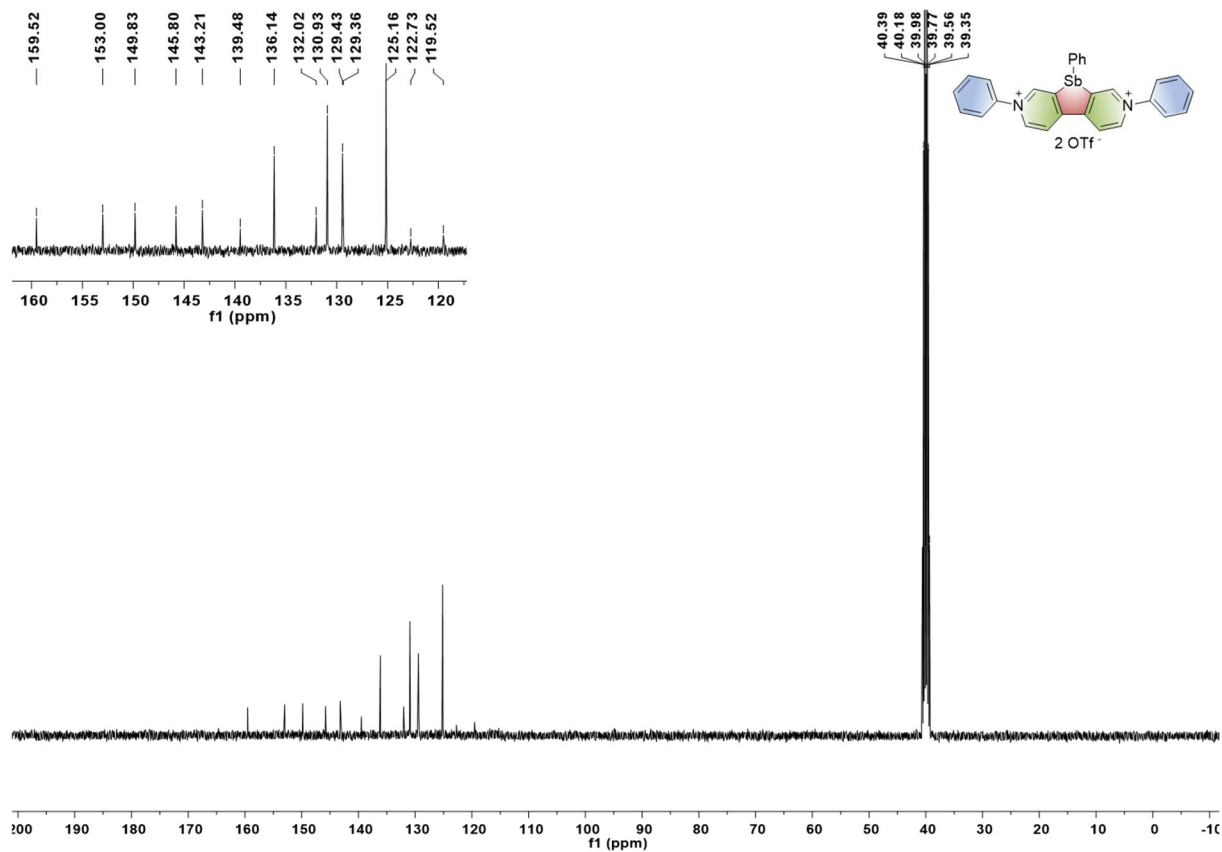
^{19}F NMR (376 MHz, DMSO-*d6*) spectrum of **4**.

— -77.76

2 OTf $^-$

f1 (ppm)

S58
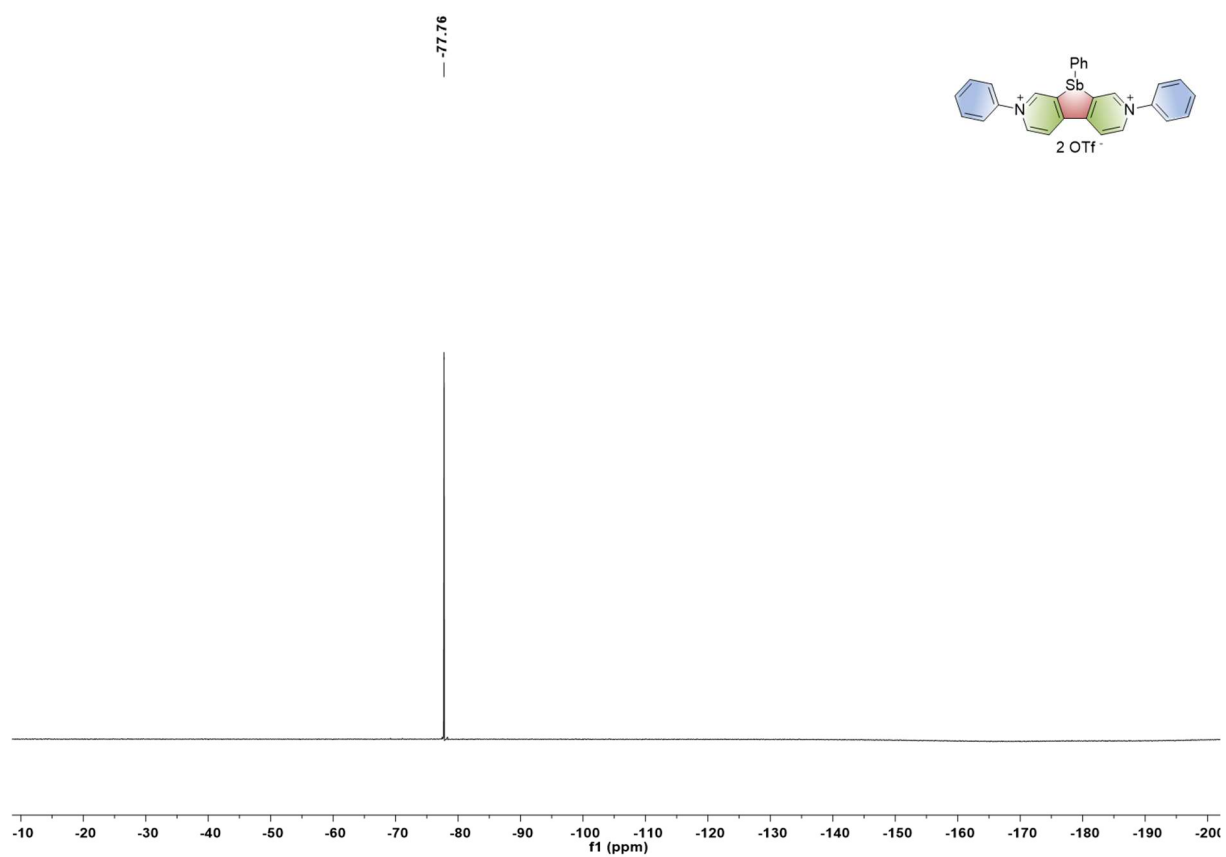
^{1}H NMR (400 MHz, DMSO-*d6*) spectrum of **5.**

^{13}C NMR (101 MHz, DMSO-*d6*) spectrum of **5.**
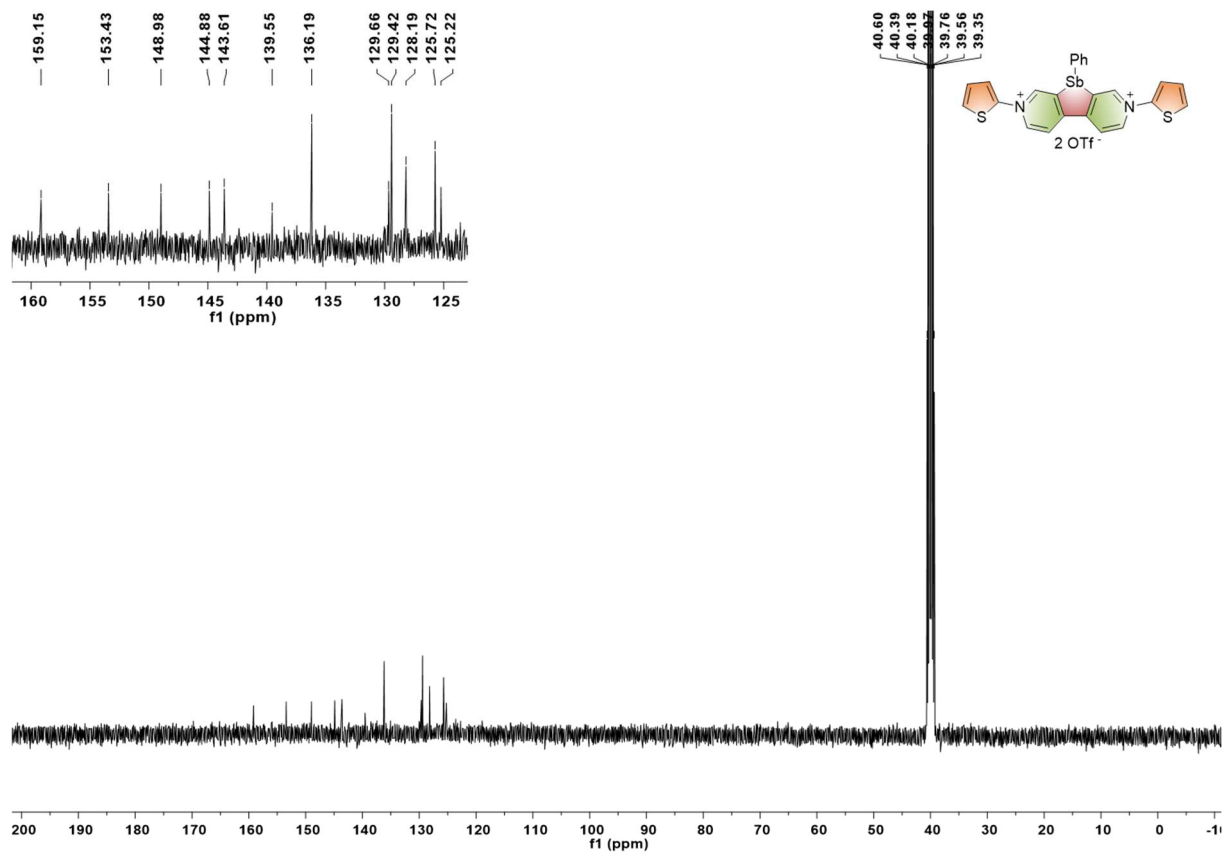
^{19}F NMR (376 MHz, DMSO-*d6*) spectrum of **5**.

—— -77.76
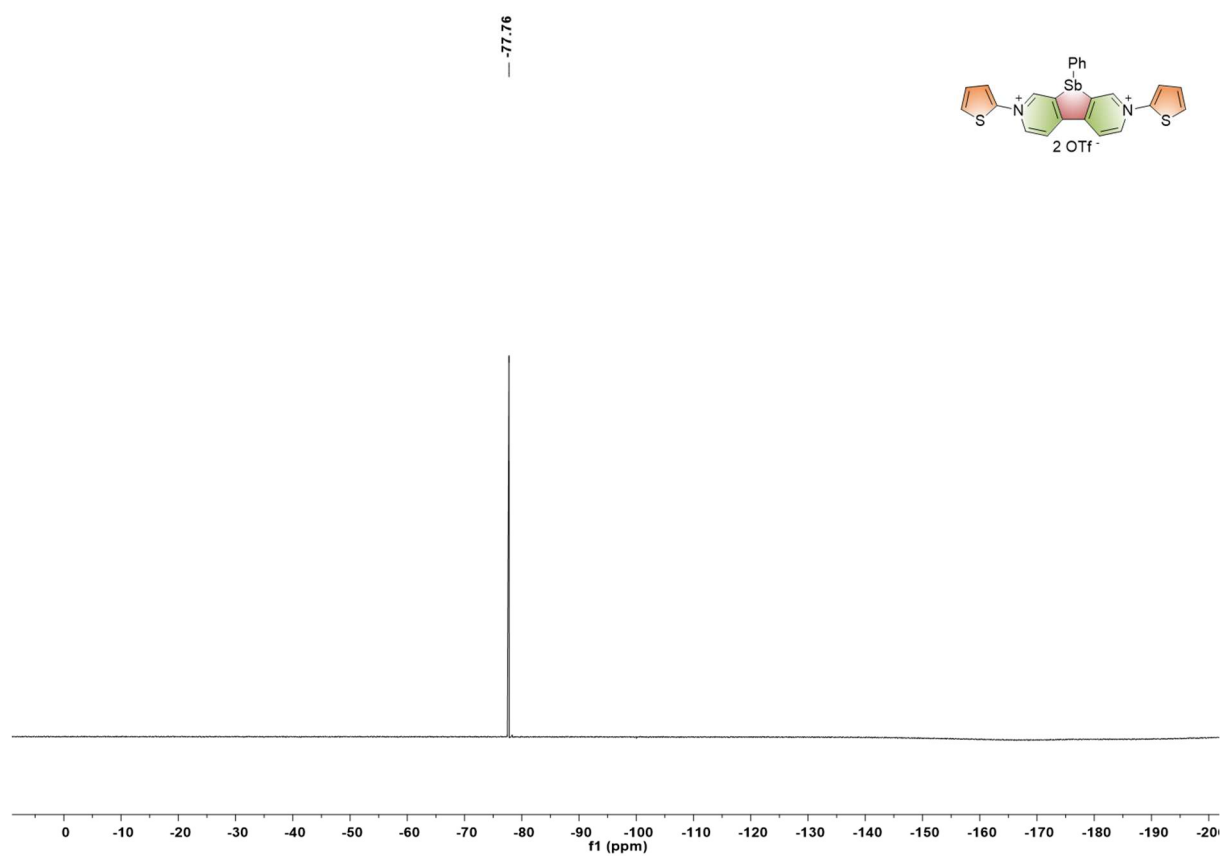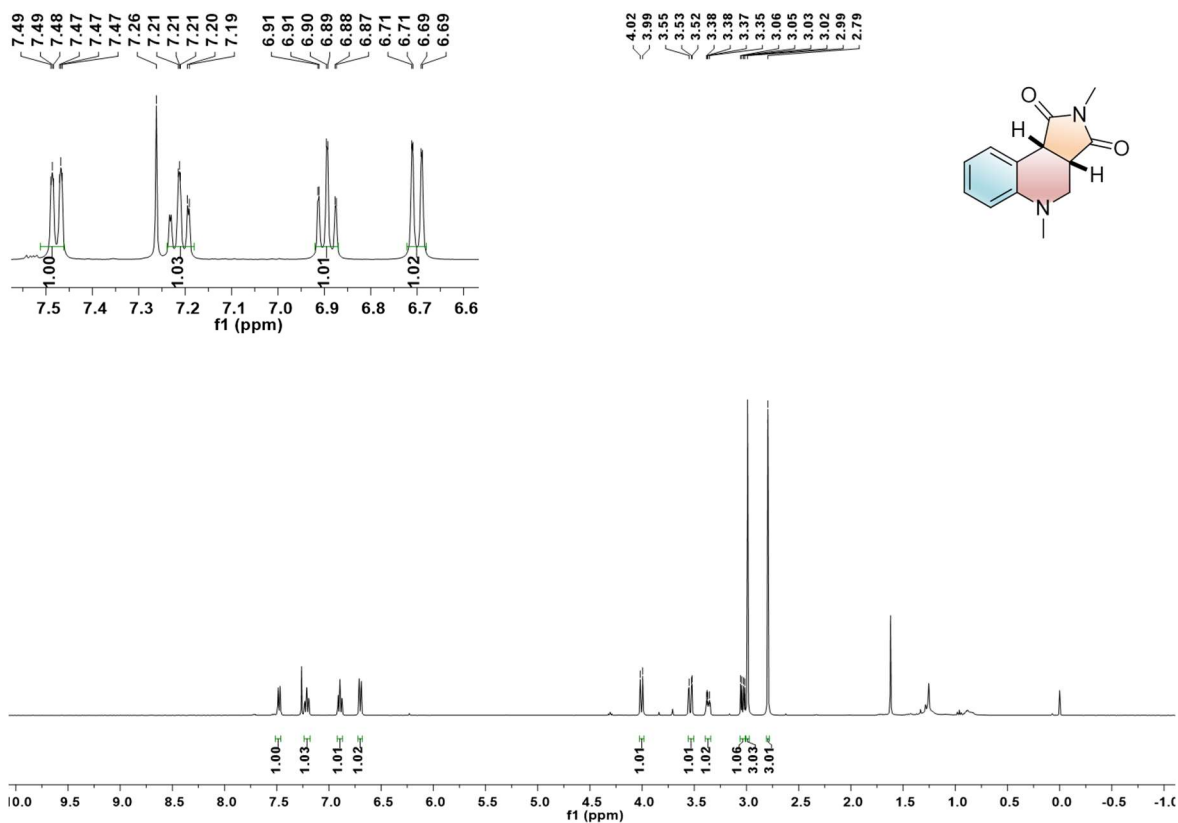
1H NMR (400 MHz, CDCl3) spectrum of 3aa.

13C NMR (101 MHz, CDCl3) spectrum of 3aa.
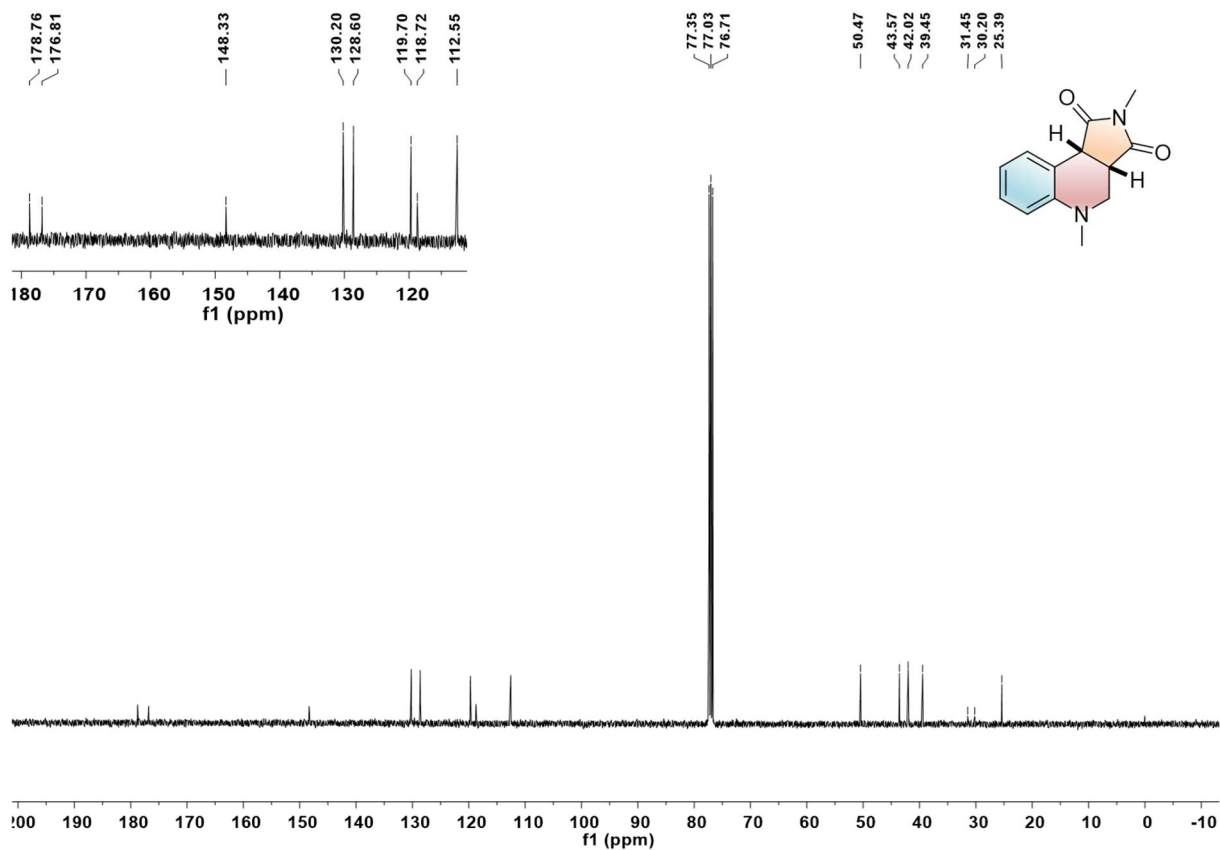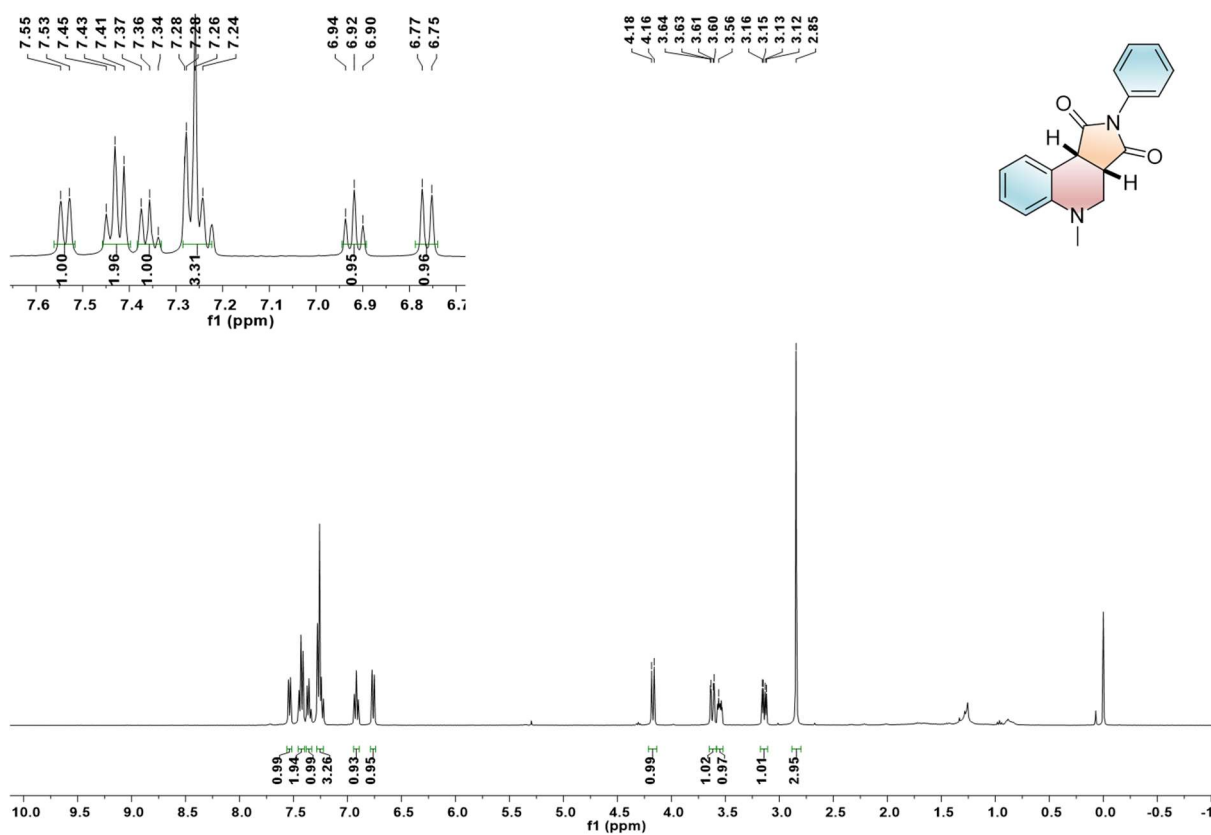
¹H NMR (400 MHz, CDCl₃) spectrum of 3ab.

¹³C NMR (101 MHz, CDCl₃) spectrum of 3ab.
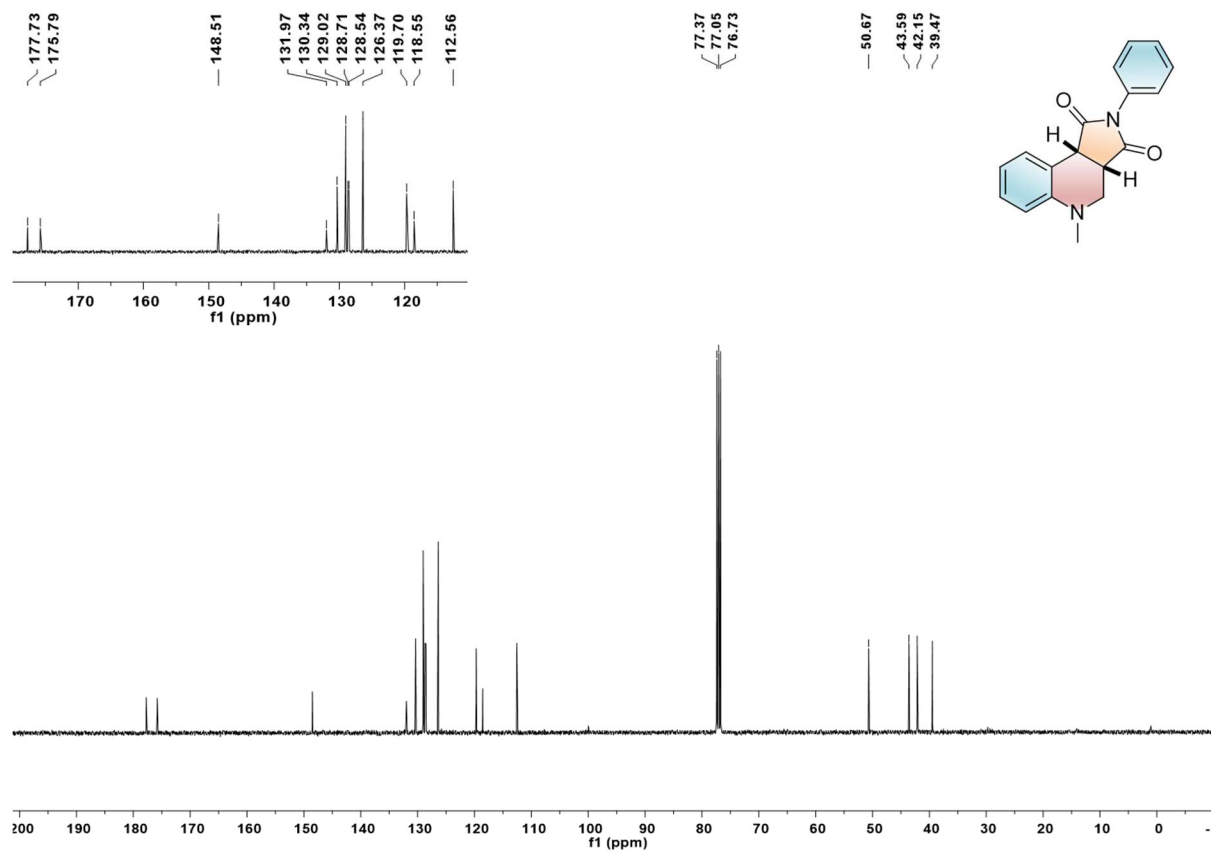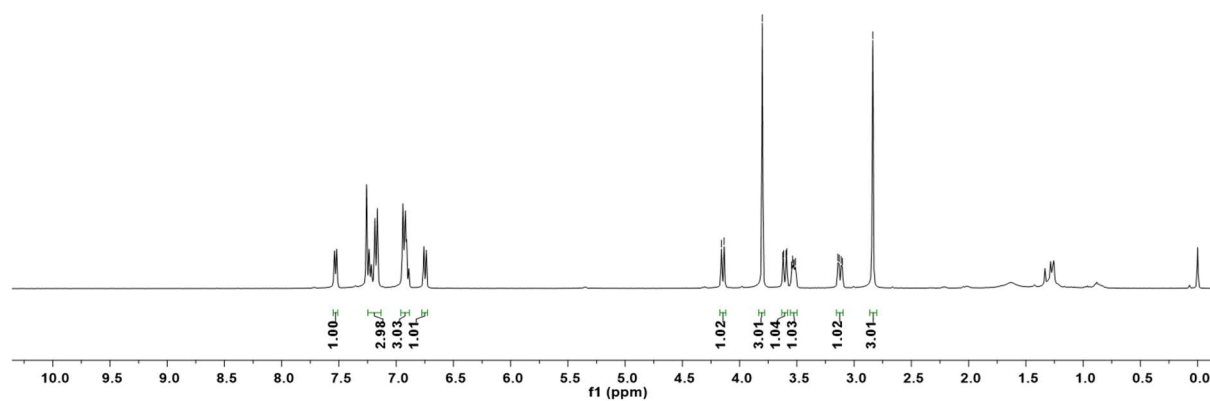
¹H NMR (400 MHz, CDCl₃) spectrum of 3ac.

¹³C NMR (101 MHz, CDCl₃) spectrum of 3ac.
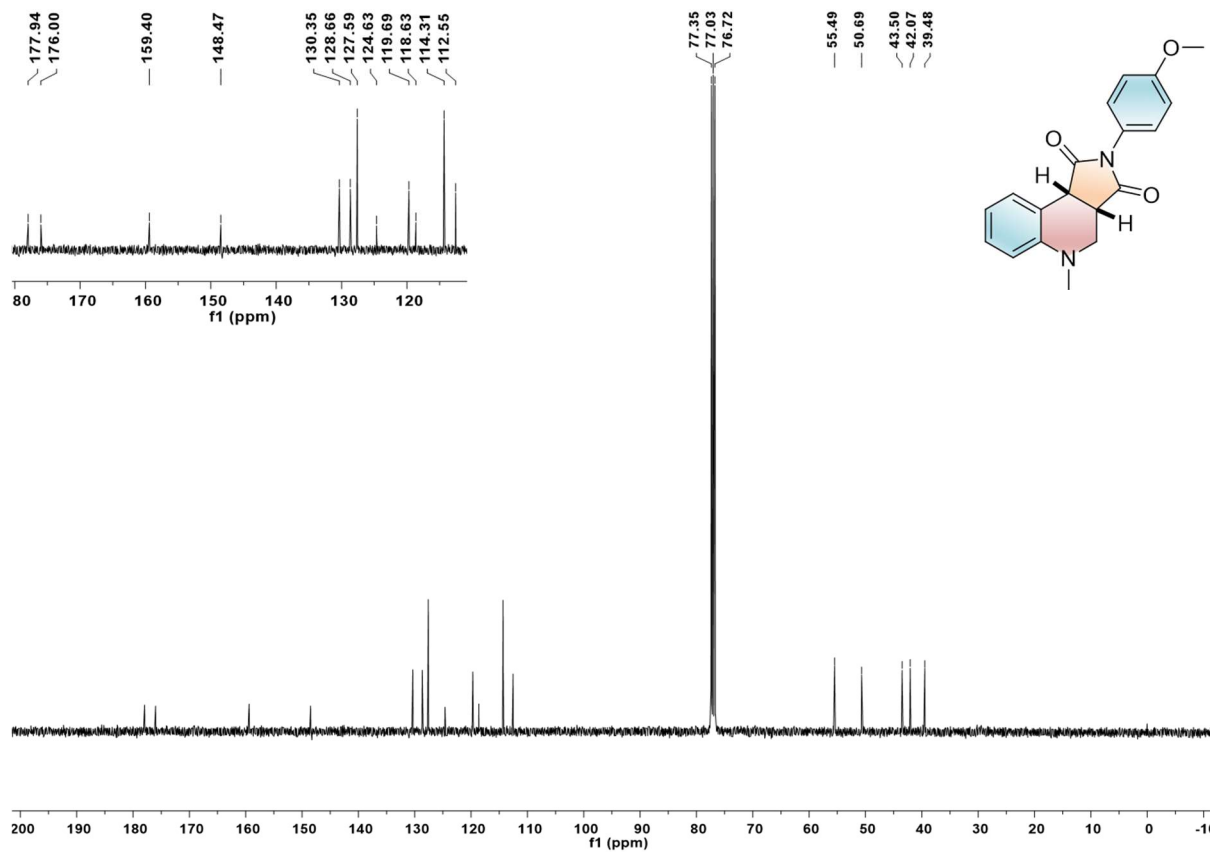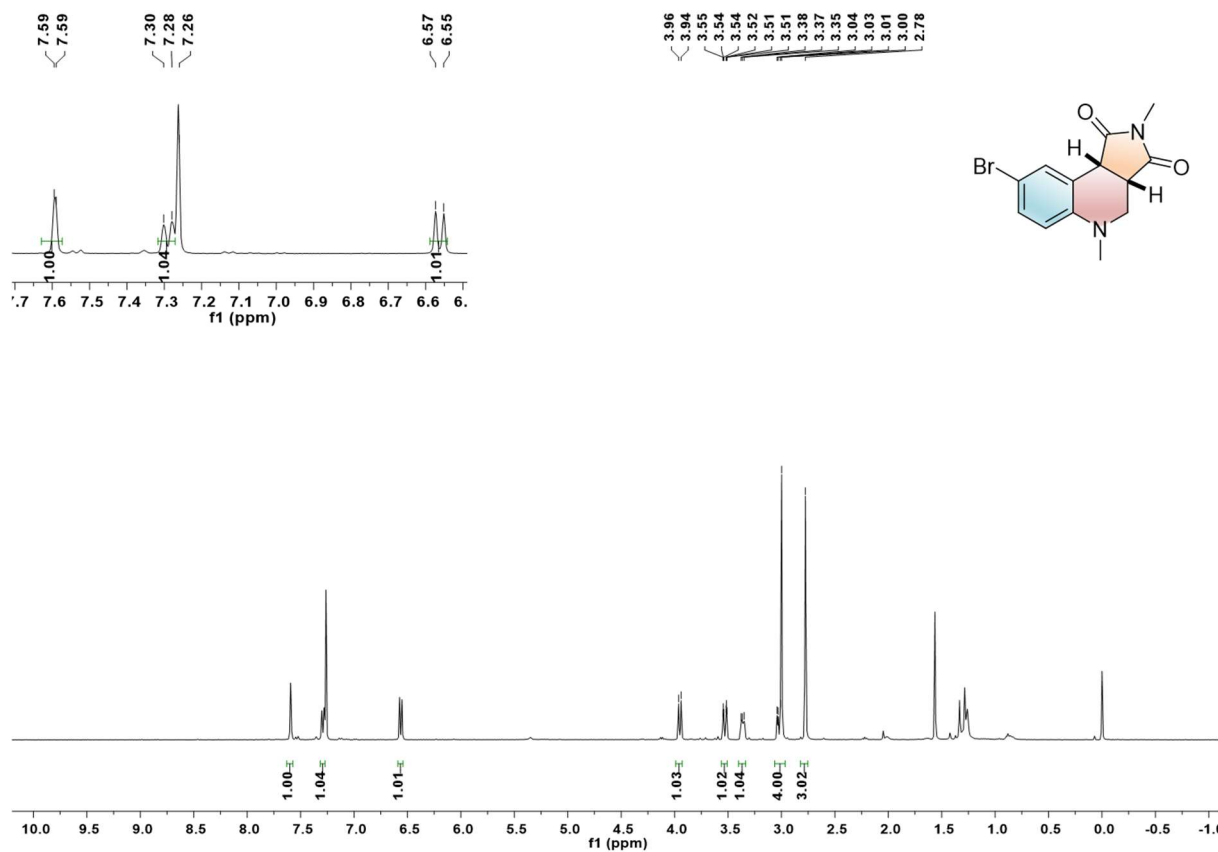
¹H NMR (400 MHz, CDCl₃) spectrum of 3ad.

¹³C NMR (101 MHz, CDCl₃) spectrum of 3ad.
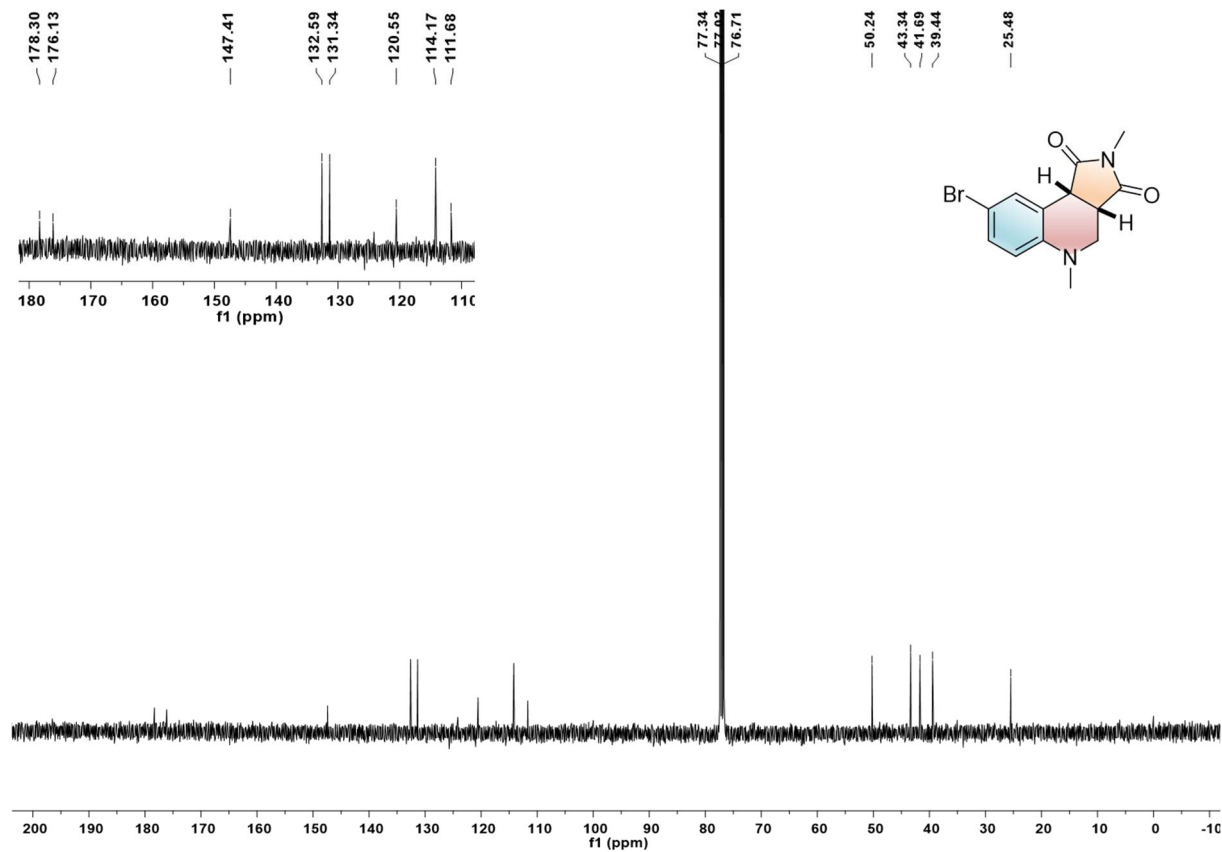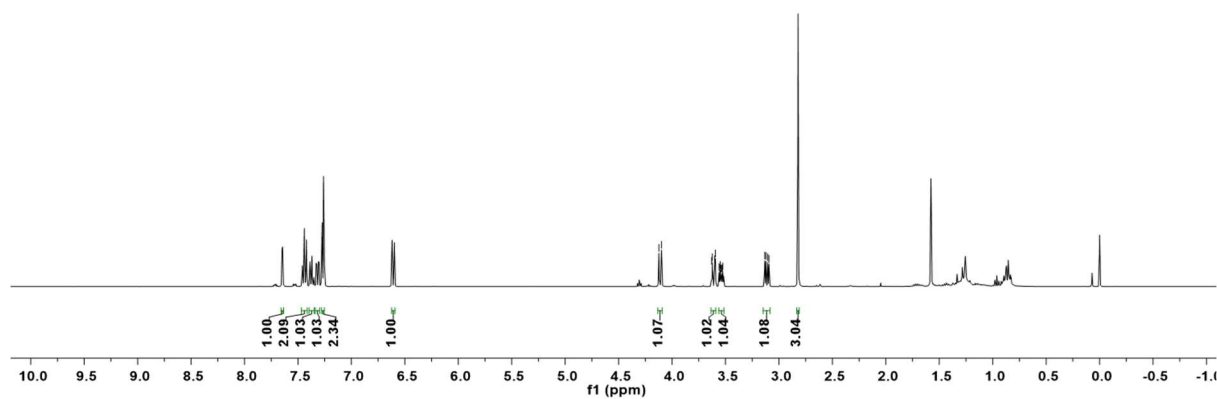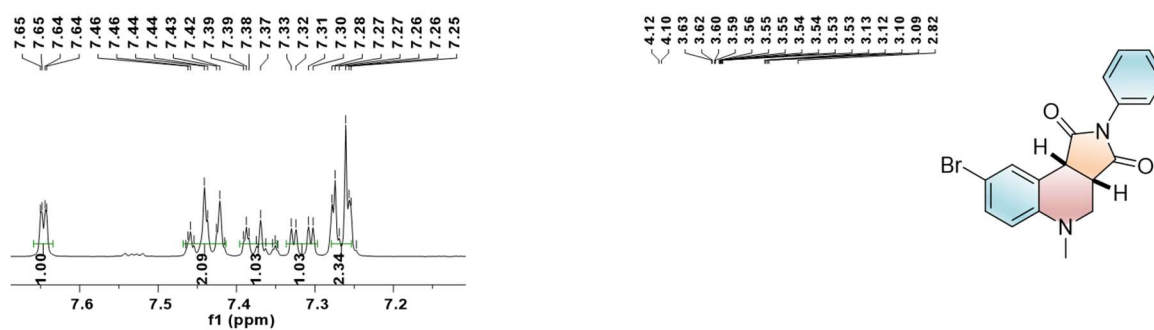
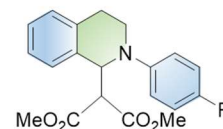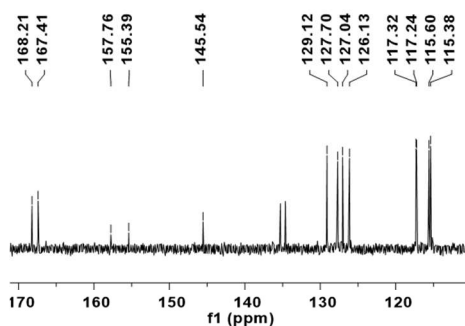¹H NMR (400 MHz, CDCl₃) spectrum of 3ae.

¹³C NMR (101 MHz, CDCl₃) spectrum of 3ae.
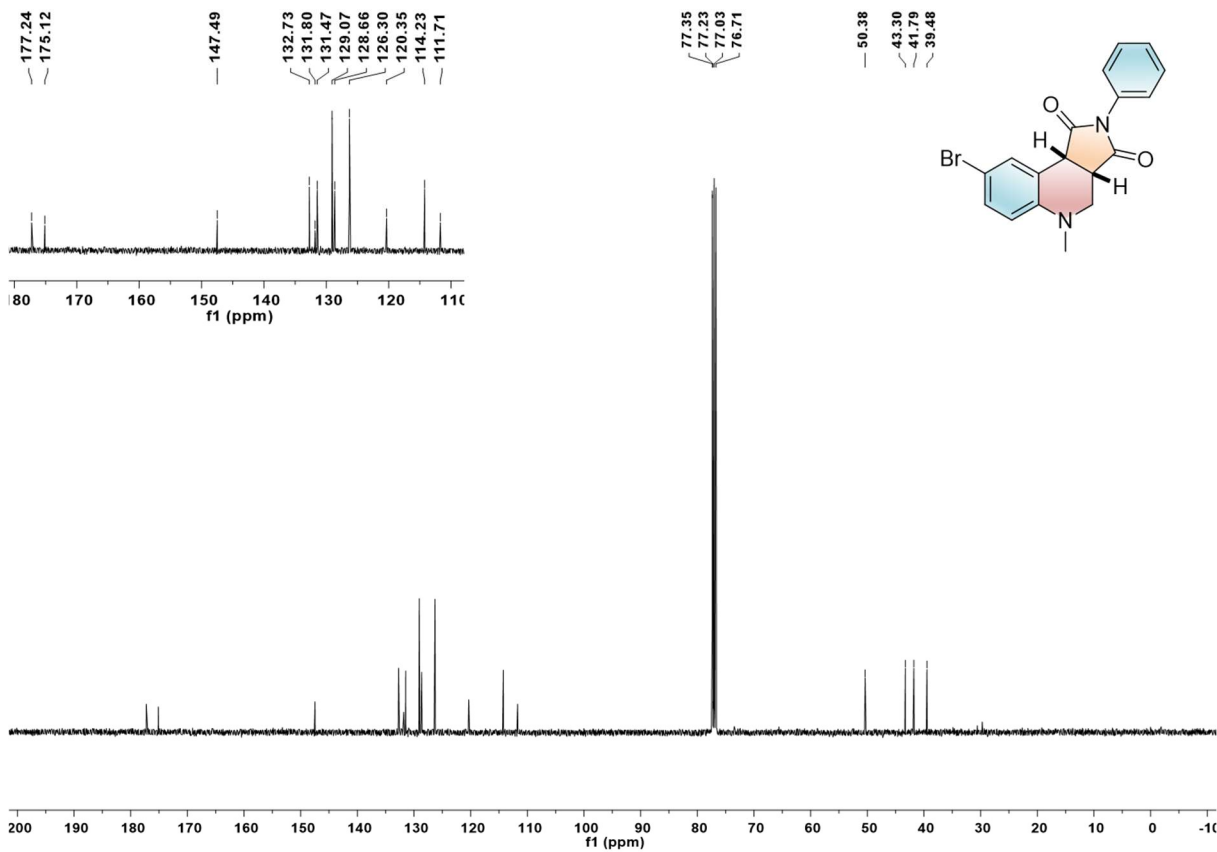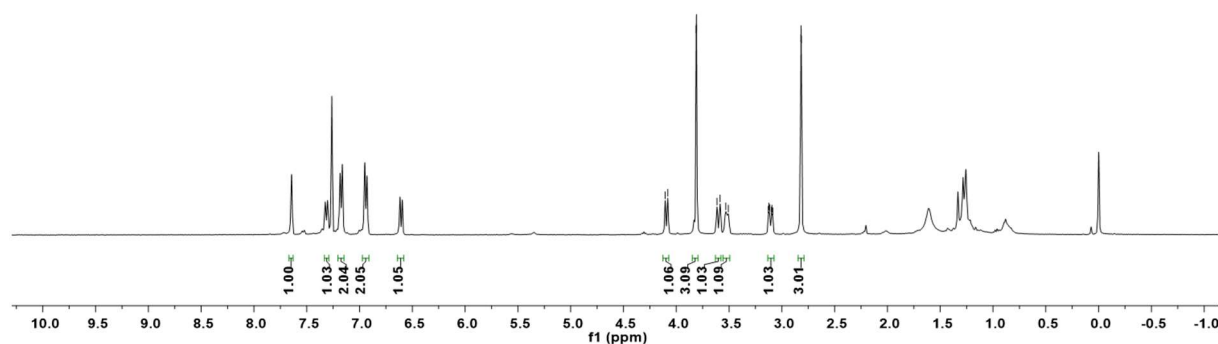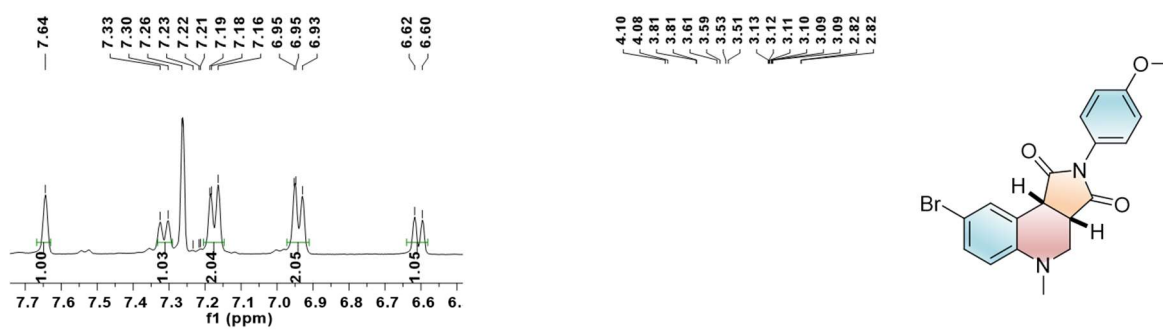
1H NMR (400 MHz, CDCl₃) spectrum of 3af.

13C NMR (101 MHz, CDCl₃) spectrum of 3af.
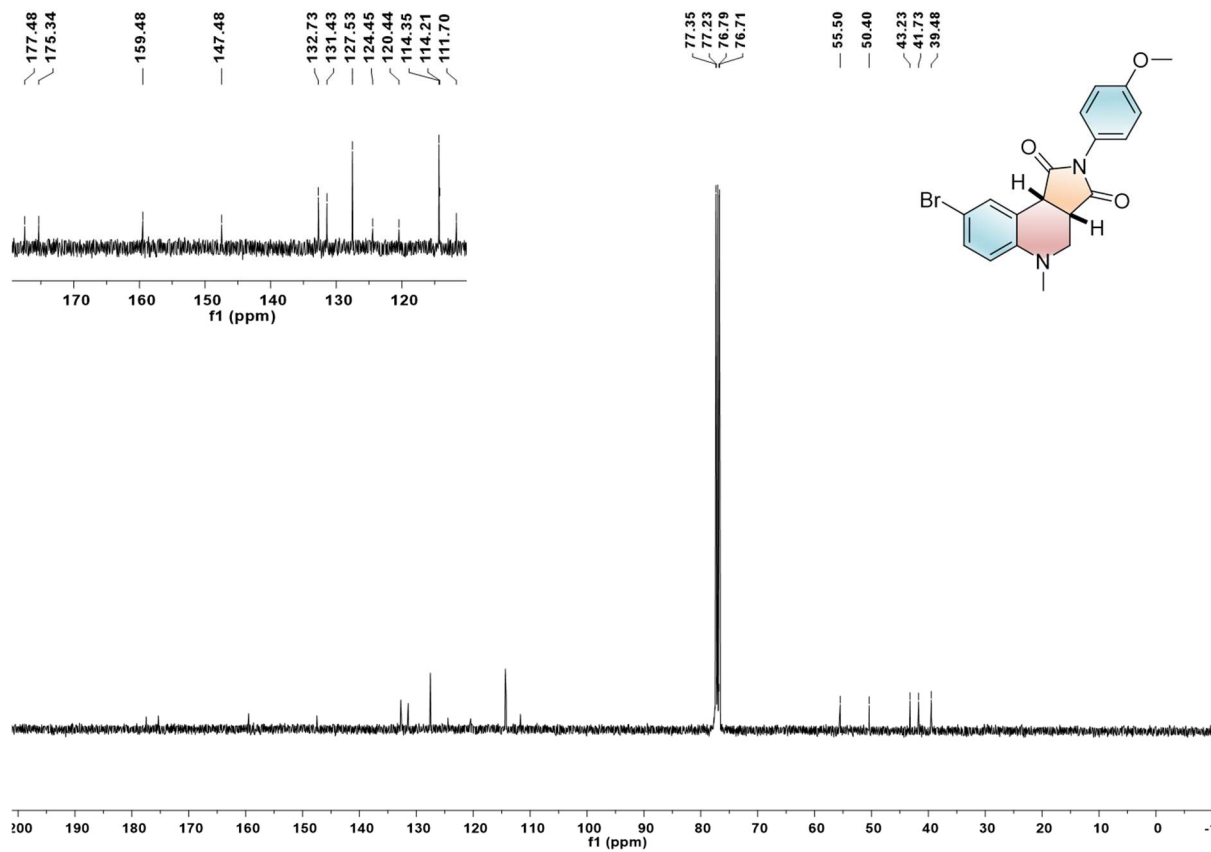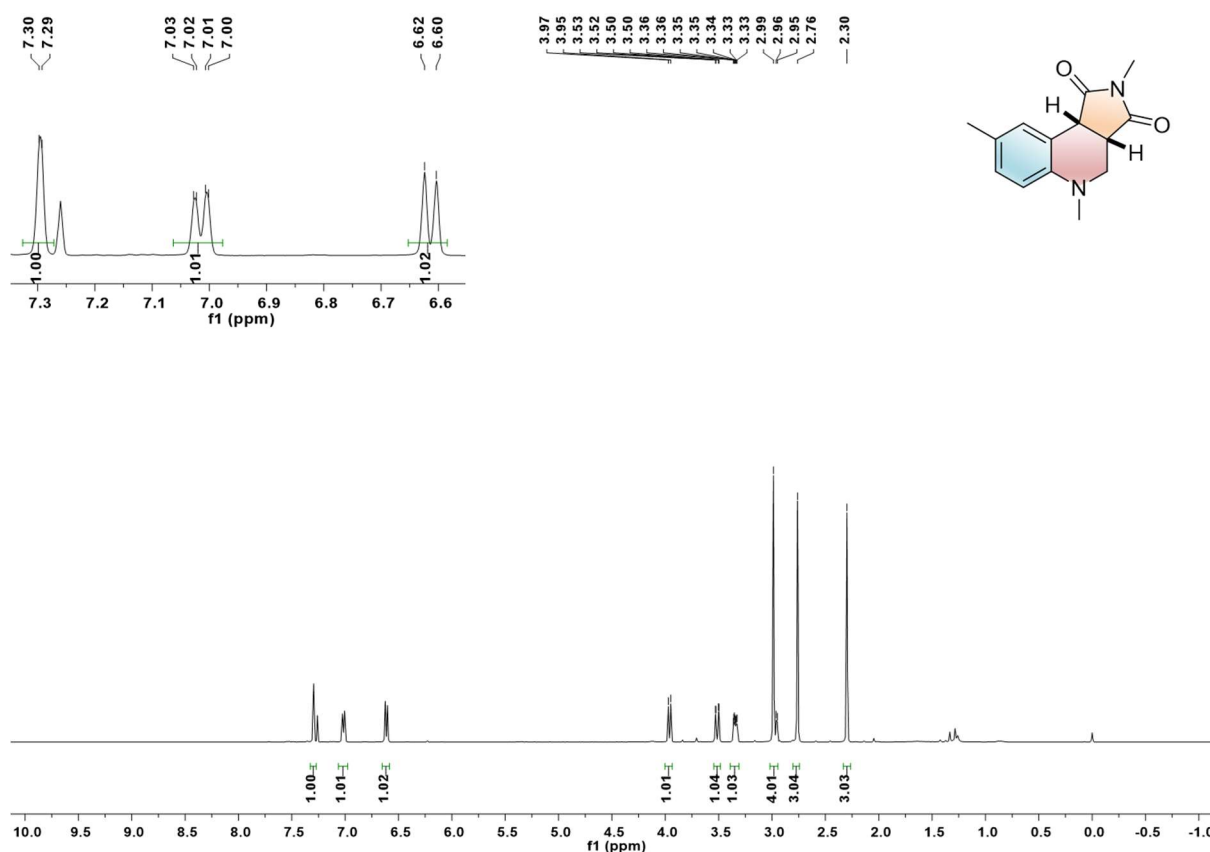
¹H NMR (400 MHz, CDCl₃) spectrum of 3ag.

¹³C NMR (101 MHz, CDCl₃) spectrum of 3ag.
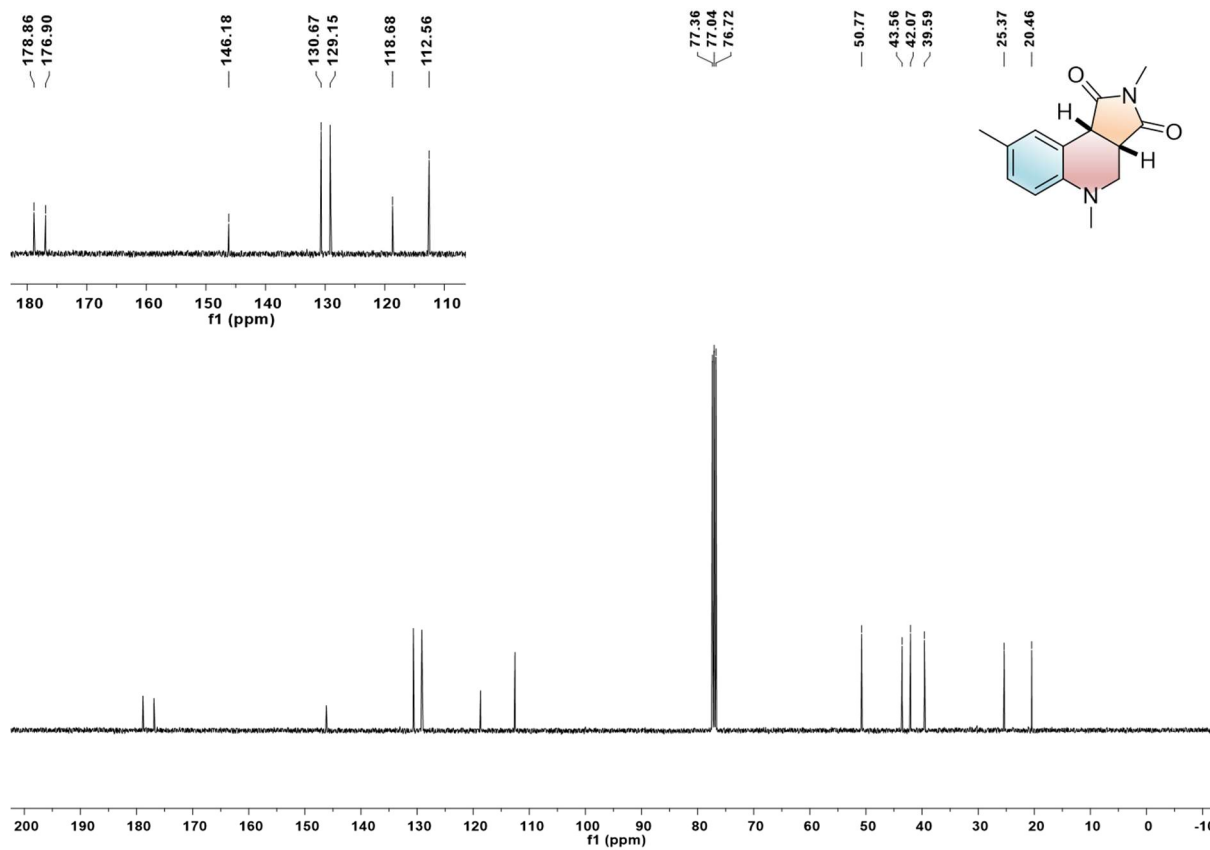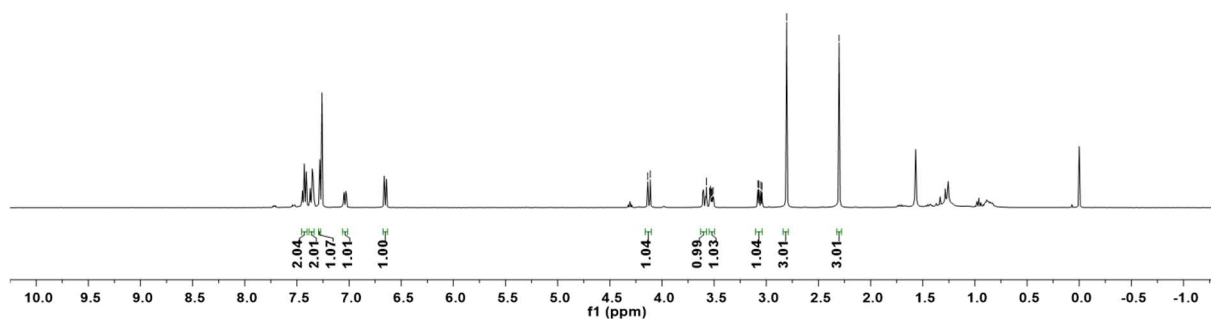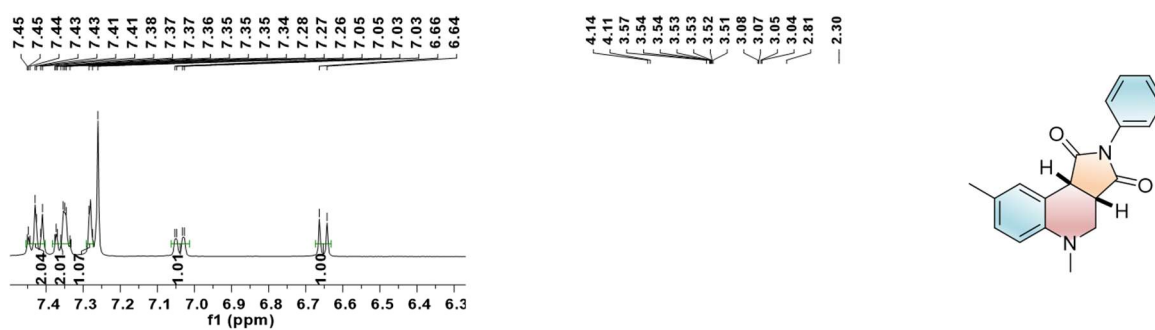
¹H NMR (400 MHz, CDCl₃) spectrum of 3ah.

¹³C NMR (101 MHz, CDCl₃) spectrum of 3ah.
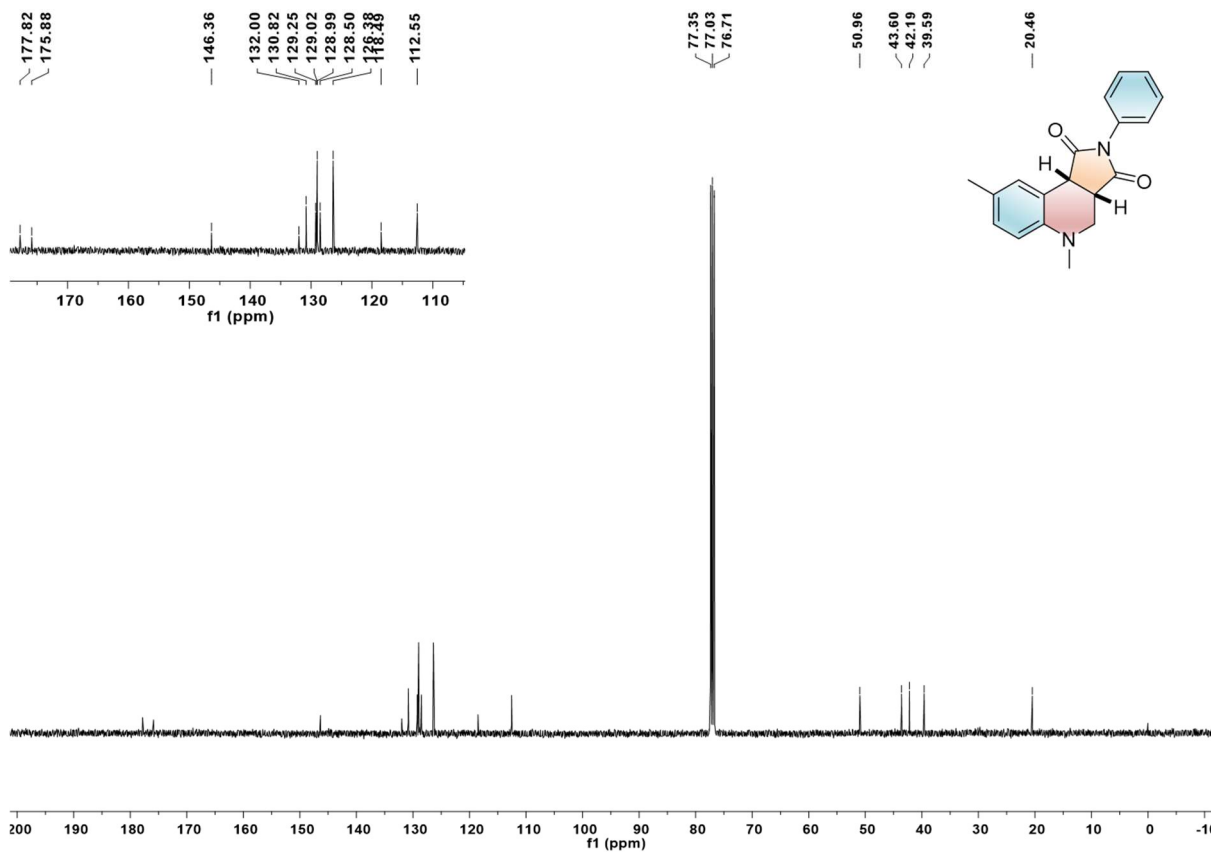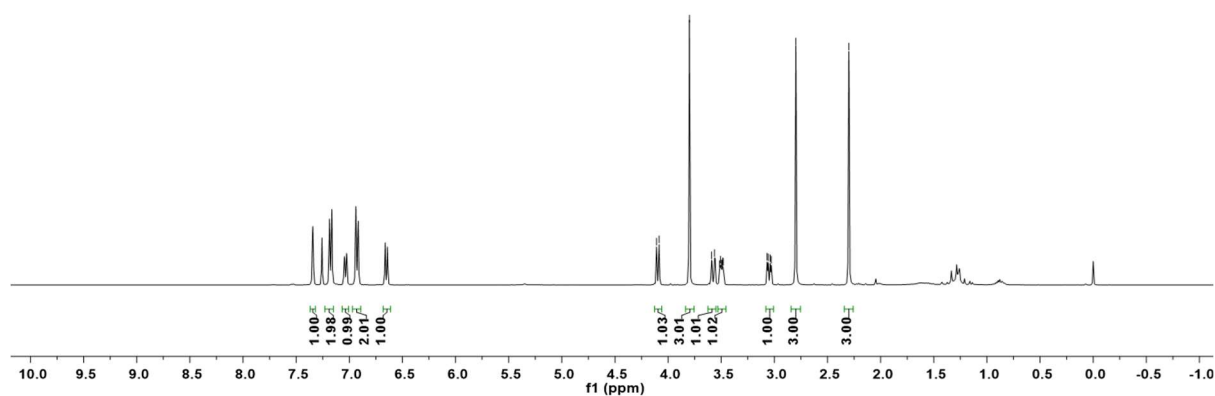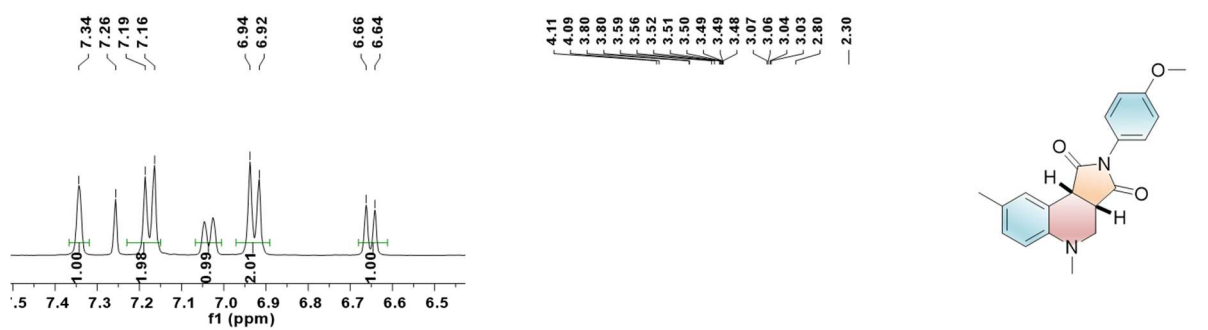
^{1}H NMR (400 MHz, CDCl$_3$) spectrum of 3ai.

^{13}C NMR (101 MHz, CDCl$_3$) spectrum of 3ai.
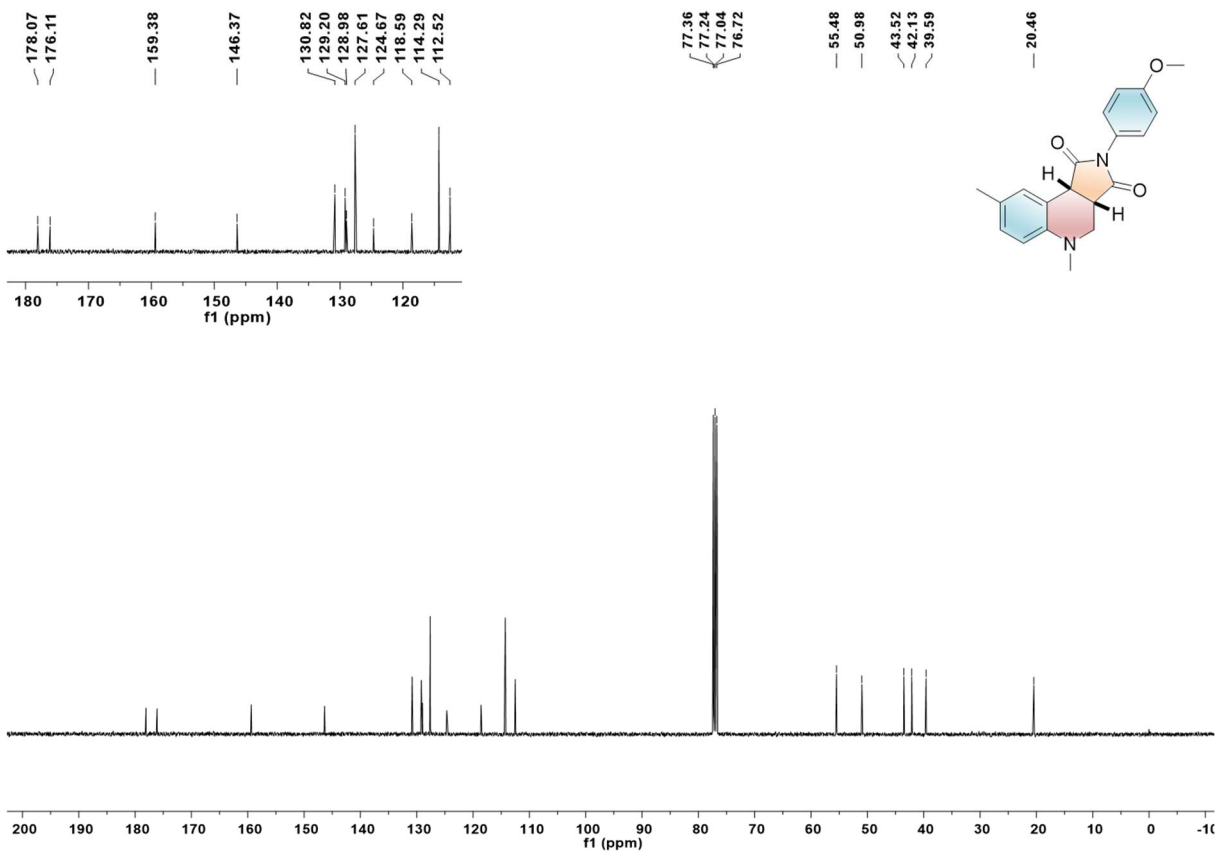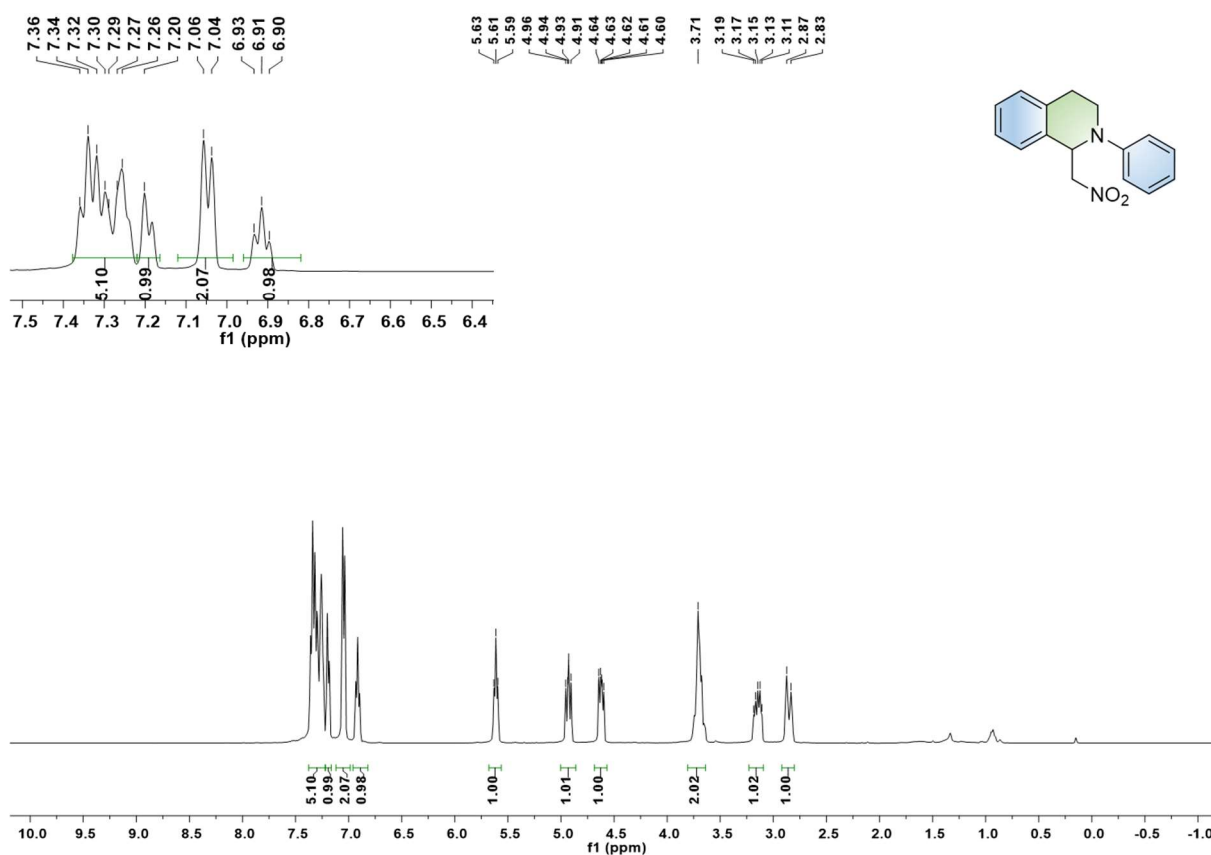
¹H NMR (400 MHz, CDCl₃) spectrum of 3ba.

¹³C NMR (101 MHz, CDCl₃) spectrum of 3ba.
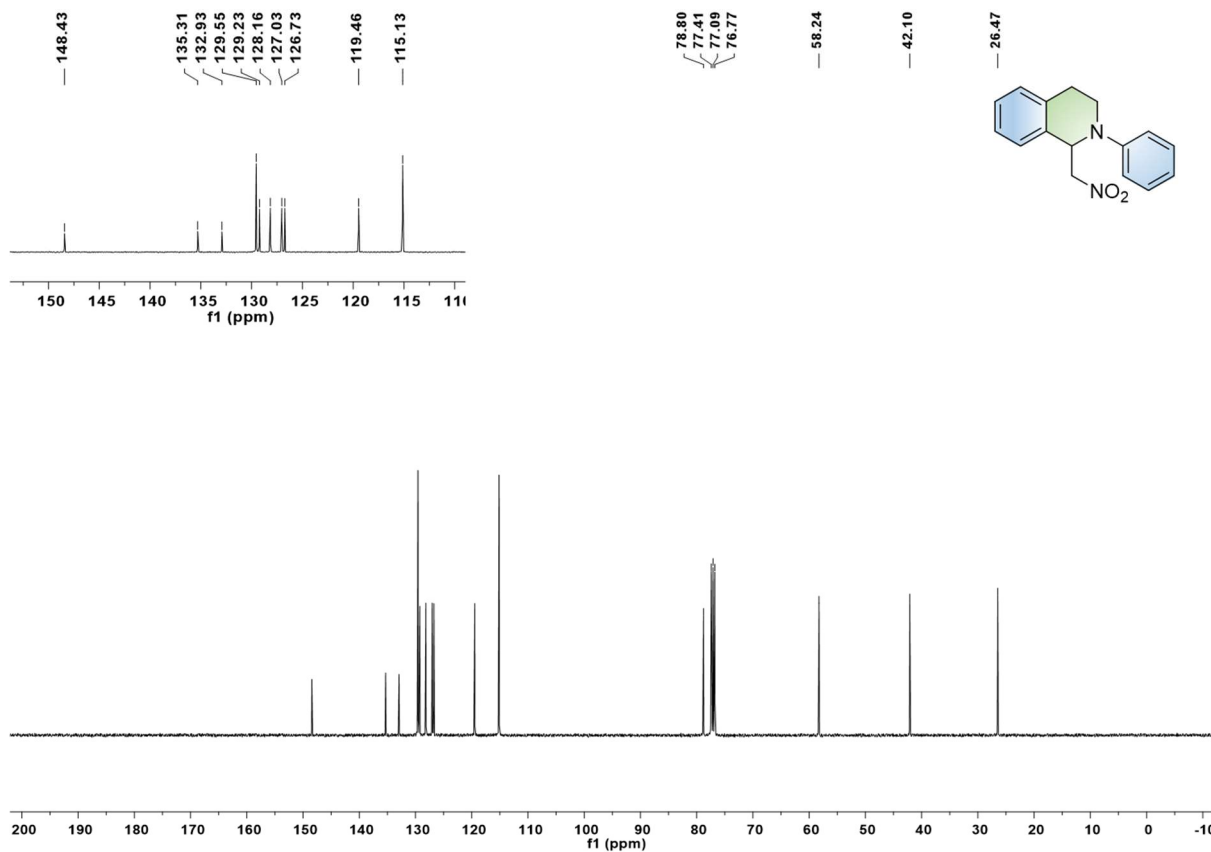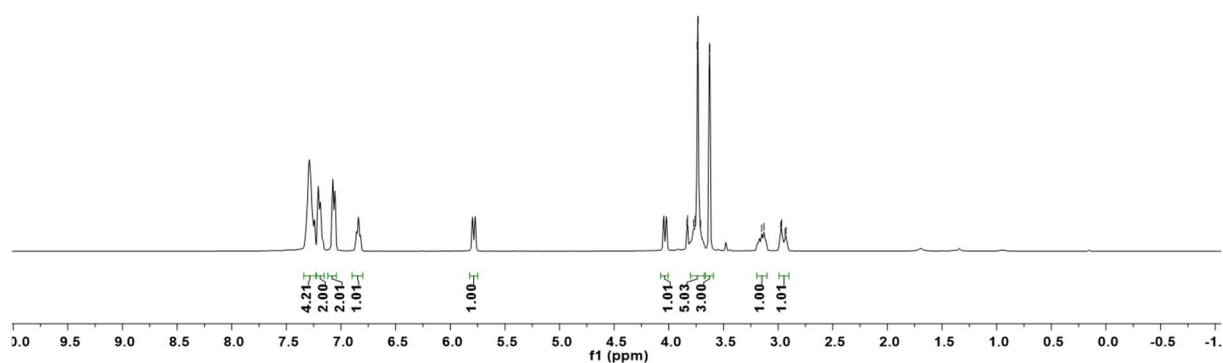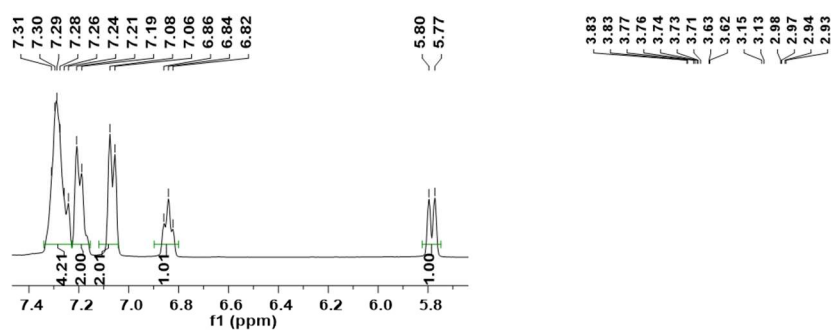
¹H NMR (400 MHz, CDCl₃) spectrum of 3bb.

¹³C NMR (101 MHz, CDCl₃) spectrum of 3bb.
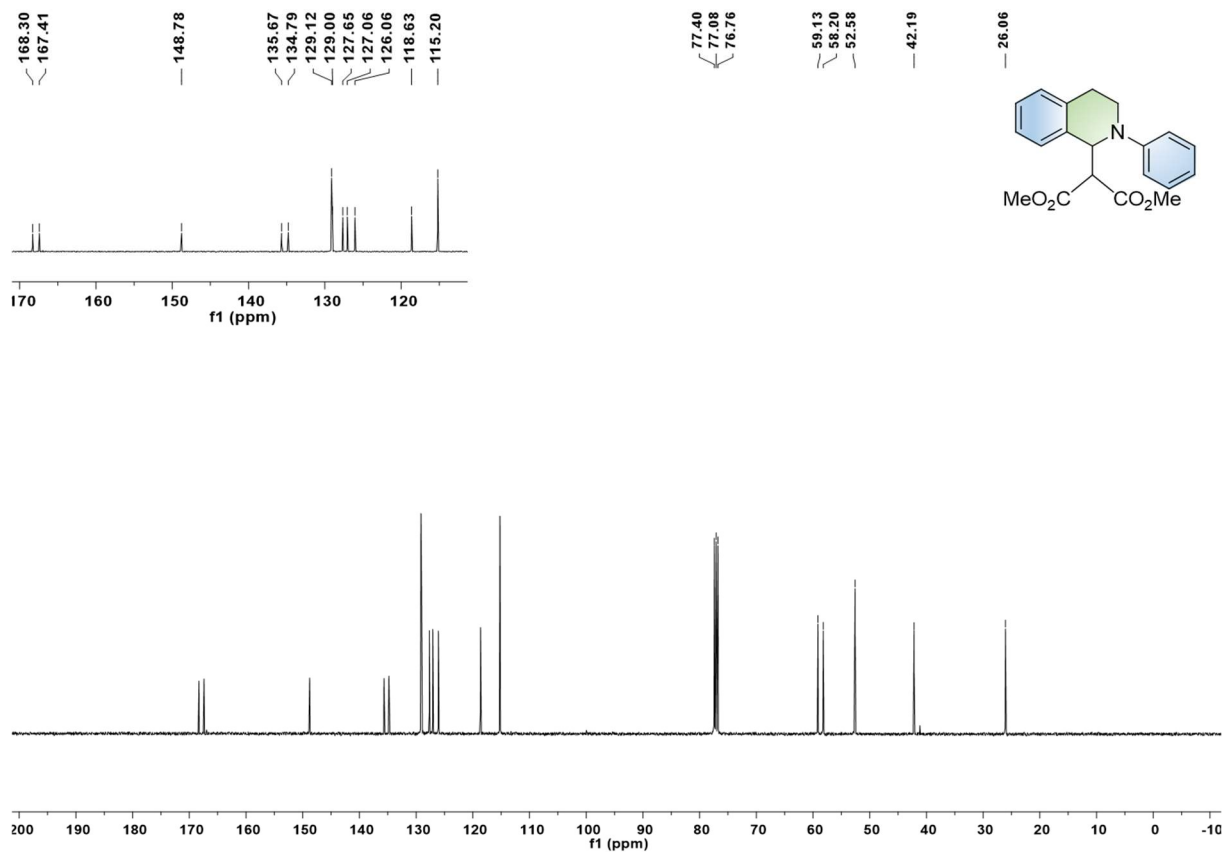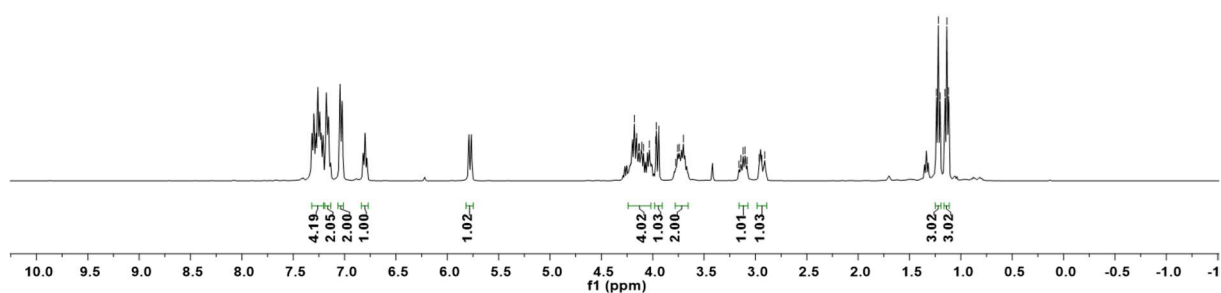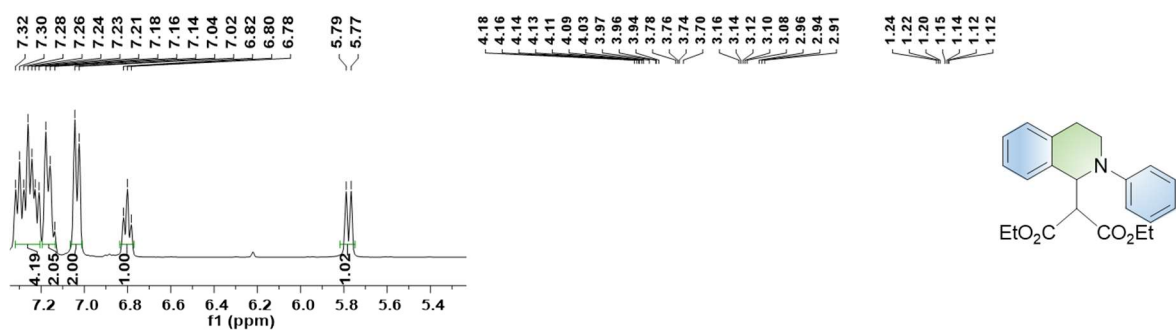
¹H NMR (400 MHz, CDCl₃) spectrum of 3bc.

¹³C NMR (101 MHz, CDCl₃) spectrum of 3bc.
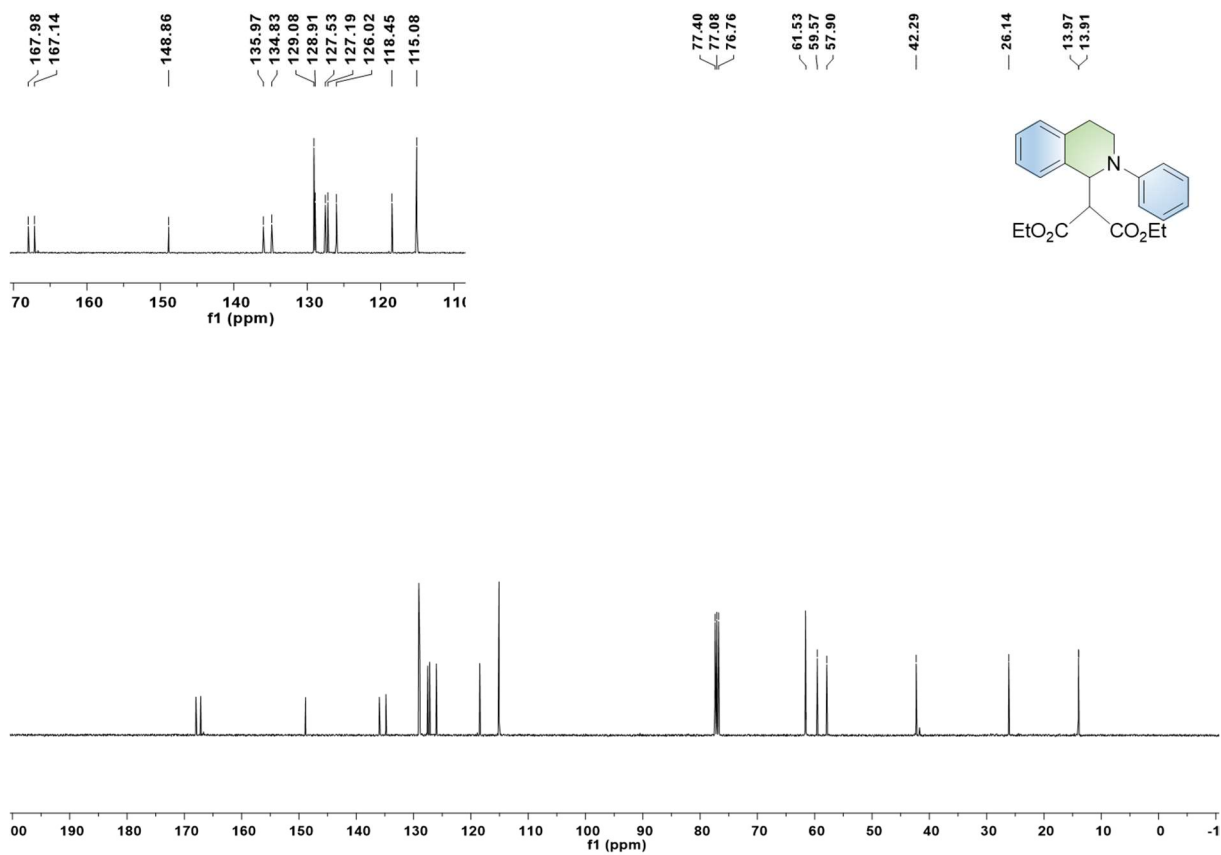
^{1}H NMR (400 MHz, CDCl₃) spectrum of 3bd.

^{13}C NMR (101 MHz, CDCl₃) spectrum of 3bd.
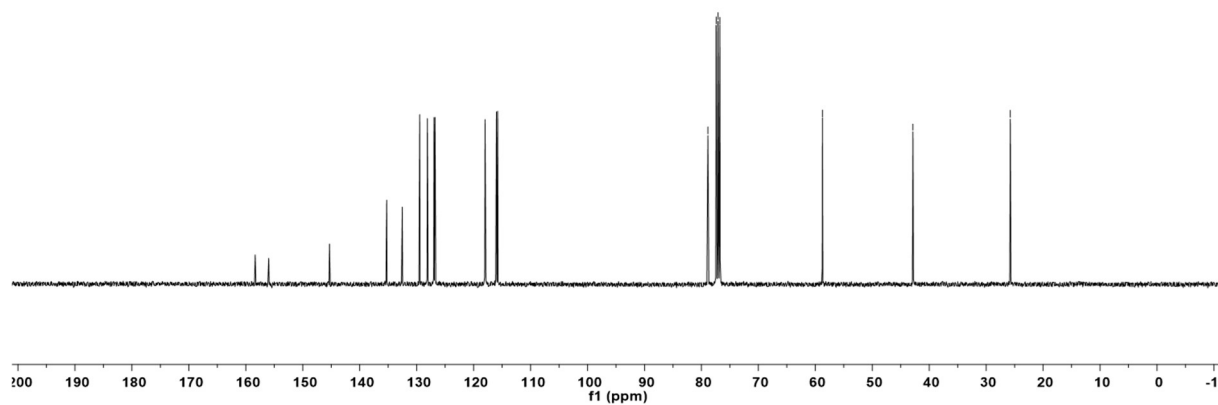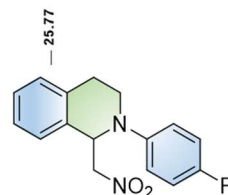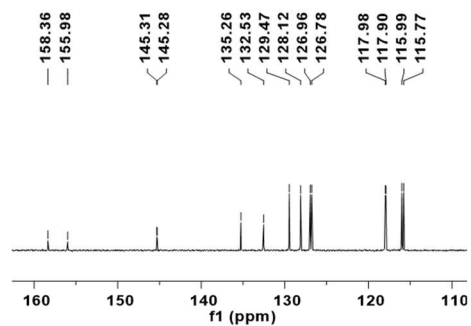
¹⁹F NMR (376 MHz, CDCl₃) spectrum of 3bd.

^{19}F NMR (376 MHz, CDCl$_3$) spectrum of 3bd.

—124.25
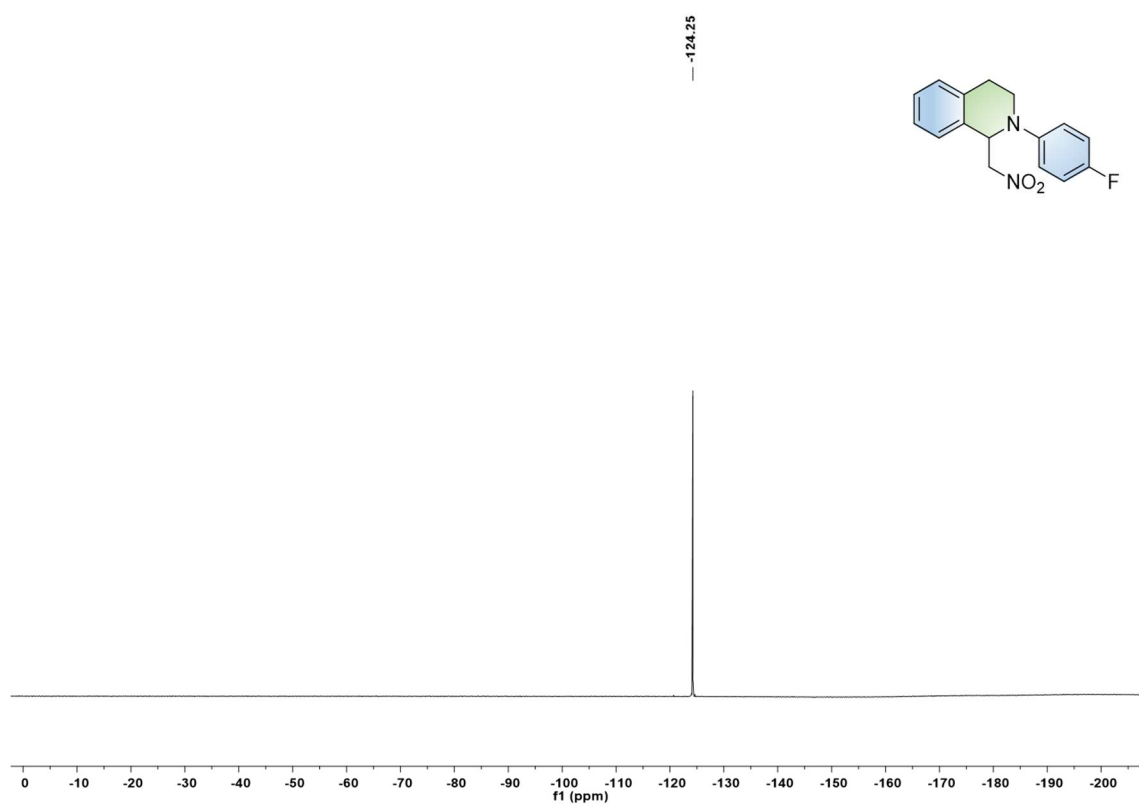
¹H NMR (400 MHz, CDCl₃) spectrum of 3be.

¹³C NMR (101 MHz, CDCl₃) spectrum of 3be.
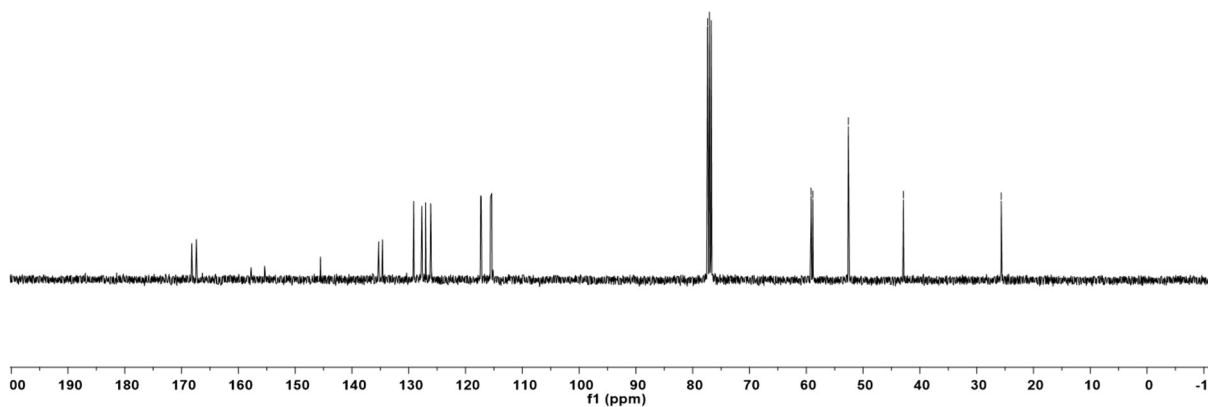
^{19}F NMR (376 MHz, CDCl$_3$) spectrum of 3be.

-125.78
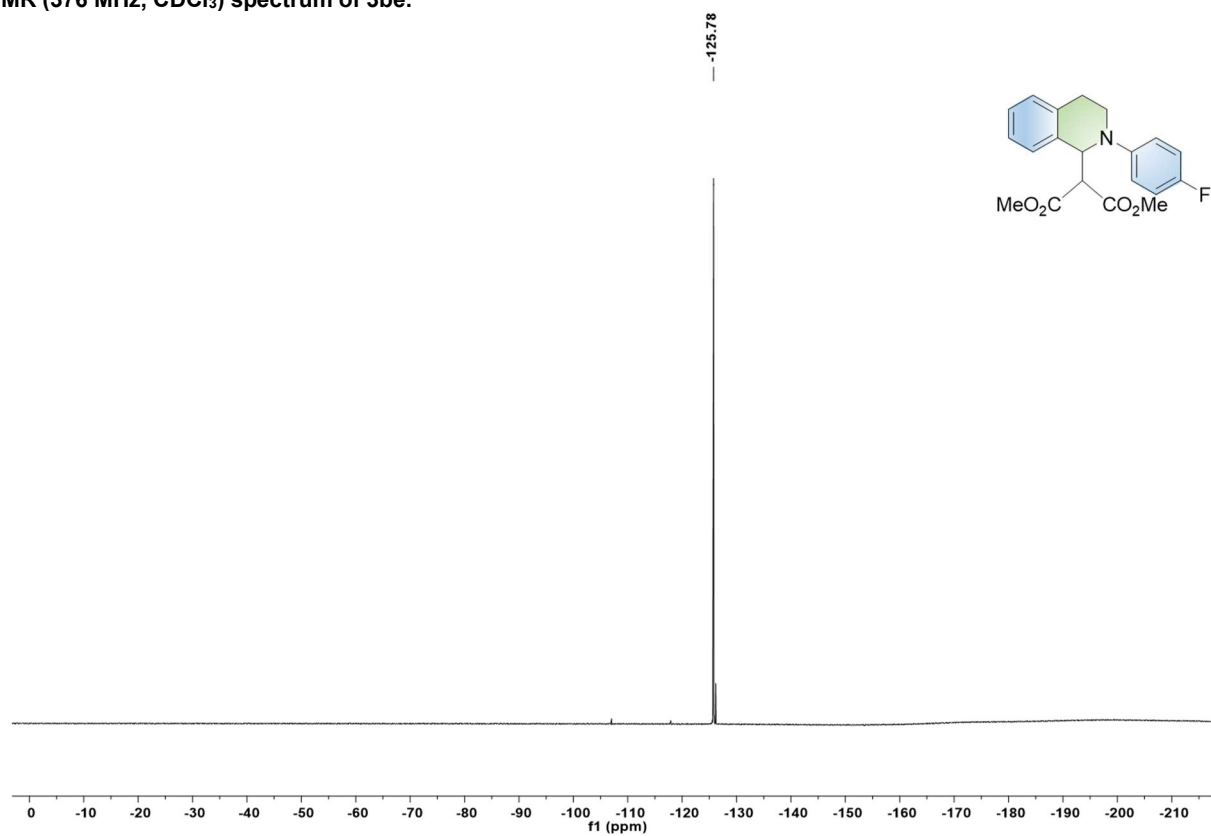
^{1}H NMR (400 MHz, CDCl$_3$) spectrum of 3bf.

^{13}C NMR (101 MHz, CDCl$_3$) spectrum of 3bf.

¹⁹F NMR (376 MHz, CDCl₃) spectrum of 3bf.

— −126.11
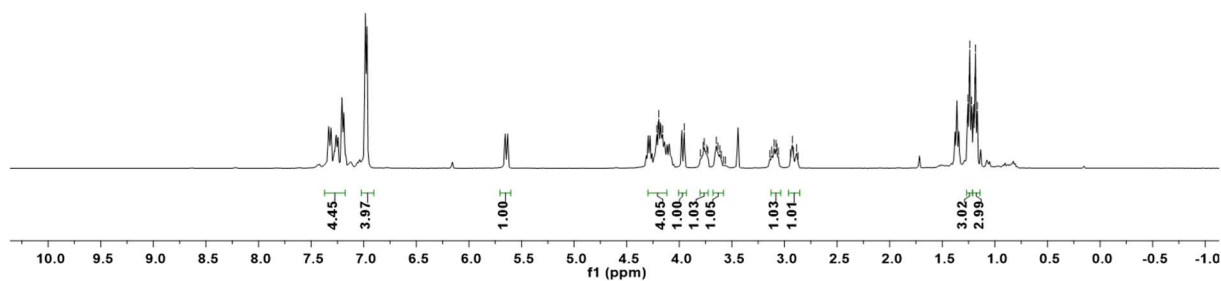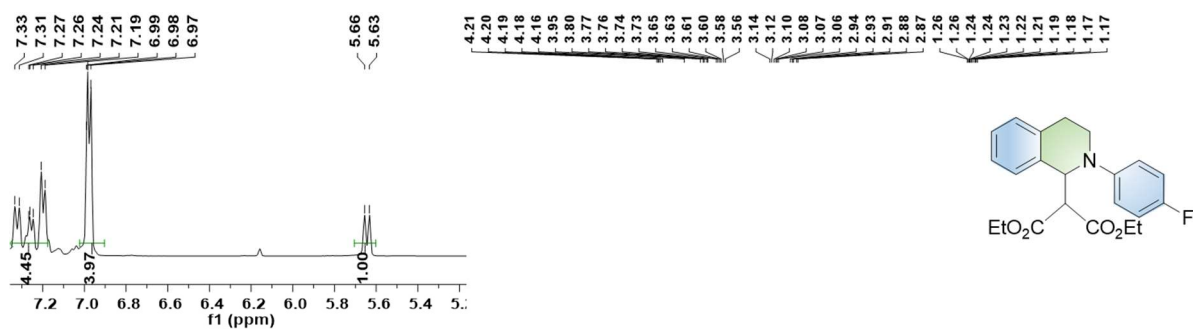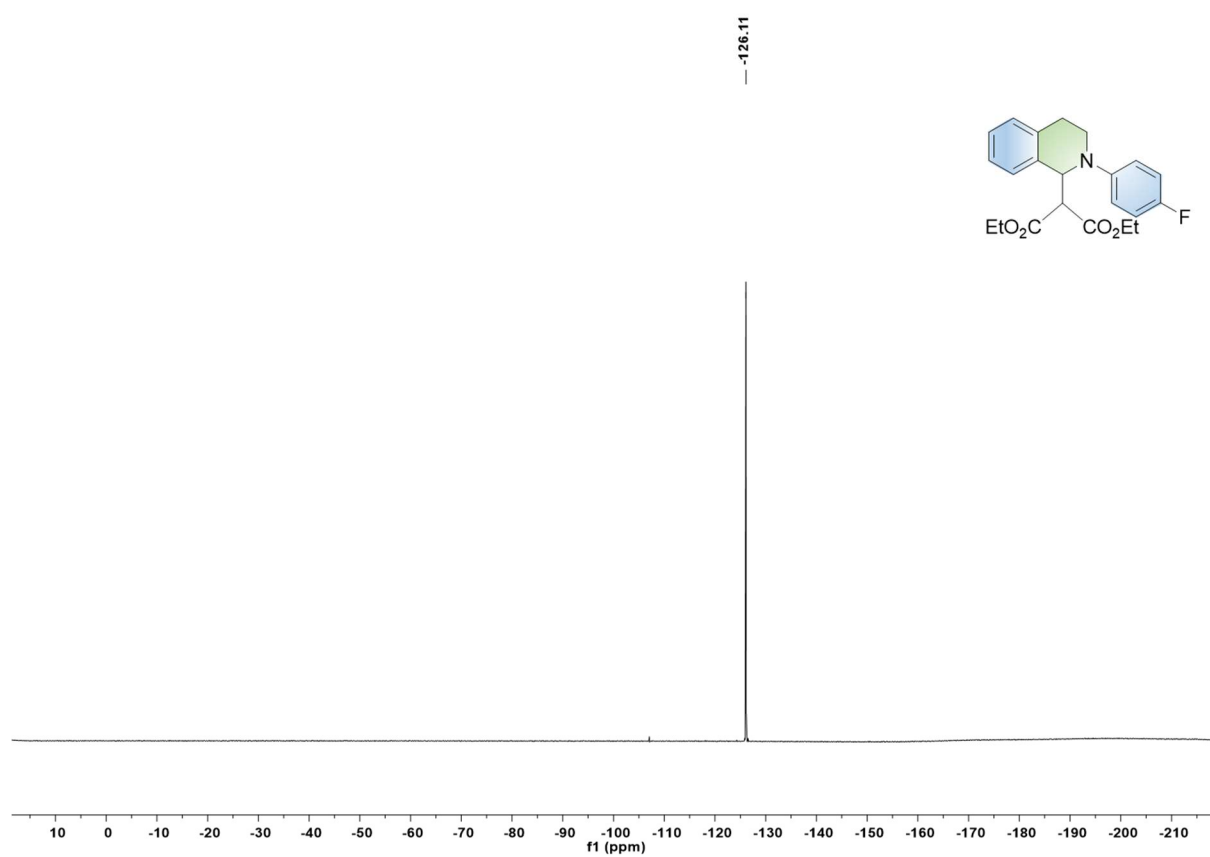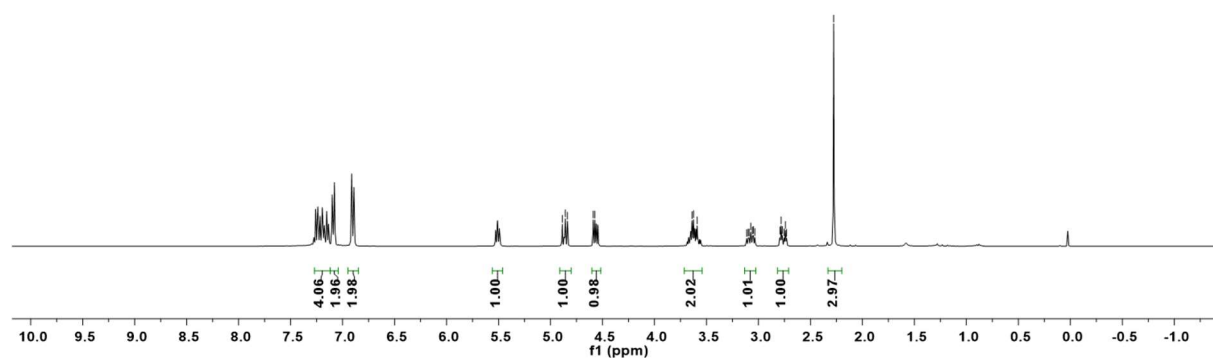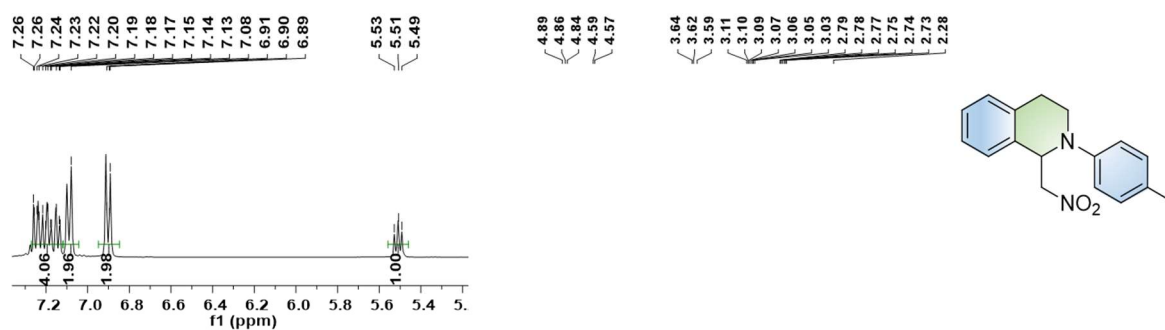
¹H NMR (400 MHz, CDCl₃) spectrum of 3bg.

¹³C NMR (101 MHz, CDCl₃) spectrum of 3bg.
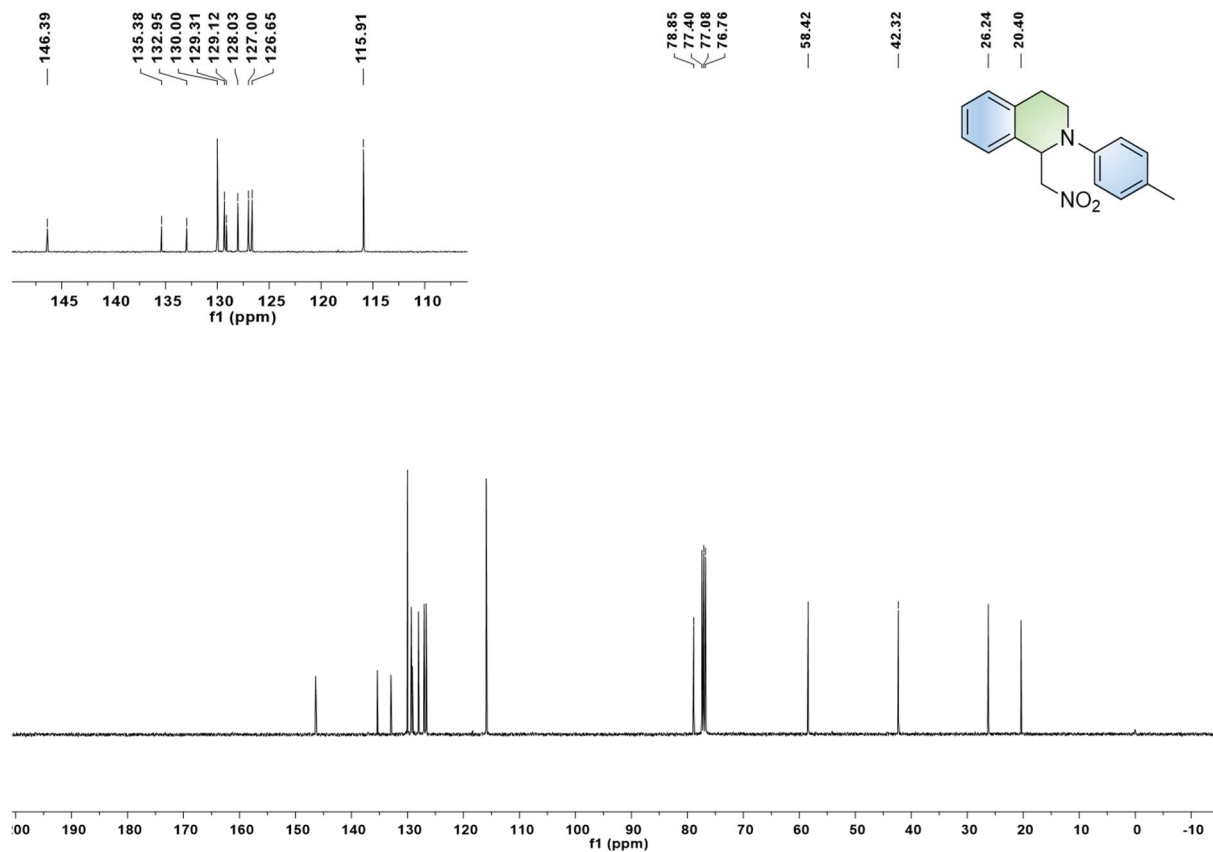
^{1}H NMR (400 MHz, CDCl$_3$) spectrum of 3bh.
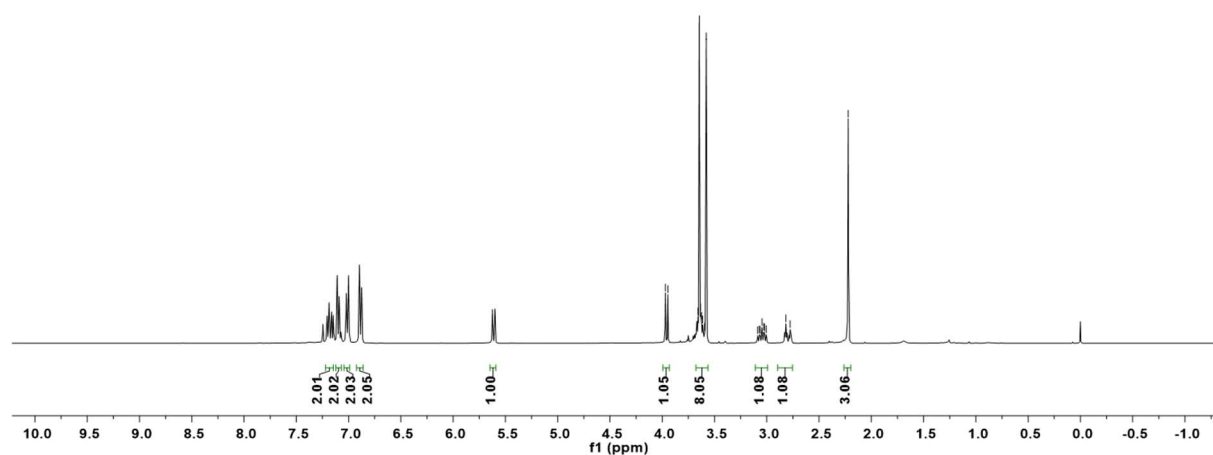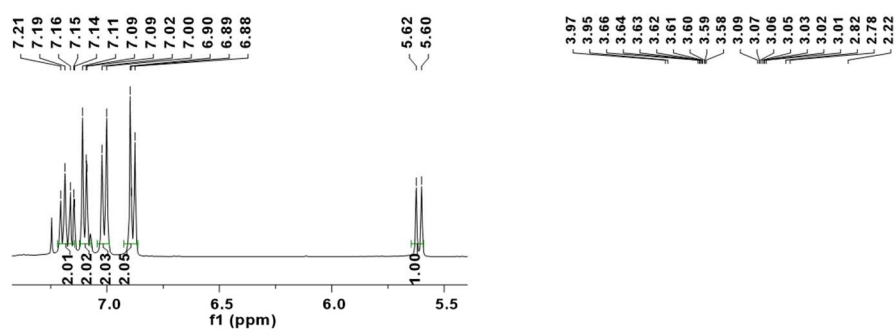
^{13}C NMR (101 MHz, CDCl$_3$) spectrum of 3bh.

S80
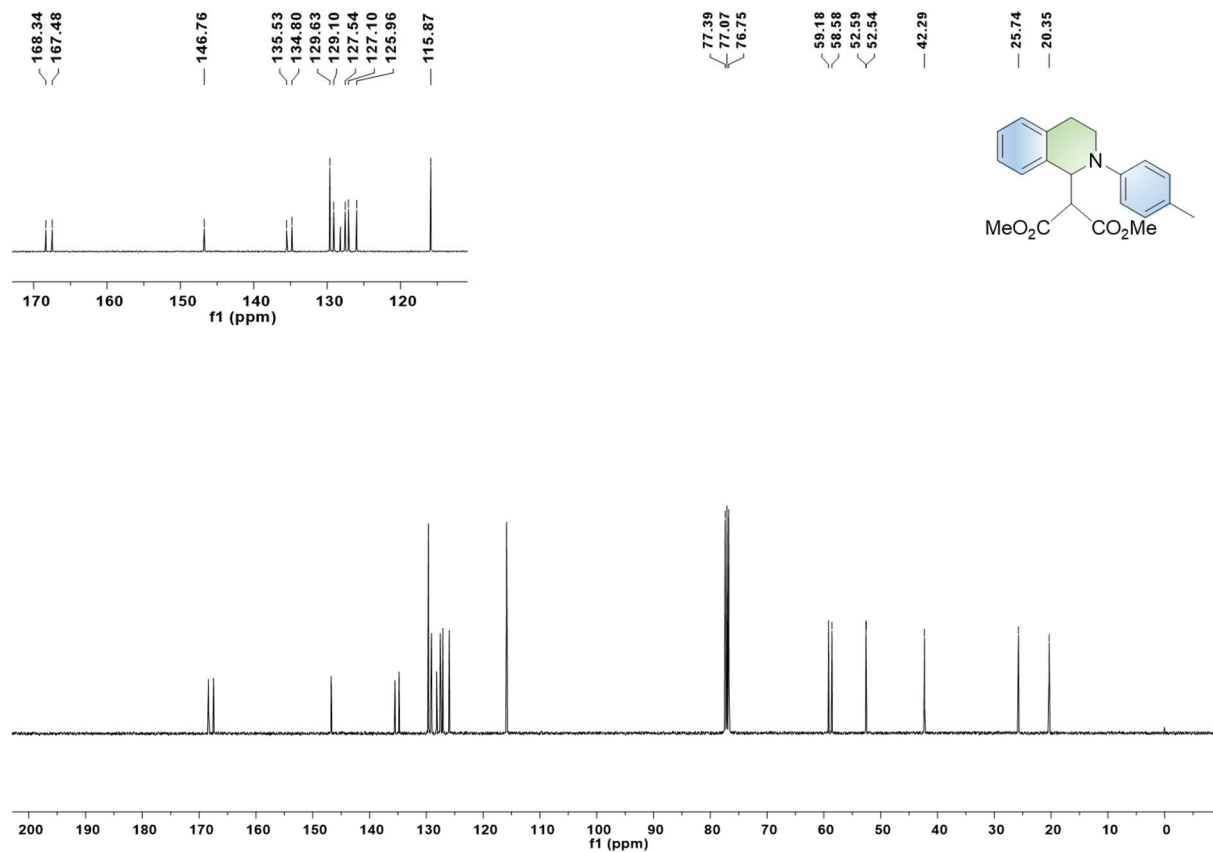
^{1}H NMR (400 MHz, CDCl$_3$) spectrum of 3bi.
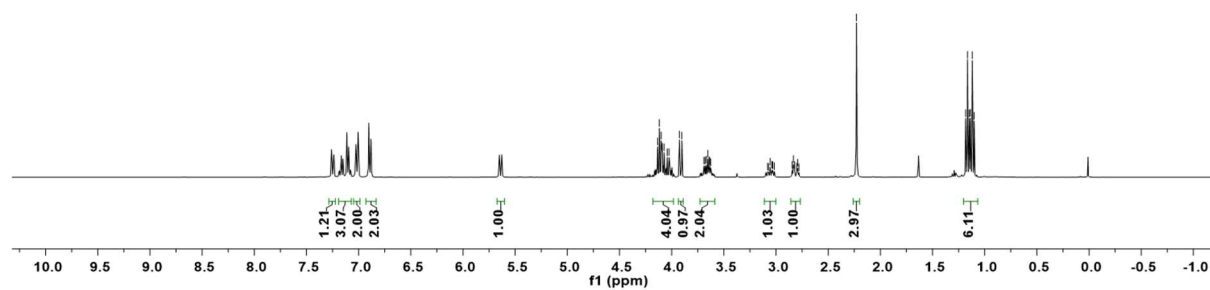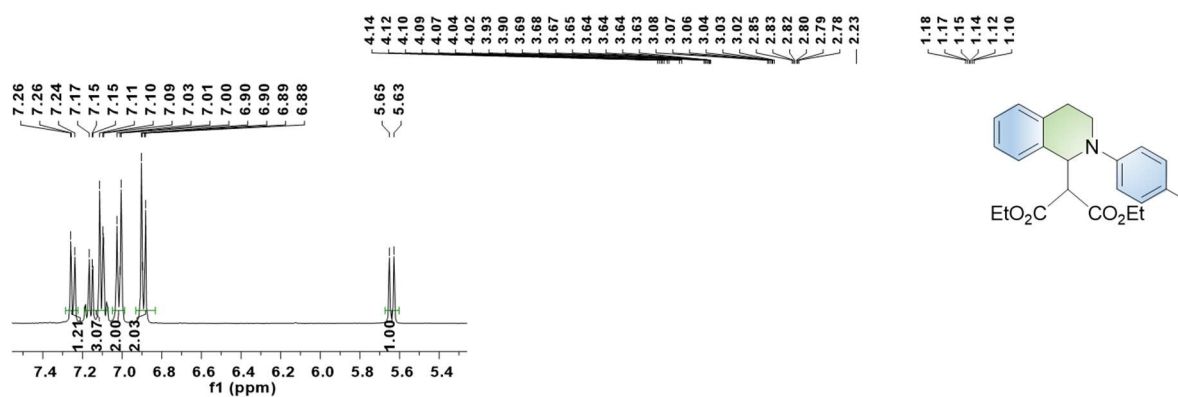
^{13}C NMR (101 MHz, CDCl$_3$) spectrum of 3bi.
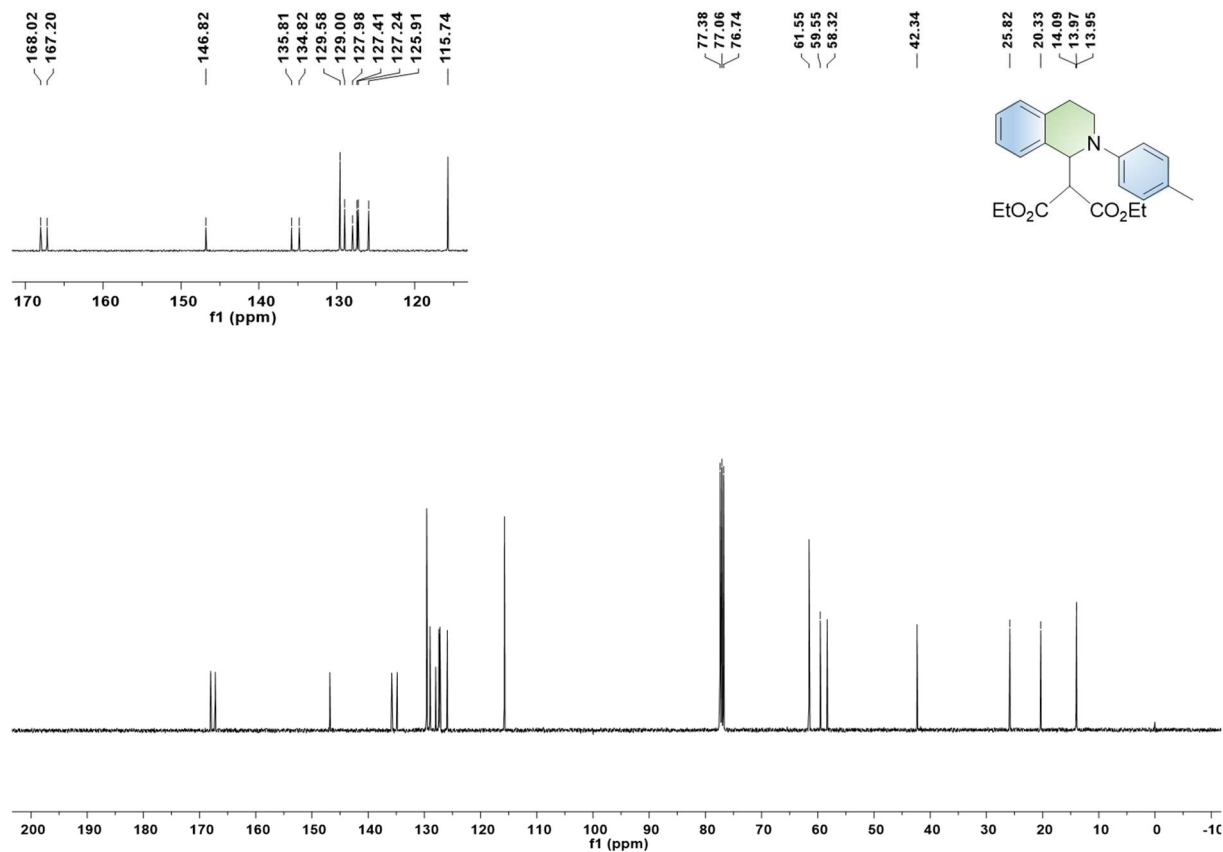
Reference

[1]   M. Bielawski, M. Zhu, B. Olofsson, *Adv. Synth. Catal.* **2007**, *349*, 2610-2618.

[2]   B. Olofsson, M. Zhu, N. Jalalian, *Synlett* **2008**, *2008*, 592-596.

[3]   W. V. Taylor, Z. L. Xie, N. I. Cool, S. A. Shubert, M. J. Rose, *Inorg. Chem.* **2018**, *57*, 10364-10374.

[4]   M. Rueping, S. Zhu, R. M. Koenigs, *ChemComm* **2011**, *47*, 8679-8681.

[5]   M. Stolar, J. Borau-Garcia, M. Toonen, T. Baumgartner, *J. Am. Chem. Soc.* **2015**, *137*, 3366-3371.

[6]   S. Durben, T. Baumgartner, *Angew. Chem. Int. Ed.* **2011**, *50*, 7948-7952.

[7]   B. He, S. Zhang, Y. Zhang, G. Li, B. Zhang, W. Ma, B. Rao, R. Song, L. Zhang, Y. Zhang, G. He, *J. Am. Chem. Soc.* **2022**, *144*, 4422-4430.

[8]   S. Zhang, L. Ma, W. Ma, L. Chen, K. Gao, S. Yu, M. Zhang, L. Zhang, G. He, *Angew. Chem. Int. Ed.* **2022**, *61*, e202209054.

[9]   G. Li, K. Zhou, Q. Sun, W. Ma, X. Liu, X. Zhang, L. Zhang, B. Rao, Y. L. He, G. He, *Angew. Chem. Int. Ed.* **2022**, *61*, e202115298.

[10]   J. Y. Hwang, A. Y. Ji, S. H. Lee, E. J. Kang, *Org. Lett.* **2020**, *22*, 16-21.

[11]   X. Z. Wang, Q. Y. Meng, J. J. Zhong, X. W. Gao, T. Lei, L. M. Zhao, Z. J. Li, B. Chen, C. H. Tung, L. Z. Wu, *ChemComm* **2015**, *51*, 11256-11259.

[12]   S.-S. Zhu, Y. Liu, X.-L. Chen, L.-B. Qu, B. Yu, *ACS Catal.* **2021**, *12*, 126-134.

Author Contributions

Liang Xu and Gang He conceived the idea for the study. Liang Xu prepared the samples and conducted characterizations. Liang Xu, Lei Zhang, Wenqiang Ma, Yi Qiao helps to prepare and characterize the samples. Liang Xu and Haifeng Zheng analyzed the electrochemical data. Liang Xu and Guoping Li contributed to the application of electrochromic devices. Liang Xu, Bin Rao and Mingming Zhang contributed to the DFT calculations. Liang Xu, and Gang He wrote the manuscript and all the authors revised and polished the manuscript.